# Optimal Resource Allocation in Wireless Networks with Non-Orthogonal Multiple Access

by

Fudong Li

A thesis submitted in partial fulfillment of the requirements for the degree of

Doctor of Philosophy

in

Communications

Department of Electrical & Computer Engineering

University of Alberta

# Abstract

Due to the unprecedentedly high demand of wireless spectrum, one of the central missions in wireless networks is to technically improve the spectrum efficiency. Thus, many techniques have been devised, in which non-orthogonal multiple access (NOMA) is quite promising. In NOMA, the strengthened spectrum efficiency is majorly due to the intelligent superimposition and detection of users' signals. Resource allocation plays a pivotal role in NOMA networks, by which the system performance can be maximized at the optimality. Accordingly, a lot of efforts have been made to achieve optimal resource allocation under a wide variety of objectives.

In this research, driven by the needs of spectrum-efficient and energy-efficient designs, we aim to identify the optimal solutions in several NOMA-based wireless networks. To be specific, resource allocation problems are investigated in three wireless networks. Firstly, in an overlay cognitive NOMA network enabled with wireless energy harvesting, we investigate the maximization of secondary throughput under the case with successive interference cancellation (SIC) and the case without SIC. Secondly, the maximization of network utility is studied in one downlink NOMA network. Thirdly, one design of energy-aware resource allocation is investigated in one NOMA multi-access edge computing (MEC) network.

# Acknowledgements

I would like to express my greatest appreciation to my supervisor, Prof. Hai Jiang, who offers me such an invaluable opportunity to pursue my PhD degree. Thanks for his generosity in providing me with the financial support. From his world-class scholarly expertise, he always guides and inspires me to make progress in my research. His dedication on pursuing high caliber academic works is more like the exploration of perfect artworks from an artist. Being his student is my lifelong honor.

I gratefully acknowledge Dr. Chintha Tellambura, Dr. Hao Liang, Dr. Xihua Wang, Dr. Zhijun Qiu and Dr. F. Richard Yu for being my defense committee and candidacy committee. Their professional reviews and constructive comments bring improvements to my thesis.

I would like to thank Dr. Rongfei Fan for his warm-hearted help and inspiring discussions on many academic directions. He is always willing to share his latest academic results with me. My thanks go to my lab-mates and friends. Their friendship and companionship bring me so many happy memories during my study.

Lastly, I sincerely thank my parents Guocai Li and Zhenmei Teng. I have been greatly indebted to them. Without their love and support, I could not even keep studying for so many years.

# Table of Contents

# List of Tables

# List of Figures

# Glossary of Terms

| Acronyms | Definition |
|---|---|
| **AWGN** | Additive White Gaussian Noise |
| **BS** | Base Station |
| **CR** | Cognitive Radio |
| **EPA** | Equal Power Allocation |
| **IoT** | Internet of Things |
| **MEC** | Multi-access Edge Computing |
| **NOMA** | Non-orthogonal Multiple Access |
| **OMA** | Orthogonal Multiple Access |
| **PT** | Primary Transmitter |
| **PR** | Primary Receiver |
| **PU** | Primary User |
| **SIC** | Successive Interference Cancellation |
| **SINR** | Signal-to-interference-plus-noise Ratio |
| **SR** | Secondary Receiver |
| **ST** | Secondary Transmitter |

| | |
|---|---|
| **SU** | Secondary User |
| **SWIPT** | Simultaneous Wireless Information and Power Transfer |
| **TS** | Time Switching |

# Chapter 1

# Introduction

In the era of information technology, the convenience provided by the wireless service has been revolutionizing every corner where we live. It promotes the productivity of our work and study, entertains us with a variety of enjoyable means, and so on. For example, people can meet each other via video conferencing. Emails and text messages can be sent at anytime. Live sport events can be broadcasted and enjoyed at anywhere through the mobile TV service.

In the future, the wireless networks will be more advanced and complicated. Even broader spectrum band will be available to guarantee the delivering of wireless service. The usable spectrum will be larger than 30 GHz in beyond-5G (B5G) networks [1]. Moreover, the support of massive connectivity is envisioned. Driven by the portability and low cost of mobile device, the connections of huge amount of devices over wireless networks have been shifting the networks into the age of Internet of Things (IoT). In addition, future networks are also featured by low latency. For example, the tactile Internet requires a latency as low as 1 ms.

However, providing wireless services in wireless networks are bottlenecked by two fundamental technical issues: energy efficiency and spectrum efficiency [2–4].

## 1.1 Efficiencies in Wireless Commutations

### 1.1.1 Energy Efficiency

Energy efficiency is one major concern in wireless communication systems, which has the target of minimizing the energy consumption on wireless data traffic. Mobile terminals usually have limited energy supply. Basically, there are two main reasons to conduct an efficient utilization of energy.

Firstly, many mobile applications have very high energy consumption. For example, an augmented reality (AR) based gaming application needs the interaction of a player with the real world, which involves high volume of data computations. These computations drain the battery at a fast pace.

Secondly, many devices may work on the scenarios that require low power consumptions. We take two types of sensors as examples. For one type, some medical sensors are embedded inside human bodies, which can be designed to monitor specific diseases [5]. For the other type, some sensors are designed to monitor the temperature of water in deep sea environment. To prolong the lifetime of battery and avoid the inconvenience of battery replacement, these sensors should be designed to consume as little energy as possible.

To enhance the energy efficiency, many technical approaches provide viable solutions, which include energy harvesting, multi-access edge computing (MEC), and so on.

### 1.1.2 Spectrum Efficiency

As the evolution of mobile systems, the system performances and offered wireless services are constantly enhanced [1] [2]. The 1G systems are designed with analog transmission, in which the frequency-division multiple access (FDMA) technique

[1] We use data rate as the example of system performance in Section 1.1.2.

is employed. Only the voice call service can be provided for users. From 2G onwards, digital transmissions are utilized. Based on the time-division multiple access (TDMA) technique, the 2G systems can offer a data rate of 64 kbps, and support improved services such as text message. In the 3G systems, by adopting the code-division multiple access (CDMA) scheme, a 2 Mbps data rate can be achieved. The users in 3G networks also enjoy further enhanced services, which include video call, Internet service, and so on. The 4G systems utilize the orthogonal frequency-division multiple access (OFDMA) scheme, which can reach a data rate of 1 Gbps, and offer numerous high quality services such as high-definition (HD) mobile TV. In the 5G systems, the data rate is expected to reach 20 Gbps in downlink network [6]. A broader class of services can be enjoyed by users, which include low latency service, massive IoT, and so on.

To guarantee the even better system performances and services in wireless networks, it calls for incredibly high demand of wireless spectrum. However, the usage of wireless spectrum has limitations, which include scarce supply, limited capacity, interference, and so on. As for the supply issue, the usable spectrum is usually restricted to a certain range. For example, in the currently adopted 4G Long Term Evolution (LTE) systems [7], the commonly used frequency band is around 2 GHz. Also, as pointed out by information theory [8], the data rate over wireless channel is upper-bounded by the channel capacity. Furthermore, when multiple users transmit signals simultaneously on the same channel, the co-channel interference degrades the signal-to-interference-plus-noise ratio (SINR) for signal detection at the receiver side.

Due to these limitations of spectrum usage, it is required that the spectrum efficiency should be technically improved into its best-effort manner. Accordingly, many approaches are devised to enhance the spectrum efficiency in future wire-

less networks, which include non-orthogonal Multiple Access (NOMA), cognitive radio (CR), and so on. In our research, we focus on NOMA.

## 1.2 An Introduction to NOMA

In traditional cellular networks, to coordinate the channel access of multiple users, the Orthogonal Multiple Access (OMA) technique is adopted [3]. In OMA, the wireless spectrum is partitioned into orthogonal resource blocks, which include frequency bands, time slots, spreading codes and subcarriers [2]. By exclusively assigning each resource block to one single user, multiple users can get channel accesses simultaneously.

In recent few years, emerged as a novel transmission technique, NOMA can further boost the spectrum efficiency [9–15]. Different from OMA, NOMA can transmit multiple users' signals by using the same resource block. There are two types of NOMA schemes, which include the power domain NOMA and code domain NOMA. We focus on the power domain NOMA.

We introduce a typical downlink NOMA system serving $N$ users, denoted as $\mathcal{N} = \{1, 2, \ldots, N\}$. Based on the superposition coding, the base station (BS) transmits signal $x_i$, $i \in \mathcal{N}$, for user $i$ with power $p_i$. And the channel coefficient from the BS to user $i$ is denoted as $h_i$, which has the corresponding channel power gain as $g_i$. Moreover, it is assumed that $g_1 \leq g_2 \leq \ldots \leq g_N$. To guarantee fairness, one widely adopted strategy is to perform power allocation in the descending order [11]. That is, user 1 is assigned with the largest power, while user $N$ is assigned with the lowest power. In such a manner, the quality-of-service (QoS) for the weak user can be guaranteed. When successive interference cancellation (SIC) is adopted, the signal decoding order at the receiver is from $x_1$ to $x_N$.

As for the receiver's signal detection by using SIC, an example for the two-user case is given here. The received signal at user $i$ is $y_i = (\sqrt{p_1}x_1 + \sqrt{p_2}x_2)h_i + n_i$, $i \in \{1, 2\}$, where $n_i$ is the Additive White Gaussian Noise (AWGN), distributed with $n_i \sim \mathcal{CN}(0, \sigma^2)$. User 1 is the weak user (with weak channel), and user 2 is the strong user (with strong channel). At user 1, it only decodes its own information $x_1$ at the rate of $R_1 = \log(1 + \frac{p_1 g_1}{p_2 g_1 + \sigma^2})$. At user 2, it decodes user 1's information $x_1$ at the rate of $R_{2,1} = \log(1 + \frac{p_1 g_2}{p_2 g_2 + \sigma^2})$. Due to $g_2 \geq g_1$, we have $R_{2,1} \geq R_1$, which means user 2 can always successfully decode $x_1$. Afterwards, user 2 subtracts $x_1$'s component from its received signal, and thus, user 2 decodes its own information $x_2$ at the rate of $R_2 = \log(1 + \frac{p_2 g_2}{\sigma^2})$. As for the SIC decoding for the $N$-user case, we can follow a similar process as the two-user case.

It can be seen that by leveraging superposition coding and SIC, multiple users' information can be delivered in only one time slot. As a comparison, if OMA transmission is adopted, we need multiple time slots to serve multiple users. Moreover, as discussed in [16], NOMA can achieve a higher sum rate than OMA. Thus, NOMA brings about the improvement of spectrum efficiency. Also, NOMA meets the massive connectivity requirement for B5G systems [1, 17]. Furthermore, it can be flexibly combined with other emerging techniques. Therefore, it is treated as one promising technique to realize the advanced features in future networks. Since many of the research problems on NOMA related wireless networks are still not fully studied, there are many research gaps to be filled.

## 1.3 Research Motivation and Thesis Contributions

To achieve the objective of spectrum-efficient and energy-efficient designs, we conduct our research on resource allocation in NOMA systems. When NOMA is enabled in various networking scenarios, it may involve the allocation of resources including power, time, frequency, and so on. By adopting different optimization frameworks, for many specific resource allocation problems, the formulated optimization problems may become non-convex. It is usually challenging to obtain the optimal solutions for such non-convex problems.

Therefore, in our research, to unveil the optimal solutions, we investigate three research topics on the resource allocation in different NOMA enabled wireless networks.

Firstly, we consider the resource allocation in cognitive NOMA systems with wireless energy harvesting. In the literature, the cognitive NOMA systems can be majorly categorized into three different systems: Cognitive Radio (CR)-inspired NOMA, underlay cognitive NOMA and overlay cognitive NOMA. Some related systems have been investigated in [18–20]. In wireless energy harvesting, the simultaneous wireless information and power transfer (SWIPT) technique is widely adopted. When SWIPT is introduced into cognitive NOMA systems, research efforts have been conducted to tackle the resource allocation problems in CR-inspired NOMA and underlay cognitive NOMA systems in [21] and [22], respectively. However, the research on overlay cognitive NOMA with the enhancement of SWIPT has not been studied, which motivates us to investigate the resource allocation problem on it.

Secondly, we consider the Stackelberg game based resource allocation in multi-user NOMA downlink system, with the maximization of network utility. For fixed

total allocated transmit power for users, two initial works in [23] and [24] studied the power allocation of downlink NOMA systems by using the Stackelberg game, which give an optimal solution for two-user case, and sub-optimal solutions for multi-user case. This motivates us to investigate the optimal solution for a novel multi-user game by considering more general game formulations (for example, the total allocated transmit power is a variable, and a more general utility function is adopted).

Thirdly, we consider the design of energy-aware resource allocation in NOMA MEC networks under the framework of Stackelberg game. In MEC networks, user's energy consumption can be effectively reduced through performing data offloading. To promote energy saving by using Stackelberg game, resource allocation can be conducted in a hierarchical manner. In OMA MEC networks, a payment-based resource allocation is investigated in [25]. The work in [26] investigates a game theoretical approach of sub-channel allocation for users in NOMA MEC networks. However, to save energy through making payments, a game theoretical approach of resource allocation within the same channel has not been studied for NOMA MEC networks, and thus, it has motivated us to solve the research problem.

To fill the research gaps for the aforementioned research topics in NOMA systems, we present three research works from Chapter 3 to Chapter 5 in our thesis. The contributions of our thesis are summarized as follows.

- In Chapter 3, we study a novel overlay cognitive NOMA system enabled with wireless energy harvesting. In our system, the secondary transmitter (ST), which harvests energy from the primary transmitter's wireless signal, is allowed to access the channel by cooperatively helping the primary system to forward information. The ST can also adopt NOMA to transmit

its own information. Our objective is to guarantee a target rate of the primary system and try to maximize the secondary throughput. Thus, an optimization framework is used. By considering the impact of SIC, two optimization problems are formulated, which include the case that the secondary receiver (SR) chooses to perform SIC and the case that the SR chooses not to perform SIC. The time portion for harvesting energy and power ratio for transmitting the primary signal are optimized. Since the formulated optimization problems are non-convex, we develop a method to convert the optimization problems into equivalent problems. As for the objective functions in the equivalent problems, they are theoretically proved to be quasiconcave. With the aid of the two-level bisection, the optimal solutions are found for our research problems. We provide one interesting and counter-intuitive insight. It is not guaranteed that the SIC case will always outperform the non-SIC case.

- In Chapter 4, we study the resource allocation in one downlink NOMA system. As all users are selfish, and there exists a hierarchy between the BS and users, we adopt the Stackelberg game approach, which is promising to deal with a hierarchy between multiple selfish players. The seller maximizes the profit per unit power, while each user maximizes the profit. We provide the optimal solution to the formulated game. To be specific, after finding the solution at the user side, the optimization problem at the seller has a non-convex form. Afterwards, we solve the problem at the seller by devising a two-stage algorithm. In the first stage, we obtain a tractable form for the original problem by using transformations. Then we develop an iterative method to solve the optimal solution in this stage. Moreover, we prove the solution in the first stage is concave, and the objective function in the

second stage is quasiconcave. Based on these features, we optimally obtain the solution to the formulated problem.

- In Chapter 5, we provide a design of energy-aware resource allocation in NOMA MEC networks. As there is a hierarchy between the MEC server and the users, we adopt the Stackelberg game approach. To minimize the overall costs, each user purchases the interference to transmit information. To maximize its profit, the BS decides the price for the interference and offloading time. We optimally solve the formulated game. We find the solution to the power at each user first. Then an approach is devised to obtain the optimal solution to the non-convex problem at the BS. Specifically, when the allocated time is given, we show the utility is separable and solvable. Afterwards, to determine the time allocation, the Polyblock algorithm is leveraged to solve it.

# Chapter 2

# Background and Literature Review

In this chapter, some background knowledge is first introduced. Then a literature review is provided for the research on NOMA-based wireless networks.

## 2.1 Background

### 2.1.1 Cognitive NOMA

CR is an important technique to effectively tackle the issue of spectrum scarcity [27–31], in which secondary users (SUs) can intelligently access the spectrum licensed to primary users (PUs) in a controlled manner such that the SUs do not cause too much harmful impacts on PUs. The combination of CR with NOMA is termed as cognitive NOMA. The three architectures of cognitive NOMA are introduced as follows.

In a basic CR-inspired NOMA system, it serves two users [18]. The weak user with a low channel power gain is treated as the PU, while the strong user with a high channel power gain is treated as the SU. When the PU's target rate is satisfied, the SU's information can be transmitted based on downlink NOMA.

In underlay cognitive NOMA systems, one typical scenario is that the sec-

ondary network works under the downlink NOMA transmission [19]. When the secondary BS transmits signal to a group of SUs, the transmitted signal causes interference to the PRs. The transmit power at the secondary BS should be well-adjusted such that the maximal interference power at the PR does not exceed a predefined value.

In overlay cognitive NOMA networks, a two-phase transmission is usually adopted [20]. Specifically, during the first phase, the primary transmitter (PT) transmits information, from which the ST can decode PT's information. During the second phase, through helping the PT to deliver information, the ST is allowed to use the spectrum. Meanwhile, the ST can also transmit information to the SRs based on the principle of NOMA.

### 2.1.2 Wireless Energy Harvesting

Mobile devices are usually powered by batteries. In many scenarios, it is not convenient to re-charge a battery or to replace a battery.

To overcome the issues, energy harvesting is a viable technique. In energy harvesting, energy is scavenged from a wide variety of energy sources. Then the harvested energy is utilized for information transmission. In such a way, a sustainable utilization of energy is expected. Generally speaking, the energy sources fall into two categories, natural sources (such as wind, and solar power) and wireless RF sources [32–35].

We primarily focus on the wireless RF signal based energy harvesting. In specific, we further concentrate on SWIPT. In SWIPT, besides transmitting information, the wireless RF signal also acts another role of transferring energy. There are two types of protocols for the SWIPT system, which are power splitting (PS) and time switching (TS).

In the PS protocol, the received power from the wireless RF signal is separated into two different parts. One part of the power is directed into the energy harvester. The other part of the power is directed into the information decoder to recover information.

In the TS protocol, each time slot is partitioned into two portions. During the first portion of the slot, energy harvesting is carried out. During the rest portion of the slot, information is decoded from the received signal.

Compared with the natural energy sources based energy harvesting, wireless RF signal based energy harvesting has many superior advantages. Since we are surrounded by RF signals almost at anytime and anywhere, the availability of RF signal is always guaranteed, and not restricted by the environments. Moreover, the amount of harvested energy is also manageable, which can be adaptively controlled by adjusting the transmit power at the transmitter.

### 2.1.3 Multi-access Edge Computing

In future wireless networks, many advanced wireless services are expected to be supported [1], such as AR, virtual reality (VR), autonomous driving, and so on. However, these services usually require low latency and high energy consumption.

To effectively strengthen the energy efficiency and reduce the latency, MEC is deemed as one viable solution. The basic idea of MEC is to transfer the computation of information and some other related operations to the edge server in the network [36–39].

In a typical MEC system, one mobile user has a task consisting of certain amount of information bits to be computed. Basically, two types of offloading strategies can be adopted by the user, including fully offloading and partial offloading. To be specific, for the fully offloading strategy, all the information bits

are offloaded to the edge server. For the partial offloading strategy, the mobile user chooses to offload part of the information bits, and computes the rest by itself.

At the edge server, since it has a powerful computational capacity, the time used for computing the offloaded information bits will be very small, which indeed reduces the overall latency at the user side. Furthermore, after performing data offloading, the user's energy consumption on computation will also be effectively reduced.

As for the deployment of MEC, a technical white paper [40] has been proposed by ETSI (European Telecommunications Standards Institute). And the technical standards are being developed. The real deployment of MEC is still under development as well. ETSI has provided a Proofs of Concepts (PoC) Framework [41] to let third party get involved and propose a PoC, with the aim of validating the viability of MEC. For example, one project, named "Video Analytics", has been proposed to verify MEC by Nokia, Vodafone Hutchison Australia and SeeTec [42].

When NOMA is combined with MEC, it provides promising information transmission. The AR and VR based wireless applications involve intensive data computations at the user side, which can be considered as applications of NOMA MEC. For example, multiple AR or VR based users can offload their data to the edge servers for computation by using uplink NOMA. Compared with a system without MEC, the overall latency for data computation can be reduced when MEC offloading is conducted. Also, compared with traditional OMA transmission, a higher spectrum efficiency can be achieved in NOMA. More information can also be offloaded through NOMA transmission. Thus, NOMA MEC can reduce the latency for the wireless applications.

### 2.1.4 Application of Game Theory in Wireless Networks

The conventional resource allocation falls into the category of the centralized approach, in which all participants in the network follow a common rule. However, due to the inherent selfish nature of each user, following the same rule may not be applicable when each user has a different objective to optimize. Thus, to overcome this drawback, game theoretical approach is widely leveraged [43, 44]. There are many types of games in the literature, which include Stackelberg game, evolutionary game, coalitional game, potential game, and so on.

When game theory is applied in wireless networks, each transmitter or receiver in the network is treated as a player. Each player has its own utility function to maximize/minimize. The solution to a non-cooperative game is the so called nash equilibrium (NE) [43]. The NE solution is optimal in the sense that the user cannot achieve a better utility by adopting the unilateral deviation.

In game theoretical approach of resource allocation over wireless networks, users are allowed to make decisions for themselves. This is because by letting users involved in the decision making process, the system resources can be more efficiently utilized from the economic view.

## 2.2 Literature Review of NOMA

In the literature, there are extensive research efforts on NOMA-based wireless networks. Basically, we can group the relevant research into two major categories: performance analysis and optimal resource allocation. Under each category, various topics are considered, in which each topic covers one network scenario.

These topics include downlink NOMA, cooperative NOMA [1], cognitive NOMA [2], NOMA with energy harvesting, NOMA MEC and NOMA with other advanced topics. In other advanced topics, there are millimeter-wave (mmWave), Massive Multiple-Input Multiple-Output (MIMO), physical layer security, caching, and so on [12–14, 45].

### 2.2.1 Performance Analysis in NOMA-based Networks

#### 1) Downlink NOMA and Cooperative NOMA

The work in [46] investigates the performance of downlink NOMA system, by assuming that users have random spatial distribution. The works in [47–49] evaluate the performances for cooperative NOMA systems. A two-phase transmission is adopted in [47]. The BS transmits information signal to all downlink users during the first phase, which is followed by the information forwarding from the stronger user to other users during the second phase. In the systems of [48, 49], two destination nodes are served by one source node, which is aided by a group of relays. Different two-stage relay selection strategies are proposed, with the aim of achieving the optimal outage performances.

#### 2) NOMA with Energy Harvesting

In [50], downlink users are grouped into far users and near users based on users' distances from the BS. From the BS's signal, the near user harvests energy and decodes information first. Afterwards, according to the designed user pairing strategies, one near user helps to forward one far user's information by consuming the harvested energy. The work in [51] analyzes one cooperative NOMA

[1] For a better presentation, the topics of downlink NOMA and cooperative NOMA are combined together in Section 2.2.1 and Section 2.2.2.

[2] The literature review of cognitive NOMA will be provided at the beginning of Chapter 3, and thus it is not listed in this section.

system, in which one source node communicates with two users through the help of one energy harvesting relay. By employing different power allocation strategies at the relay, the system performance is studied. For the NOMA network with cooperation in [52], the near user is capable of energy harvesting and working on full-duplex mode. Then the outage performance is analyzed for such a system.

**3) NOMA MEC**

In the NOMA MEC scenario of [53], different schemes are designed to compare NOMA with OMA on the impacts of both delay and energy consumption. It is shown that the performances of NOMA transmissions outperform OMA transmissions. In the NOMA MEC network of [54], two uplink users are selected to perform data offloading based on the principle of NOMA, for which the probability of successful computation is evaluated. Based on the method of stochastic geometry, when multiple users conduct data offloading through uplink NOMA, the probability to offload data information is investigated in [55].

**4) NOMA with Other Advanced Topics**

In the mmWave system of [56], by adopting NOMA technique, strategies are designed to pair IoT users. Then the outage performances for users are provided. Through applying NOMA in Massive MIMO system, the outage performance is evaluated under designed precoding matrixes in [57]. The work in [58] studies a typical cooperative NOMA system consisting of one BS, two users and one relay, in which one eavesdropper intercepts the user's information. The secrecy outage probability is analyzed for the system. In [59], a NOMA caching system is modeled by using the Poisson cluster processes. Then based on the NOMA principle, the performances of different designed push and delivery strategies are evaluated.

### 2.2.2 Optimal Resource Allocation in NOMA-based Networks

#### 1) Downlink NOMA and Cooperative NOMA

The works in [60–64] study the optimal resource allocation for downlink NOMA systems. To guarantee the max-min and $\alpha$ fairness among users in terms of achievable rate and outage probability, the optimal strategies of power allocation are investigated in [60] and [61], respectively. To achieve the target outage probability for each user, the minimization of power consumption, which is based on the knowledge of average channel statistics, is studied in [62]. In [63], to achieve the Pareto optimality, the beamforming design, power allocation, user scheduling are optimized under a two-user system. The works in [65, 66] investigate the optimal resource allocation for cooperative NOMA systems. In [65], with the help of one decode-and-forward relay, two users' information is delivered. To achieve the target of maximizing the energy efficiency, optimization is conducted to allocate transmit powers at the source node and the relay. In the two-user downlink network of [66], the near user, who is able to work in either half-duplex or full-duplex mode, can help the far user to transmit information. The power allocation strategy to achieve the max-min fairness is optimized for such a system.

#### 2) NOMA with Energy Harvesting

The works in [67, 68] consider NOMA networks with wireless energy harvesting, in which two-phase transmissions are adopted. In [67], users harvest energy from the BS's signal in downlink first. Subsequently, users use the harvested energy to deliver their information back to the BS in uplink. To maximize different types of data rate, how to allocate time and design decoding order for SIC are studied. In [68], a dedicated power beacon is equipped to transfer energy to the

mobile users in one phase, which is followed by the information delivery to the BS in another phase. The spectrum and energy efficiencies are evaluated and compared for NOMA and TDMA transmissions. The work in [69] studies one heterogeneous network with NOMA, in which the BS is considered to be capable of energy harvesting. The energy efficiency is maximized by allocating the power resource and sub-channels.

**3) NOMA MEC**

Under the guaranteeing of one user's offloading data amount, the minimization of offloading delay of one opportunistic user is investigated for the NOMA MEC network in [70]. For such a system, the minimization of energy consumption is also studied in [71]. In [72], multiple single-antenna users offload information to one multi-antenna edge server through uplink NOMA. The resource allocation problem to minimize the energy expenditure is investigated. The work in [73] studies one NOMA MEC network, which is enhanced with the dual connectivity. With the aim of optimizing the energy in the network, the related data amount and time resources are allocated.

**4) NOMA with Other Advanced Topics**

In the mmWave NOMA system of [74], the problem of maximization of sum rate for users is studied by designing the strategies of user scheduling, power allocation and beamforming. The work in [75] investigates the downlink NOMA system, in which users' information is intercepted by one eavesdropper. The maximization of the secrecy sum rate is studied under the constraint of budgeted transmit power. The work in [76] studies the scenario that one full-duplex BS serves multiple downlink and uplink users at the same time, in which some users are untrusted. Then the maximization of sum throughput is investigated under

the guarantee of the secrecy performance. The work in [77] considers a two-user scenario with caching ability at each user. The decoding order and rate region are studied for such a system.

# Chapter 3

# Optimal Resource Allocation in Cognitive Non-orthogonal Multiple Access System with Energy Harvesting [1]

Since both CR and NOMA can promote spectrum efficiency, cognitive NOMA yields an even spectrum-efficient communications [18–20,80–84]. The CR inspired NOMA is conceptually introduced in [18], in which one PU and one SU are paired on one resource block to conduct NOMA transmission. The work in [80] extends the CR inspired NOMA concept to the scenario with multiple PUs and one single SU, in which the SU, having better channel gain than those of the PUs, is served together with all the PUs simultaneously by using NOMA. The transmission strategy of the multiple-antenna transmitter is designed such that the energy efficiency is maximized. By further extending CR inspired NOMA with multiple PUs and multiple SUs, the work in [81] proposes a distributed matching method, which pairs an SU with a PU and assigns transmit power levels for them, targeting system throughput maximization. In [19], underlaid with the primary network, the secondary network sets up an interference guard zone to limit the

[1] A version of this chapter has been published in IEEE Transactions on Vehicular Technology [78], and presented in part in the Proceedings of Vehicular Technology Conference [79].

primary interference, and transmits information from one ST to multiple SRs by employing NOMA. For secondary transmissions, the outage performance and diversity order are analyzed. A two-user underlay cognitive NOMA system is investigated in [82], in which a dedicated full-duplex relay is resorted to help a far user to forward information from the BS. The power allocation, beamformer design and the outage performance are investigated. The work in [20] considers an overlay cognitive NOMA system, in which the primary network has one PT and one PR, and the secondary network has one ST and one SR. The primary network is assisted by the secondary network that applies NOMA principe in its transmissions. The work in [83] considers an overlay cognitive NOMA system with a number of STs, in which one ST is scheduled to use NOMA to forward primary signals and send its own signals to its receivers. Two scheduling schemes, targeting reliability and fairness, respectively, are proposed. A survey of cognitive NOMA techniques and future research trends is given in [84].

Since SWIPT technique has the advantage of transferring energy and delivering information simultaneously, by integrating SWIPT into cognitive NOMA framework, a greener and more sustainable communication is expected. In the literature, some research efforts on SWIPT-based cognitive NOMA are conducted, such as [21, 22]. The work in [22] studies an underlay cognitive NOMA system, in which multiple STs harvest energy from one energy transmitter and transmit to one common BS by using NOMA. The secure energy efficiency maximization problem for secondary system is investigated. The work in [21] can be viewed as a CR inspired NOMA system enhanced with SWIPT. To serve a weak user, a strong user uses PS protocol to harvest energy from the transmitter's signals and decode its own and the weak user's information during the first phase. Afterwards, during the second phase, the strong user forwards the weak user's information.

With a condition that the reception quality of the weak user is satisfied, the strong user's throughput is maximized, by optimally designing the beamformers of the multiple-antenna transmitter and the PS ratio at the strong user.

In this chapter, we investigate an overlay cognitive NOMA scenario equipped with SWIPT, in which an ST uses TS protocol for energy harvesting and information decoding, and uses NOMA to help a PT and deliver its own information. The optimal solution, deriving the time ratio for energy harvesting as well as the NOMA power allocation of the ST, is provided. Our main contributions are summarized as follows.

1) A new SWIPT-enhanced cognitive NOMA framework: In the literature, SWIPT is integrated with underlay cognitive NOMA in [22], and with CR-inspired NOMA in [21]. However, SWIPT-enhanced overlay cognitive NOMA is not investigated in the literature, and its performance is unclear. To address this research gap, we investigate a SWIPT-enhanced overlay cognitive NOMA framework.

2) Optimal solution: The formulated problems are nonconvex, and are generally hard to solve. We devise a method to transform the formulated problems to equivalent problems under different cases. We theoretically prove that the objective functions of the equivalent problems are quasiconcave. We then develop an effective algorithm, by using a two-level bisection search, to find the optimal solution of each equivalent problem. We also develop a method that could reduce the number of iterations in the inner bisection search.

3) Interesting insights: Interestingly, different from existing NOMA works in which SIC is always applied, performing SIC in our work does not guarantee a better performance than the scenario without performing SIC. The insight behind this observation is also discussed.

The remainder of this chapter is organized as follows. In Section 3.1, our system model is described. The optimal solution to Problem P1 is presented in Section 3.2. Section 3.3 offer the optimal solutions to Problem P2. Section 3.4 shows the simulation results. In Section 3.5, we draw the conclusion of this chapter. In Table 3.1, we illustrate the used symbols.

## 3.1 System Model

We consider a cognitive system, consisting of one pair of PT and PR, and one pair of ST and SR, as depicted in Fig. 3.1. The spectrum is licensed to the primary system. The PT has a stable power supply, which transmits data with a fixed transmit power $P_p$. The ST is powered by harvested energy from RF signals transmitted by the PT. The ST opportunistically gains spectrum access opportunities in an overlay mode, i.e., when the link from the PT to the PR is not good enough, the ST could help forward the PT's signal and send its own signal to the SR as well by using NOMA.

The system is time slotted, and each time slot has a unit length. The channel coefficients between PT and PR, PT and SR, ST and PR, and ST and SR are denoted as $h_{pp}$, $h_{ps}$, $h_{sp}$, and $h_{ss}$, respectively. In subscript of the channel coefficients, the first symbol $p$ or $s$ means the primary or secondary transmitter, and the second symbol $p$ or $s$ means the primary or secondary receiver. In addition, the channel coefficient between PT and ST is denoted as $h_{tt}$. Accordingly, the channel gains (square of channel coefficient magnitude) of those channels are denoted as $g_{pp}$, $g_{ps}$, $g_{sp}$, $g_{ss}$, and $g_{tt}$, respectively. Block fading is assumed, which means that all the channel gains keep unchanged in each time slot and may change independently from slot to slot.

Basically, in a particular time slot, the system works in one of two transmission

| **Symbol** | **Meaning** |
|---|---|
| $x_p$ | The primary information signal |
| $x_s$ | The secondary information signal |
| $x_{st}$ | ST's transmit signal |
| $P_p$ | PT's transmit power |
| $R_{ss}$ | The secondary throughput for the scenario that the SR performs SIC |
| $R_{ss}^{w/o}$ | The secondary throughput for the scenario that the SR does not perform SIC |
| $h_{tt}, h_{pp}, h_{ps}, h_{sp}, h_{ss}$ | Channel coefficients between different transmitters and receivers |
| $g_{tt}, g_{pp}, g_{ps}, g_{sp}, g_{ss}$ | Channel gains between different transmitters and receivers |
| $\gamma^T$ | The target throughput of PT |
| $\alpha$ | The power ratio in NOMA transmission at the ST |
| $\rho$ | The time portion for energy harvesting at the ST |
| $E_0$ | The ST's battery's energy at the beginning of the slot |
| $E_h$ | The ST's battery's energy after energy harvesting |
| $E_c$ | The energy expenditure due to the circuit operation and channel estimation |
| $\eta$ | Energy conversion efficiency |
| $\sigma^2$ | The variance of the AWGN in our system |
| $P_e$ | The ST's transmit power |
| $\epsilon_t$ | The tolerance for the outer level bisection |
| $\epsilon_\rho$ | The tolerance for the inner level bisection |

Table 3.1: The notations used in Chapter 3

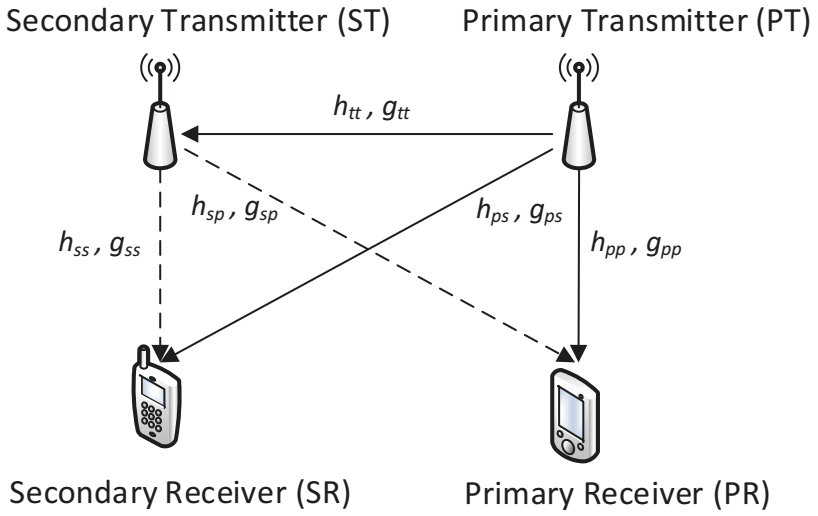


Figure 3.1: System model ('$h$' means channel coefficient, and '$g$' means channel gain).

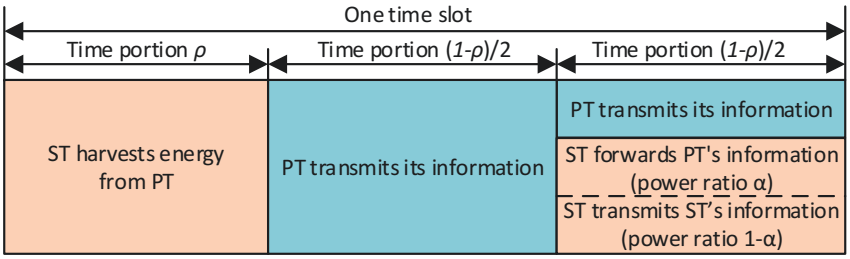


Figure 3.2: The slotted structure of the energy harvesting cognitive NOMA system.

modes:

- Direct primary transmission mode
- Cooperative transmission mode.

### 3.1.1 Direct Primary Transmission Mode

We assume that the PT and ST always have enough information to be transmitted to the PR and SR, respectively. The PT has a target throughput[2], denoted as

[2]In this chapter, "throughput" is defined as the amount of information bits that can be transmitted in a target slot.

$\gamma^T$, for each time slot. At a slot, the achievable throughput of the direct link from the PT to the PR is expressed as $\log(1 + \frac{P_p g_{pp}}{\sigma^2})$, where $\sigma^2$ is variance of the background AWGN.

If the achievable throughput is not less than the PT's target throughput $\gamma^T$ (which equivalently means that the channel gain of the direct primary link PT→PR satisfies $g_{pp} \geq (2^{\gamma^T} - 1)\sigma^2/P_p$), then the system works in *direct primary transmission mode*. In this mode, the PT transmits data to the PR during the whole slot, whereas the ST is not allowed to access the spectrum. Thus, the ST harvests energy during the whole slot, which yields the battery energy at the end of the slot as $\max\{E_0 + \eta P_p g_{tt} - E_c, 0\}$,[3] where $E_0$ is the ST's battery energy at the beginning of the slot, $\eta \in (0, 1)$ is the energy conversion efficiency, and $E_c$ means the energy expenditure in a time slot due to circuit operation and channel estimation.

### 3.1.2 Cooperative Transmission Mode

If the achievable throughput $\log(1 + \frac{P_p g_{pp}}{\sigma^2})$ of the direct primary link PT→PR is lower than the PT's target throughput $\gamma^T$ (which equivalently means that $g_{pp} < (2^{\gamma^T} - 1)\sigma^2/P_p$), the ST is requested to help to forward the PT's message to PR by using decode-and-forward (DF) relaying. The ST can simultaneously send its own message to the SR based on downlink NOMA. In other words, the system works in the *cooperative transmission mode*.

In this mode, the slot is partitioned into three phases, as shown in Fig. 3.2. The first phase has length $\rho \in [0, 1]$, while the second and third phases both have length $(1 - \rho)/2$, where the value of $\rho$ is a designed parameter, to be optimized hereafter.

[3]This amount of energy is also the battery energy at the beginning of the next slot.

**1) The First Phase**

During the first phase, the PT transmits wireless RF signals with power $P_p$, from which the ST harvests energy.[4] Then the ST's battery energy, after harvesting, has the form of $E_h = E_0 + \eta\rho P_p g_{tt}$. If $E_h$ is less than $E_c$, then the ST is not able to help the PT, and thus, the system has to work in the direct primary transmission mode. Therefore, for the system to work in the cooperative transmission mode, we should have $E_h \geq E_c$, which leads to $\rho \geq \max\{\frac{E_c - E_0}{\eta P_p g_{tt}}, 0\}$.

**2) The Second Phase**

During the second phase, the PT transmits its information signal $x_p$ with power $P_p$, which is received by the PR and ST, as well as the SR.

At the PR, the received signal in the second phase of the slot is represented by $\sqrt{P_p}h_{pp}x_p + n_{pr}$, in which $n_{pr}$ is the AWGN at the PR.

The received signal at the ST in the second phase of the slot is written as $\sqrt{P_p}h_{tt}x_p + n_{st}$, in which $n_{st}$ is the AWGN at the ST. The achievable information rate for the transmission from the PT to the ST in the second phase of the slot is expressed as $R_{tt} = \frac{1-\rho}{2}\log(1 + \frac{P_p g_{tt}}{\sigma^2})$. As the ST needs to decode the PT's signal, the achievable information rate $R_{tt}$ should be not less than the target throughput $\gamma^T$ of the primary system. Thus, we should have constraint $R_{tt} \geq \gamma^T$, based on which we have constraint $\rho \in \mathcal{A}_1 \triangleq \left[\max\{\frac{E_c - E_0}{\eta P_p g_{tt}}, 0\}, 1 - \frac{2\gamma^T}{\log(1+\frac{P_p g_{tt}}{\sigma^2})}\right]$.

At the SR, the received signal in the second phase of the slot is represented by $\sqrt{P_p}h_{ps}x_p + n_{sr}$, in which $n_{sr}$ is the AWGN at the SR.

[4]Note that in the first phase, the wireless RF signals can actually be information signals of the PT for the PR. In other words, in the first phase, from the PT's signals, the ST tries to harvest energy while the PR tries to decode information. This portion of information for the PR will be investigated in Section 3.2.6.

### 3) The Third Phase

During the third phase, the PT transmits a copy of the primary signal $x_p$ with power $P_p$. The ST applies downlink NOMA to transmit a superimposed signal consisting of the PT's signal $x_p$ and the ST's own signal $x_s$, by using the harvested energy in a greedy manner, i.e., it uses up all the available energy stored in battery in this phase.[5] In specific, the ST transmits $x_{st} = \sqrt{\alpha P_e}x_p + \sqrt{(1-\alpha)P_e}x_s$, where $\alpha$, a parameter to be optimized, is the power ratio for $x_p$, $(1-\alpha)$ is the power ratio for $x_s$, and $P_e$ is the transmit power of ST, shown as

$$P_e = \frac{2(E_h - E_c)}{1-\rho} = \frac{2(\eta\rho P_p g_{tt} + E_0 - E_c)}{1-\rho}. \tag{3.1}$$

Accordingly, the received signal at the PR in the third phase is $\sqrt{P_p}h_{pp}x_p + h_{sp}x_{st} + n_{pr}$. As the PR receives the PT's signal $x_p$ in the second phase (from the PT) and the third phase (from the PT and ST), the PR employs maximal ratio combining (MRC) to combine the received PT's signal portions, which yields the overall throughput of the PT's signal $x_p$ (also called the throughput of the primary system) in the time slot as

$$R_{pp} = \frac{1-\rho}{2}\log\left(1 + \frac{P_p g_{pp}}{\sigma^2} + \frac{P_p g_{pp} + \alpha P_e g_{sp}}{(1-\alpha)P_e g_{sp} + \sigma^2}\right). \tag{3.2}$$

In the third phase, the received signal at the SR is $y_{ss} = \sqrt{P_p}h_{ps}x_p + h_{ss}x_{st} + n_{sr}$. In the received signal $y_{ss}$, the PT's signal portion $x_p$ is interference to the SR's own signal $x_s$. Thus, similar to NOMA works in the literature, the SR can use SIC, i.e., it first decodes the PT's signal $x_p$, removes $x_p$ from $y_{ss}$, and then decodes its own signal $x_s$.

[5]Note that our method can be straightforwardly extended to the case when there exists a limit for the energy level that the ST can use in the third phase of the slot (i.e., there is some energy left at the end of the slot).

When the SR decodes the PT's signal portion $x_p$, the achievable information rate is given as

$$R_{ps} = \frac{1-\rho}{2} \log \left( 1 + \frac{P_p g_{ps}}{\sigma^2} + \frac{P_p g_{ps} + \alpha P_e g_{ss}}{(1-\alpha) P_e g_{ss} + \sigma^2} \right), \tag{3.3}$$

where MRC is used to combine the received PT's signal portions in the second and third phases. When performing SIC at the SR, $\rho$ and $\alpha$ should be set up such that $R_{ps} \geq \gamma^T$, which means that the SR can successfully decode $x_p$, and perform SIC to remove $x_p$ in $y_{ss}$. Subsequently, the achievable throughput of the secondary signal $x_s$ (also called the secondary system's throughput) can be written as

$$R_{ss} = \frac{1-\rho}{2} \log \left( 1 + \frac{(1-\alpha) P_e g_{ss}}{\sigma^2} \right). \tag{3.4}$$

Our objective is to maximize the secondary system's throughput while guaranteeing that the throughput of the primary system is not smaller than $\gamma^T$. Thus we formulate the following optimization problem.

**Problem P1:**

$$\max_{\alpha,\rho} \quad R_{ss} = \frac{1-\rho}{2} \log \left( 1 + \frac{(1-\alpha) P_e g_{ss}}{\sigma^2} \right) \tag{3.5a}$$

$$\text{s.t.} \quad \rho \in \mathcal{A}_1; \tag{3.5b}$$

$$\min\{R_{pp}, R_{ps}\} \geq \gamma^T; \tag{3.5c}$$

$$0 \leq \alpha \leq 1. \tag{3.5d}$$

In Problem P1, to perform SIC at the SR, we have constraint $R_{ps} \geq \gamma^T$. If the SR does not perform SIC, interference from the PT's signal is not cancelled, which harms the secondary throughput. On the other hand, if the SR does not perform SIC, the constraint $R_{ps} \geq \gamma^T$ can be removed, and we can have a larger feasible region of $\alpha$ and $\rho$, which benefits the secondary throughput. It is not clear whether the overall effect of not performing SIC is beneficial or harmful.

Thus, we should also investigate an optimization problem, in which the SR does not perform SIC.

When the SR does not perform SIC, the achievable throughput of the secondary system is

$$R_{ss}^{w/o} = \frac{1-\rho}{2} \log \left( 1 + \frac{(1-\alpha) P_e g_{ss}}{\alpha P_e g_{ss} + P_p g_{ps} + \sigma^2} \right), \tag{3.6}$$

in which superscript $(\cdot)^{w/o}$ stands for "without performing SIC." Accordingly, the following optimization problem can be formulated.

**Problem P2:**

$$\max_{\alpha,\rho} \quad R_{ss}^{w/o} = \frac{1-\rho}{2} \log \left( 1 + \frac{(1-\alpha) P_e g_{ss}}{\alpha P_e g_{ss} + P_p g_{ps} + \sigma^2} \right) \tag{3.7a}$$

$$\text{s.t.} \quad \rho \in \mathcal{A}_1; \tag{3.7b}$$

$$R_{pp} \geq \gamma^T; \tag{3.7c}$$

$$0 \leq \alpha \leq 1. \tag{3.7d}$$

As a summary, the optimal solution of the system is the better one between the optimal solutions of Problems P1 and P2, which has larger secondary throughput.[6]

## 3.2 Optimal Solution of Problem P1

Problem P1 is non-convex since the objective and the constraint functions are not jointly concave. Generally, it is hard to solve such a problem. In this work, we provide an efficient method to solve our Problem P1.

By careful inspection, there exists the following useful lemma.

[6]If both Problems P1 and P2 are infeasible, which means the cooperative transmission mode cannot make the throughput of the primary system be at least $\gamma^T$, then the system will work in direct primary transmission mode.

**Lemma 1.** *When the optimality of Problem P1 is achieved, constraint* $\min\{R_{pp}, R_{ps}\} \geq \gamma^T$ *should be active, i.e., we should have* $\min\{R_{pp}, R_{ps}\} = \gamma^T$.

*Proof.* We use proof by contradiction. Suppose that when the optimality of Problem P1 is achieved, we have $\min\{R_{pp}, R_{ps}\} > \gamma^T$.

From (3.2) and (3.3), we know that $R_{pp}$ and $R_{ps}$ both are increasing functions of $\alpha$. Furthermore, when $\alpha = 0$, we have $\min\{R_{pp}, R_{ps}\}|_{\alpha=0} \leq R_{pp}|_{\alpha=0} = \frac{1-\rho}{2}\log\left(1 + \frac{P_p g_{pp}}{\sigma^2} + \frac{P_p g_{pp}}{P_e g_{sp}+\sigma^2}\right) < \gamma^T$, in which the last inequality comes from the fact that

$$\begin{aligned} &\frac{1-\rho}{2}\log\left(1 + \frac{P_p g_{pp}}{\sigma^2} + \frac{P_p g_{pp}}{P_e g_{sp} + \sigma^2}\right) \\ &\leq \frac{1-\rho}{2}\log(1 + \frac{2P_p g_{pp}}{\sigma^2}) \\ &\leq \frac{1}{2}\log(1 + \frac{P_p g_{pp}}{\sigma^2})^2 \\ &= \log\left(1 + \frac{P_p g_{pp}}{\sigma^2}\right) < \gamma^T. \end{aligned} \tag{3.8}$$

In (3.8), the last inequality comes from the fact that the system works in the cooperative transmission mode when the achievable throughput $\log(1 + \frac{P_p g_{pp}}{\sigma^2})$ of the direct primary link from the PT to the PR is less than the PT's target throughput $\gamma^T$.

Thus, from the optimality point of Problem P1, we can decrease the value of $\alpha$ such that we still have $\min\{R_{pp}, R_{ps}\} \geq \gamma^T$ but we have a larger objective function $R_{ss}$ (noting that $R_{ss}$ is a decreasing function of $\alpha$ according to (3.4)). This is a contradiction.

This completes the proof. □

Lemma 1 indicates that, at optimality of Problem P1, either $R_{pp}$ or $R_{ps}$ should be equal to $\gamma^T$.

If $R_{pp} = \gamma^T$, then from (3.2), we can see that $\alpha$ can be expressed by a function

of $\rho$ as

$$\alpha = F_p(\rho) \triangleq \frac{\mu_p(P_e g_{sp} + \sigma^2) - P_p g_{pp}}{(\mu_p + 1) P_e g_{sp}} \tag{3.9}$$

with

$$\mu_p \triangleq 2^{\frac{2\gamma^T}{1-\rho}} - \frac{P_p g_{pp}}{\sigma^2} - 1. \tag{3.10}$$

Note that by using (3.8), we can see $\mu_p > 0$.

When $\alpha$ is expressed as a function of $\rho$ as in (3.9), the constraint $0 \leq \alpha \leq 1$ should be satisfied. Note that $\alpha > 0$ is satisfied automatically, since from (3.8), we have $\frac{1-\rho}{2}\log(1 + \frac{2P_p g_{pp}}{\sigma^2}) < \gamma^T$, based on which we have $\mu_p \sigma^2 - P_p g_{pp} > 0$, yielding $\alpha > 0$. Thus, only $\alpha \leq 1$ is considered here, which is equivalent to

$$\rho \in \mathcal{A}_2 \triangleq \left\{\rho | \rho \geq 0 \text{ and } P_e g_{sp} - \mu_p \sigma^2 + P_p g_{pp} \geq 0\right\}. \tag{3.11}$$

**Lemma 2.** *Set $\mathcal{A}_2$ is a closed interval of $\rho$, with closed-form starting and ending points.*

*Proof.* See Appendix 3.6.1. □

If $R_{ps} = \gamma^T$, then from (3.3), we can see that $\alpha$ can be expressed as a function of $\rho$, as

$$\alpha = F_s(\rho) \triangleq \frac{\mu_s(P_e g_{ss} + \sigma^2) - P_p g_{ps}}{(\mu_s + 1) P_e g_{ss}} \tag{3.12}$$

with $\mu_s \triangleq 2^{\frac{2\gamma^T}{1-\rho}} - \frac{P_p g_{ps}}{\sigma^2} - 1$.

When $\alpha$ is expressed as a function of $\rho$ as in (3.12), the constraint $0 \leq \alpha \leq 1$ is equivalent to

$$\rho \in \mathcal{A}_3 \triangleq \left\{\rho | \rho \geq 0 \text{ and } \mu_s(P_e g_{ss} + \sigma^2) - P_p g_{ps} \geq 0\right\} \cap \left\{\rho | \rho \geq 0 \text{ and } P_e g_{ss} - \mu_s \sigma^2 + P_p g_{ps} \geq 0\right\}. \tag{3.13}$$

In $\mathcal{A}_3$, set $\{\rho | \rho \geq 0 \text{ and } \mu_s(P_e g_{ss} + \sigma^2) - P_p g_{ps} \geq 0\}$ comes from $\alpha \geq 0$, which is a closed interval, since $\mu_s(P_e g_{ss} + \sigma^2) - P_p g_{ps}$ is an increasing function of $\rho$. Similar

to set $\mathcal{A}_2$, set $\{\rho|\rho \geq 0 \text{ and } P_e g_{ss} - \mu_s \sigma^2 + P_p g_{ps} \geq 0\}$ is also a closed interval. Thus, $\mathcal{A}_3$ is a closed interval.

Afterwards, by comparing (3.2) and (3.3), we have the following four cases for Problem P1.

### 3.2.1 Case 1: When $g_{pp} \leq g_{ps}$ and $g_{sp} \leq g_{ss}$

For a specific value of $\rho$, $R_{pp}$ in (3.2) and $R_{ps}$ in (3.3) can be viewed as functions of $\alpha$.

**1) Intersections of Curves $R_{pp}$ vs. $\alpha$ and $R_{ps}$ vs. $\alpha$ over $\alpha \in [0,1]$**

By considering two curves: $R_{pp}$ vs. $\alpha$ and $R_{ps}$ vs. $\alpha$ over $\alpha \in [0,1]$, we have the following lemma.

**Lemma 3.** *For a specific value of $\rho$, the two curves $R_{pp}$ vs. $\alpha$ and $R_{ps}$ vs. $\alpha$ over $\alpha \in [0,1]$ have up to two intersections.*

*Proof.* For a given $\rho$, from (3.2) and (3.3), if we set $R_{pp} = R_{ps}$, we can obtain

$$L_1 P_e^2 (1-\alpha)^2 + \left[ L_1 (\frac{\sigma^2}{g_{ss}} + \frac{\sigma^2}{g_{sp}}) + \frac{\frac{P_p g_{ps}}{g_{ss}} - \frac{P_p g_{pp}}{g_{sp}}}{\frac{\sigma^2}{g_{ss}} - \frac{\sigma^2}{g_{sp}}} + 1 \right] P_e (1-\alpha) + 2L_1 \frac{\sigma^4}{g_{ss} g_{sp}} - P_e = 0, \tag{3.14}$$

where $L_1 = \frac{\frac{P_p g_{ps}}{\sigma^2} - \frac{P_p g_{pp}}{\sigma^2}}{\frac{\sigma^2}{g_{ss}} - \frac{\sigma^2}{g_{sp}}} < 0$. Considering the left hand-side of (3.14) as a function of $\alpha$, the two roots of (3.14) are

$$\text{ROOT}_1 = 1 - \frac{-L_2 + \sqrt{L_2^2 - 4L_1 L_3}}{2L_1 P_e}, \tag{3.15}$$

$$\text{ROOT}_2 = 1 - \frac{-L_2 - \sqrt{L_2^2 - 4L_1 L_3}}{2L_1 P_e}, \tag{3.16}$$

in which $L_2 = L_1 (\frac{\sigma^2}{g_{ss}} + \frac{\sigma^2}{g_{sp}}) + \frac{\frac{P_p g_{ps}}{g_{ss}} - \frac{P_p g_{pp}}{g_{sp}}}{\frac{\sigma^2}{g_{ss}} - \frac{\sigma^2}{g_{sp}}} + 1$ and $L_3 = 2L_1 \frac{\sigma^4}{g_{ss} g_{sp}} - P_e < 0$. Note that when $L_2 < 0$, both $\text{ROOT}_1$ and $\text{ROOT}_2$ are larger than 1 and infeasible.

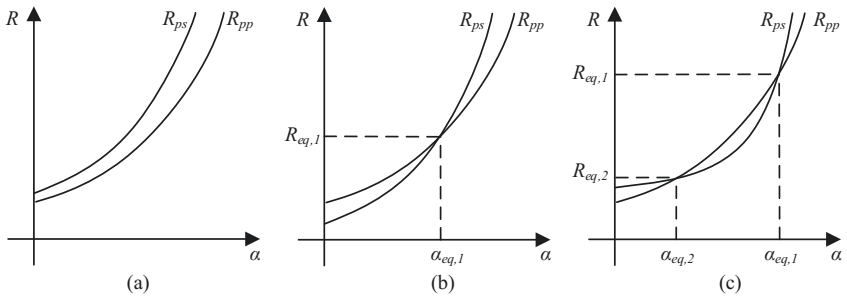


Figure 3.3: An illustration of two curves $R_{pp}$ vs. $\alpha$ and $R_{ps}$ vs. $\alpha$ (for a specific $\rho$) in Case 1, in which two curves have up to two intersections.

To make $\mathrm{ROOT}_1$ shown in (3.15) feasible, we should have $0 \leq \mathrm{ROOT}_1 \leq 1$, which equivalently means that $\rho \in \mathcal{A}_4 \triangleq \{\rho | 0 \leq \rho \leq 1, L_2 \geq 0, L_2^2 - 4L_1L_3 \geq 0, 2L_1P_e + L_2 - \sqrt{L_2^2 - 4L_1L_3} \leq 0\}$.[7] The set $\mathcal{A}_4$ is a closed interval of $\rho$.

To make $\mathrm{ROOT}_2$ shown in (3.16) feasible, we should have $0 \leq \mathrm{ROOT}_2 \leq 1$, which equivalently means $\rho \in \mathcal{A}_5 \triangleq \{\rho | 0 \leq \rho \leq 1, L_2 \geq 0, L_2^2 - 4L_1L_3 \geq 0, 2L_1P_e + L_2 + \sqrt{L_2^2 - 4L_1L_3} \leq 0\}$. The set $\mathcal{A}_5$ is an interval of $\rho$, and is a subset of $\mathcal{A}_4$.

Overall, for any specific $\rho$, if $\rho \in \bar{\mathcal{A}}_4 \triangleq [0,\ 1] \backslash \mathcal{A}_4$, then the two curves $R_{pp}$ vs. $\alpha$ and $R_{ps}$ vs. $\alpha$ do not have intersection; if $\rho \in \mathcal{A}_4 \backslash \mathcal{A}_5$, then the two curves have one intersection denoted as $(\alpha_{eq,1}, R_{eq,1})$, with $\alpha_{eq,1} = \mathrm{ROOT}_1$; if $\rho \in \mathcal{A}_5$, then the two curves have two intersections denoted as $(\alpha_{eq,1}, R_{eq,1})$ and $(\alpha_{eq,2}, R_{eq,2})$, with $\alpha_{eq,1} = \mathrm{ROOT}_1$ and $\alpha_{eq,2} = \mathrm{ROOT}_2$. An illustration is given in Fig. 3.3.

This completes the proof. □

Below we show some features of $R_{eq,1}$ and $R_{eq,2}$.

[7] $L_2$ is not a function of $\rho$. By including "$L_2 \geq 0$" in the expression of $\mathcal{A}_4$, we mean that $\mathcal{A}_4$ will be a null set if $L_2 < 0$.

$R_{eq,1}$ is expressed as

$$R_{eq,1} = R_{pp}|_{\alpha=\mathrm{ROOT}_1} = \frac{1-\rho}{2}\log\Bigg[1 + \frac{P_p g_{pp}}{\sigma^2} + \frac{P_p\frac{g_{ps}}{g_{ss}} - P_p\frac{g_{pp}}{g_{sp}}}{\frac{\sigma^2}{g_{ss}} - \frac{\sigma^2}{g_{sp}}} + L_1\bigg(\frac{-L_2 + \sqrt{L_2^2 - 4L_1L_3}}{2L_1} + \frac{\sigma^2}{g_{ss}}\bigg)\Bigg]. \quad (3.17)$$

The second order derivative of $R_{eq,1}$ is given by

$$\frac{\mathrm{d}^2 R_{eq,1}}{\mathrm{d}\rho^2} = \frac{1}{(\ln 2)H_1(\rho)}\frac{L_1}{\sqrt{L_2^2 - 4L_1L_3}}\Big(\frac{1-\rho}{2}\frac{\mathrm{d}^2P_e}{\mathrm{d}\rho^2} - \frac{\mathrm{d}P_e}{\mathrm{d}\rho}\Big) - \frac{1-\rho}{2(\ln 2)\big(H_1(\rho)\big)^2}\frac{L_1^2}{L_2^2 - 4L_1L_3}(\frac{\mathrm{d}P_e}{\mathrm{d}\rho})^2 - \frac{1-\rho}{(\ln 2)H_1(\rho)}\frac{L_1^2}{\big(L_2^2 - 4L_1L_3\big)^{\frac{3}{2}}}(\frac{\mathrm{d}P_e}{\mathrm{d}\rho})^2, \quad (3.18)$$

where $H_1(\rho) = 1 + \frac{P_p g_{pp}}{\sigma^2} + \frac{P_p\frac{g_{ps}}{g_{ss}} - P_p\frac{g_{pp}}{g_{sp}}}{\frac{\sigma^2}{g_{ss}} - \frac{\sigma^2}{g_{sp}}} + L_1\big(\frac{-L_2+\sqrt{L_2^2-4L_1L_3}}{2L_1} + \frac{\sigma^2}{g_{ss}}\big)$, and

$$\begin{cases} \frac{\mathrm{d}P_e}{\mathrm{d}\rho} &= \frac{2(\eta P_p g_{tt} + E_0 - E_c)}{(1-\rho)^2}, \\ \frac{\mathrm{d}^2P_e}{\mathrm{d}\rho^2} &= \frac{4(\eta P_p g_{tt} + E_0 - E_c)}{(1-\rho)^3}. \end{cases} \quad (3.19)$$

From (3.18), since $\frac{1-\rho}{2}\frac{\mathrm{d}^2P_e}{\mathrm{d}\rho^2} - \frac{\mathrm{d}P_e}{\mathrm{d}\rho} = 0$, $\frac{\mathrm{d}^2P_e}{\mathrm{d}\rho^2} > 0$ and $\frac{\mathrm{d}P_e}{\mathrm{d}\rho} > 0$, one can obtain that $\frac{\mathrm{d}^2R_{eq,1}}{\mathrm{d}\rho^2} < 0$, which indicates that $R_{eq,1}$ is a concave function of $\rho$.

$R_{eq,2}$ is expressed as

$$R_{eq,2} = R_{pp}|_{\alpha=\mathrm{ROOT}_2} = \frac{1-\rho}{2}\log\Bigg[1 + \frac{P_p g_{pp}}{\sigma^2} + \frac{P_p\frac{g_{ps}}{g_{ss}} - P_p\frac{g_{pp}}{g_{sp}}}{\frac{\sigma^2}{g_{ss}} - \frac{\sigma^2}{g_{sp}}} + L_1\bigg(\frac{-L_2 - \sqrt{L_2^2 - 4L_1L_3}}{2L_1} + \frac{\sigma^2}{g_{ss}}\bigg)\Bigg]. \quad (3.20)$$

The second order derivative of $R_{eq,2}$ is given by

$$\frac{\mathrm{d}^2 R_{eq,2}}{\mathrm{d}\rho^2} = \frac{-1}{(\ln 2)H_2(\rho)}\frac{L_1}{\sqrt{L_2^2 - 4L_1L_3}}\Big(\frac{1-\rho}{2}\frac{\mathrm{d}^2P_e}{\mathrm{d}\rho^2} - \frac{\mathrm{d}P_e}{\mathrm{d}\rho}\Big) - \frac{1-\rho}{2(\ln 2)\big(H_2(\rho)\big)^2}\frac{L_1^2}{L_2^2 - 4L_1L_3}(\frac{\mathrm{d}P_e}{\mathrm{d}\rho})^2 + \frac{1-\rho}{(\ln 2)H_2(\rho)}\frac{L_1^2}{\big(L_2^2 - 4L_1L_3\big)^{\frac{3}{2}}}(\frac{\mathrm{d}P_e}{\mathrm{d}\rho})^2, \quad (3.21)$$

where $H_2(\rho) = 1 + \frac{P_p g_{pp}}{\sigma^2} + \frac{P_p\frac{g_{ps}}{g_{ss}} - P_p\frac{g_{pp}}{g_{sp}}}{\frac{\sigma^2}{g_{ss}} - \frac{\sigma^2}{g_{sp}}} + L_1\big(\frac{-L_2-\sqrt{L_2^2-4L_1L_3}}{2L_1} + \frac{\sigma^2}{g_{ss}}\big)$.

Recall that intersection $(\alpha_{eq,2}, R_{eq,2})$ exists only when $\rho \in \mathcal{A}_5$. By observing (3.21), it can be seen that 1) when $\rho \in \mathcal{A}_6 \triangleq \mathcal{A}_5 \cap \{\rho | H_2(\rho) - \frac{1}{2}\sqrt{L_2^2 - 4L_1L_3} \geq 0\}$, we have $\frac{\mathrm{d}^2 R_{eq,2}}{\mathrm{d}\rho^2} \geq 0$, which indicates that $R_{eq,2}$ is a convex function of $\rho$ over $\mathcal{A}_6$; 2) when $\rho \in \mathcal{A}_7 \triangleq \mathcal{A}_5 \cap \{\rho | H_2(\rho) - \frac{1}{2}\sqrt{L_2^2 - 4L_1L_3} < 0\}$, we have $\frac{\mathrm{d}^2 R_{eq,2}}{\mathrm{d}\rho^2} < 0$, which indicates that $R_{eq,2}$ is a concave function of $\rho$ over $\mathcal{A}_7$. Note that $\mathcal{A}_6$ and $\mathcal{A}_7$ both are closed intervals of $\rho$.

**2) Problem P1 with Case 1**

From Lemma 3, when $\rho \in \bar{\mathcal{A}}_4$, the two curves $R_{pp}$ vs. $\alpha$ and $R_{ps}$ vs. $\alpha$ do not have intersection, which means that we always have $R_{pp} < R_{ps}$, as shown in Fig. 3.3(a). Thus, at optimality of Problem P1, we should have $R_{pp} = \gamma^T$. Then Problem P1 is equivalent to

$$\max_{\rho} \quad R_{ss}|_{\alpha=F_p(\rho)} \tag{3.22a}$$

$$\text{s.t.} \quad \rho \in \mathcal{A}_1 \cap \mathcal{A}_2 \cap \bar{\mathcal{A}}_4, \tag{3.22b}$$

with $R_{ss}|_{\alpha=F_p(\rho)} = \frac{1-\rho}{2}\log\left(1 + \frac{(P_e g_{sp} - \mu_p\sigma^2 + P_p g_{pp})g_{ss}}{(\mu_p+1)g_{sp}\sigma^2}\right)$.

When $\rho \in \mathcal{A}_4 \backslash \mathcal{A}_5$, the two curves have one intersection at $(\alpha_{eq,1}, R_{eq,1})$. It is interesting to point out that we further have two scenarios, as follows.

- If $R_{eq,1} \geq \gamma^T$, then at optimality of Problem P1 (i.e., when $\min\{R_{pp}, R_{ps}\} = \gamma^T$), we have $R_{ps} \leq R_{pp}$, and thus, we have $R_{ps} = \gamma^T$ at optimality of Problem P1. Accordingly, Problem P1 is equivalent to

$$\max_{\rho} \quad R_{ss}|_{\alpha=F_s(\rho)} \tag{3.23a}$$

$$\text{s.t.} \quad \rho \in \mathcal{A}_1 \cap \mathcal{A}_3 \cap [(\mathcal{A}_4 \backslash \mathcal{A}_5) \cap \mathcal{A}_8] \tag{3.23b}$$

  in which $R_{ss}|_{\alpha=F_s(\rho)} = \frac{1-\rho}{2}\log\left(1 + \frac{P_e g_{ss} - \mu_s\sigma^2 + P_p g_{ps}}{(\mu_s+1)\sigma^2}\right)$ and $\mathcal{A}_8 \triangleq \{\rho | R_{eq,1} \geq \gamma^T\}$. As aforementioned, $R_{eq,1}$ is a concave function of $\rho$. Thus, $\mathcal{A}_8$ is a closed interval of $\rho$.

- If $R_{eq,1} \leq \gamma^T$, then at optimality of Problem P1 (i.e., when $\min\{R_{pp}, R_{ps}\} = \gamma^T$), we have $R_{pp} \leq R_{ps}$, and thus, we have $R_{pp} = \gamma^T$ at optimality of Problem P1. Accordingly, Problem P1 is equivalent to

$$\max_{\rho} \quad R_{ss}|_{\alpha=F_p(\rho)} \tag{3.24a}$$

$$\text{s.t.} \quad \rho \in \mathcal{A}_1 \cap \mathcal{A}_2 \cap [(\mathcal{A}_4 \backslash \mathcal{A}_5) \cap \bar{\mathcal{A}}_8] \tag{3.24b}$$

  in which $\bar{\mathcal{A}}_8 = [0,\ 1] \backslash \mathcal{A}_8$. As $\mathcal{A}_8$ is a closed interval, $\bar{\mathcal{A}}_8$ is the union of two closed intervals.

When $\rho \in \mathcal{A}_5$, the two curves have two intersections at $(\alpha_{eq,1}, R_{eq,1})$ and $(\alpha_{eq,2}, R_{eq,2})$. It is also interesting to point out that we further have two scenarios, as follows.

- If $R_{eq,1} \leq \gamma^T$ or $R_{eq,2} \geq \gamma^T$, then at optimality of Problem P1 (i.e., when $\min\{R_{pp}, R_{ps}\} = \gamma^T$), we have $R_{pp} \leq R_{ps}$, and thus, we have $R_{pp} = \gamma^T$ at optimality of Problem P1. Accordingly, Problem P1 is equivalent to

$$\max_{\rho} \quad R_{ss}|_{\alpha=F_p(\rho)} \tag{3.25a}$$

$$\text{s.t.} \quad \rho \in \mathcal{A}_1 \cap \mathcal{A}_2 \cap \mathcal{A}_5 \cap [\bar{\mathcal{A}}_8 \cup \mathcal{A}_9] \tag{3.25b}$$

  in which $\mathcal{A}_9 = \{\rho | R_{eq,2} \geq \gamma^T \text{ and } \rho \in \mathcal{A}_6\} \cup \{\rho | R_{eq,2} \geq \gamma^T \text{ and } \rho \in \mathcal{A}_7\}$. As $R_{eq,2}$ is convex over $\mathcal{A}_6$ and concave over $\mathcal{A}_7$, $\mathcal{A}_9$ is the union of three closed intervals.

- If $R_{eq,1} \geq \gamma^T$ and $R_{eq,2} \leq \gamma^T$, then at optimality of Problem P1 (i.e., when $\min\{R_{pp}, R_{ps}\} = \gamma^T$), we have $R_{ps} \leq R_{pp}$, and thus, we have $R_{ps} = \gamma^T$ at optimality of Problem P1. Accordingly, Problem P1 is equivalent to

$$\max_{\rho} \quad R_{ss}|_{\alpha=F_s(\rho)} \tag{3.26a}$$

$$\text{s.t.} \quad \rho \in \mathcal{A}_1 \cap \mathcal{A}_3 \cap \mathcal{A}_5 \cap \mathcal{A}_8 \cap \bar{\mathcal{A}}_9 \tag{3.26b}$$

in which $\bar{\mathcal{A}}_9 = \{\rho | R_{eq,2} \leq \gamma^T \text{ and } \rho \in \mathcal{A}_6\} \cup \{\rho | R_{eq,2} \leq \gamma^T \text{ and } \rho \in \mathcal{A}_7\}$, being the union of three closed intervals.

As a summary, for Case 1, the maximal objective function of Problem P1 is the largest one among the maximal objective functions of Problem (3.22), Problem (3.23), Problem (3.24), Problem (3.25) and Problem (3.26).

### 3.2.2 Case 2: When $g_{pp} > g_{ps}$ and $g_{sp} > g_{ss}$

Similar to Lemma 3, when $\rho \in \bar{\mathcal{A}}_4$, the two curves do not have intersection, which means that we always have $R_{ps} \leq R_{pp}$. Thus, at optimality of Problem P1, we should have $R_{ps} = \gamma^T$. Then Problem P1 is equivalent to

$$\max_{\rho} \quad R_{ss}|_{\alpha=F_s(\rho)} \tag{3.27a}$$

$$\text{s.t.} \quad \rho \in \mathcal{A}_1 \cap \mathcal{A}_3 \cap \bar{\mathcal{A}}_4. \tag{3.27b}$$

When $\rho \in \mathcal{A}_4 \backslash \mathcal{A}_5$, the two curves have one intersection at $(\alpha_{eq,1}, R_{eq,1})$. We further have two scenarios, as follows.

- If $R_{eq,1} \geq \gamma^T$, then at optimality of Problem P1 (i.e., when $\min\{R_{pp}, R_{ps}\} = \gamma^T$), we have $R_{pp} \leq R_{ps}$, and thus, we have $R_{pp} = \gamma^T$ at optimality of Problem P1. Accordingly, Problem P1 is equivalent to

$$\max_{\rho} \quad R_{ss}|_{\alpha=F_p(\rho)} \tag{3.28a}$$

$$\text{s.t.} \quad \rho \in \mathcal{A}_1 \cap \mathcal{A}_2 \cap [(\mathcal{A}_4 \backslash \mathcal{A}_5) \cap \mathcal{A}_8]. \tag{3.28b}$$

- If $R_{eq,1} \leq \gamma^T$, then at optimality of Problem P1 (i.e., when $\min\{R_{pp}, R_{ps}\} = \gamma^T$), we have $R_{ps} \leq R_{pp}$, and thus, we have $R_{ps} = \gamma^T$ at optimality of Problem P1. Accordingly, Problem P1 is equivalent to

$$\max_{\rho} \quad R_{ss}|_{\alpha=F_s(\rho)} \tag{3.29a}$$

$$\text{s.t.} \quad \rho \in \mathcal{A}_1 \cap \mathcal{A}_3 \cap [(\mathcal{A}_4 \backslash \mathcal{A}_5) \cap \bar{\mathcal{A}}_8]. \tag{3.29b}$$

When $\rho \in \mathcal{A}_5$, the two curves have two intersections at $(\alpha_{eq,1}, R_{eq,1})$ and $(\alpha_{eq,2}, R_{eq,2})$. We further have two scenarios, as follows.

- If $R_{eq,1} \leq \gamma^T$ or $R_{eq,2} \geq \gamma^T$, then at optimality of Problem P1 (i.e., when $\min\{R_{pp}, R_{ps}\} = \gamma^T$), we have $R_{ps} \leq R_{pp}$, and thus, we have $R_{ps} = \gamma^T$ at optimality of Problem P1. Accordingly, Problem P1 is equivalent to

$$\max_{\rho} \quad R_{ss}|_{\alpha=F_s(\rho)} \tag{3.30a}$$

$$\text{s.t.} \quad \rho \in \mathcal{A}_1 \cap \mathcal{A}_3 \cap \mathcal{A}_5 \cap [\bar{\mathcal{A}}_8 \cup \mathcal{A}_9]. \tag{3.30b}$$

- If $R_{eq,1} \geq \gamma^T$ and $R_{eq,2} \leq \gamma^T$, then at optimality of Problem P1 (i.e., when $\min\{R_{pp}, R_{ps}\} = \gamma^T$), we have $R_{pp} \leq R_{ps}$, and thus, we have $R_{pp} = \gamma^T$ at optimality of Problem P1. Accordingly, Problem P1 is equivalent to

$$\max_{\rho} \quad R_{ss}|_{\alpha=F_p(\rho)} \tag{3.31a}$$

$$\text{s.t.} \quad \rho \in \mathcal{A}_1 \cap \mathcal{A}_2 \cap \mathcal{A}_5 \cap \mathcal{A}_8 \cap \bar{\mathcal{A}}_9. \tag{3.31b}$$

As a summary, for Case 2, the maximal objective function of Problem P1 is the largest one among the maximal objective functions of Problem (3.27), Problem (3.28), Problem (3.29), Problem (3.30) and Problem (3.31).

### 3.2.3 Case 3: When $g_{pp} \leq g_{ps}$ and $g_{sp} > g_{ss}$

Similar to the previous two cases, we also try to decide which one between $R_{pp}$ and $R_{ps}$ should be equal to $\gamma^T$.

**Lemma 4.** *For a specific value of $\rho$, the two curves $R_{pp}$ vs. $\alpha$ and $R_{ps}$ vs. $\alpha$ over $\alpha \in [0, 1]$ have at most one intersection at $(\alpha_{eq,1}, R_{eq,1})$, with $R_{eq,1}$ being a concave function of $\rho$.*

*Proof.* The proof is similar to Lemma 3. The major difference is $L_1 > 0$ and $L_2 > 0$, which makes $\text{ROOT}_2$ in (3.16) larger than 1 and infeasible, yielding at most one intersection. □

Note that we have $R_{pp}|_{\alpha=0} = \frac{1-\rho}{2}\log(1+\frac{P_p g_{pp}}{\sigma^2}+\frac{P_p g_{pp}}{P_e g_{sp}+\sigma^2}) < R_{ps}|_{\alpha=0} = \frac{1-\rho}{2}\log(1+\frac{P_p g_{ps}}{\sigma^2}+\frac{P_p g_{ps}}{P_e g_{ss}+\sigma^2})$. Thus, the two curves $R_{pp}$ vs. $\alpha$ and $R_{ps}$ vs. $\alpha$ have one intersection over $\alpha \in [0,1]$ if and only if $R_{pp}|_{\alpha=1} \geq R_{ps}|_{\alpha=1}$, which equivalently means that $\rho \in \mathcal{A}_4 = \left[\max\left\{1-\frac{\eta P_p g_{tt}+E_0-E_c}{\eta P_p g_{tt}+\frac{P_p g_{ps}-P_p g_{pp}}{g_{sp}-g_{ss}}}, 0\right\},\ 1\right]$.

Similar to Lemma 3, when $\rho \in \bar{\mathcal{A}}_4 \triangleq [0,\ 1]\backslash\mathcal{A}_4$, the two curves do not have intersection, which means that we always have $R_{pp} < R_{ps}$. Thus, at optimality of Problem P1, we should have $R_{pp} = \gamma^T$. Then Problem P1 is equivalent to

$$\max_{\rho} \quad R_{ss}|_{\alpha=F_p(\rho)} \tag{3.32a}$$

$$\text{s.t.} \quad \rho \in \mathcal{A}_1 \cap \mathcal{A}_2 \cap \bar{\mathcal{A}}_4. \tag{3.32b}$$

When $\rho \in \mathcal{A}_4$, the two curves have one intersection at $(\alpha_{eq,1}, R_{eq,1})$. We further have two scenarios, as follows.

- If $R_{eq,1} \geq \gamma^T$, then at optimality of Problem P1 (i.e., when $\min\{R_{pp}, R_{ps}\} = \gamma^T$), we have $R_{pp} \leq R_{ps}$, and thus, we have $R_{pp} = \gamma^T$ at optimality of Problem P1. Accordingly, Problem P1 is equivalent to

$$\max_{\rho} \quad R_{ss}|_{\alpha=F_p(\rho)} \tag{3.33a}$$

$$\text{s.t.} \quad \rho \in \mathcal{A}_1 \cap \mathcal{A}_2 \cap \mathcal{A}_4 \cap \mathcal{A}_8. \tag{3.33b}$$

- If $R_{eq,1} < \gamma^T$, then at optimality of Problem P1 (i.e., when $\min\{R_{pp}, R_{ps}\} = \gamma^T$), we have $R_{ps} < R_{pp}$, and thus, we have $R_{ps} = \gamma^T$ at optimality of

Problem P1. Accordingly, Problem P1 is equivalent to

$$\max_{\rho} \quad R_{ss}|_{\alpha=F_s(\rho)} \tag{3.34a}$$

$$\text{s.t.} \quad \rho \in \mathcal{A}_1 \cap \mathcal{A}_3 \cap \mathcal{A}_4 \cap \bar{\mathcal{A}}_8. \tag{3.34b}$$

As a summary, for Case 3, the maximal objective function of Problem P1 is the largest one among the maximal objective functions of Problem (3.32), Problem (3.33), and Problem (3.34).

### 3.2.4 Case 4: When $g_{pp} > g_{ps}$ and $g_{sp} \leq g_{ss}$

Similar to Case 3, we can also prove that Lemma 4 holds in Case 4. Different from Case 3, here we have $R_{pp}|_{\alpha=0} = \frac{1-\rho}{2}\log(1+\frac{P_p g_{pp}}{\sigma^2}+\frac{P_p g_{pp}}{P_e g_{sp}+\sigma^2}) > R_{ps}|_{\alpha=0} = \frac{1-\rho}{2}\log(1+\frac{P_p g_{ps}}{\sigma^2}+\frac{P_p g_{ps}}{P_e g_{ss}+\sigma^2})$. Thus, the two curves $R_{pp}$ vs. $\alpha$ and $R_{ps}$ vs. $\alpha$ have one intersection over $\alpha \in [0,1]$ if and only if $R_{pp}|_{\alpha=1} \leq R_{ps}|_{\alpha=1}$, which equivalently means that $\rho \in \mathcal{A}_4$.[8]

When $\rho \in \bar{\mathcal{A}}_4$, the two curves do not have intersection, which means that we always have $R_{pp} > R_{ps}$. Thus, at optimality of Problem P1, we should have $R_{ps} = \gamma^T$. Then Problem P1 is equivalent to

$$\max_{\rho} \quad R_{ss}|_{\alpha=F_s(\rho)} \tag{3.35a}$$

$$\text{s.t.} \quad \rho \in \mathcal{A}_1 \cap \mathcal{A}_3 \cap \bar{\mathcal{A}}_4. \tag{3.35b}$$

When $\rho \in \mathcal{A}_4$, the two curves have one intersection at $(\alpha_{eq,1}, R_{eq,1})$. We have two scenarios as follows.

- If $R_{eq,1} \geq \gamma^T$, then at optimality of Problem P1 (i.e., when $\min\{R_{pp}, R_{ps}\} = \gamma^T$), we have $R_{ps} \leq R_{pp}$, and thus, we have $R_{ps} = \gamma^T$ at optimality of

[8] In Case 3, $R_{pp}|_{\alpha=1} \geq R_{ps}|_{\alpha=1}$ is equivalent to $\rho \in \mathcal{A}_4$, while in Case 4, $R_{pp}|_{\alpha=1} \leq R_{ps}|_{\alpha=1}$ is equivalent to $\rho \in \mathcal{A}_4$. This is because we have $g_{pp} \leq g_{ps}$ and $g_{sp} > g_{ss}$ in Case 3, while we have $g_{pp} > g_{ps}$ and $g_{sp} \leq g_{ss}$ in Case 4.

Problem P1. Accordingly, Problem P1 is equivalent to

$$\max_{\rho} \quad R_{ss}|_{\alpha=F_s(\rho)} \tag{3.36a}$$

$$\text{s.t.} \quad \rho \in \mathcal{A}_1 \cap \mathcal{A}_3 \cap \mathcal{A}_4 \cap \mathcal{A}_8. \tag{3.36b}$$

- If $R_{eq,1} < \gamma^T$, then at optimality of Problem P1 (i.e., when $\min\{R_{pp}, R_{ps}\} = \gamma^T$), we have $R_{pp} < R_{ps}$, and thus, we have $R_{pp} = \gamma^T$ at optimality of Problem P1. Accordingly, Problem P1 is equivalent to

$$\max_{\rho} \quad R_{ss}|_{\alpha=F_p(\rho)} \tag{3.37a}$$

$$\text{s.t.} \quad \rho \in \mathcal{A}_1 \cap \mathcal{A}_2 \cap \mathcal{A}_4 \cap \bar{\mathcal{A}}_8. \tag{3.37b}$$

As a summary, for Case 4, the maximal objective function of Problem P1 is the largest one among the maximal objective functions of Problem (3.35), Problem (3.36), and Problem (3.37).

In Cases 1∼4, all the equivalent problems are in the format of $\max_{\rho} \ R_{ss}|_{\alpha=F_p(\rho)}$ or $\max_{\rho} \ R_{ss}|_{\alpha=F_s(\rho)}$ under a constraint that $\rho$ is within a closed interval (i.e., such as equivalent problems (3.23), (3.28), (3.32) and (3.35)) or within a union of multiple closed intervals (i.e., such as equivalent problems (3.25), (3.30), (3.34) and (3.37)). We have two observations:

- If $\rho$ is within a union of multiple closed intervals, we can first get the optimal solution over each interval and pick up the best optimal solution.

- $R_{ss}|_{\alpha=F_p(\rho)}$ and $R_{ss}|_{\alpha=F_s(\rho)}$ can be expressed in an unified form as

$$R_{ss,n} = \frac{1-\rho}{2} \log\left(1 + \frac{(P_e g_{sn} - \mu_n \sigma^2 + P_p g_{pn}) g_{ss}}{(\mu_n + 1) g_{sn} \sigma^2}\right) \tag{3.38}$$

  with $n \in \{p, s\}$. Here we have $R_{ss}|_{\alpha=F_n(\rho)} = R_{ss,n}$.

Therefore, in what follows, we focus on maximizing $R_{ss,n}$, $n \in \{p, s\}$ over $\rho \in \mathcal{B}$ with $\mathcal{B}$ being a closed interval.

### 3.2.5 Solving max $R_{ss,n}$ s.t. $\rho \in \mathcal{B}$

The objective function $R_{ss,n}$ is not a concave function. However, it is a quasiconcave function [85], as theoretically shown in the following theorem.

**Theorem 1.** *The objective function $R_{ss,n}$ is quasiconcave with respect to $\rho \in \mathcal{B}$.*

*Proof.* See Appendix 3.6.2. □

As shown in [85], super-level sets of a quasiconcave function can be represented by inequalities of concave functions. As reference [85] does not provide methods to find the inequalities of concave functions, here we develop a method to find the inequalities of concave functions that can represent super-level sets of our quasiconcave function $R_{ss,n}$. As a result, we have the following theorem.

**Theorem 2.** *For any $t \geq 0$, inequality $R_{ss,n} \geq t$ and inequality $\xi_{t,n} \geq 0$ are equivalent, in which $\xi_{t,n}$ is given as*

$$\xi_{t,n} = (\lambda_n - 2^{\frac{2t}{1-\rho}})(1-\rho)(\mu_n + 1), \tag{3.39}$$

*where*

$$\lambda_n = 1 + \frac{(P_e g_{sn} - \mu_n \sigma^2 + P_p g_{pn}) g_{ss}}{(\mu_n + 1) g_{sn} \sigma^2}. \tag{3.40}$$

*Proof.* It is readily checked that $R_{ss,n} \geq t$ is equivalent to $\lambda_n - 2^{\frac{2t}{1-\rho}} \geq 0$.

Since $1-\rho$ and $\mu_n + 1$ are larger than 0, multiplying two positive numbers to $\lambda_n - 2^{\frac{2t}{1-\rho}}$ will not change its sign. Then we can see that $R_{ss,n} \geq t$ is equivalent to $\xi_{t,n} \geq 0$.

This completes the proof. □

From Theorem 2, identifying the maximized $R_{ss,n}$ in $\rho \in \mathcal{B}$ is equivalent to finding the maximal possible value of $t$ such that there exists $\rho \in \mathcal{B}$ that makes $R_{ss,n} \geq t$, which is further equivalent to finding the maximal possible value of

$t$ such that there exists $\rho \in \mathcal{B}$ that makes $\xi_{t,n} \geq 0$. For a value of $t$, if there exists $\rho \in \mathcal{B}$ that makes $\xi_{t,n} \geq 0$, then we say that the $t$ value is *feasible*. Thus, $\max\limits_{\rho} \ R_{ss,n}$ s.t. $\rho \in \mathcal{B}$ is equivalent to finding the maximal feasible $t$ value, which can be done by using a bisection search over $t \in [0, \log(1 + \frac{P_e g_{ss}}{\sigma^2})]$ (noting that from (3.4) and (3.6), it can be seen that an upper bound of $R_{ss,n}$ is $\log(1+\frac{P_e g_{ss}}{\sigma^2})$).

In the bisection search over $t$, we need to decide whether or not a checked $t$ value is feasible. For this purpose, the following theorem, which gives a feature of $\xi_{t,n}$, is helpful.

**Theorem 3.** *For a given nonnegative value of $t$, the function $\xi_{t,n}$ is concave with respect to $\rho \in \mathcal{B}$.*

*Proof.* See Appendix 3.6.3. □

In the bisection search over $t$, if a checked $t$ value is feasible, this equivalently means that for the checked $t$ value, the maximal value of $\xi_{t,n}$ over $\rho \in \mathcal{B}$ is nonnegative. Thus, from Theorem 3, we can use a bisection search over $\rho \in \mathcal{B}$, to find the maximal value of $\xi_{t,n}$.[9] If any searched $\rho$ makes $\xi_{t,n} \geq 0$, then the checked $t$ value is feasible, and we can terminate the bisection search of $\rho$. If the found maximal value of $\xi_{t,n}$ is negative, then the checked $t$ value is infeasible. Thus, we have two levels of bisection search, and we call the bisection search over $t$ as outer bisection search, and call the bisection search over $\rho$ as inner bisection search.

Generally, each inner bisection search may need to be done over $\rho \in \mathcal{B}$. Next we reduce the number of iterations in inner bisection search.

[9]In the bisection search, we try to find a value of $\rho$ that makes $\frac{\mathrm{d}\xi_{t,n}}{\mathrm{d}\rho} = 0$ (which means the maximal value of $\xi_{t,n}$ is achieved over $\rho \in \mathcal{B}$). Note that other methods can also be used here to find the maximal value of $\xi_{t,n}$ over $\rho \in \mathcal{B}$, such as gradient descent method and Newton's method.

For a $t$ value, define $\mathcal{R}_{t,n} = \{\rho | \xi_{t,n} \geq 0, \rho \in \mathcal{B}\}$. So $\mathcal{R}_{t,n}$ is a set of $\rho$ that makes $\xi_{t,n} \geq 0$. Consider two $t$ values: $t_1$ and $t_2$, with $t_1 < t_2$. We have

$$\mathcal{R}_{t_2,n} \overset{\text{(i)}}{=} \{\rho | R_{ss,n} \geq t_2\} \overset{\text{(ii)}}{\subseteq} \{\rho | R_{ss,n} \geq t_1\} \overset{\text{(iii)}}{=} \mathcal{R}_{t_1,n}, \tag{3.41}$$

in which steps (i) and (iii) are from Theorem 2, and step (ii) is from $t_1 < t_2$.

From (3.41), we can see that, if we know that $t_1$ is feasible, then when deciding whether or not $t_2$ is feasible, we only need to search $\rho$ over $\mathcal{R}_{t_1,n}$, or over an interval of $\rho$ that includes $\mathcal{R}_{t_1,n}$ as a subset. Denote $\mathcal{F} \triangleq [f_1, f_2]$ as the interval of $\rho$ over which the inner bisection search is performed. So $\mathcal{F}$ is initially set to be $\mathcal{B}$. In the outer bisection search, for a checked $t$ value (say $t^\dagger$), if $t^\dagger$ is feasible, we get an updated $\mathcal{F}$ (which is a subset of the previous $\mathcal{F}$, and includes $\mathcal{R}_{t^\dagger,n}$ as a subset). Then, in the outer bisection search, when we check feasibility of higher $t$ values,[10] we only need to search $\rho$ over the updated interval $\mathcal{F}$ (rather than over $\mathcal{B}$) in the inner bisection search, referred to as *feasible region shrinking*.

Based on this observation, we have Algorithm 1 for our inner bisection search. In Algorithm 1, the expression of $\xi_{t,n}$ is given in (3.39), while expression of $\frac{\mathrm{d}\xi_{t,n}}{\mathrm{d}\rho}$ is given as

$$\begin{aligned}\frac{\mathrm{d}\xi_{t,n}}{\mathrm{d}\rho} = &(\frac{g_{ss}}{g_{sn}} - 1)\big(\mu_n - (1-\rho)\frac{\mathrm{d}\mu_n}{\mathrm{d}\rho}\big) + \frac{2\eta P_p g_{tt} g_{ss}}{\sigma^2} - 1 \\ &- \frac{P_p g_{pn} g_{ss}}{g_{sn}\sigma^2} - \Big((\mu_n + 1)\big(\frac{2(\ln 2)t}{1-\rho} - 1\big) + (1-\rho)\frac{\mathrm{d}\mu_n}{\mathrm{d}\rho}\Big)2^{\frac{2t}{1-\rho}}. \end{aligned} \tag{3.42}$$

In Steps 1 and 2 of Algorithm 1, we check whether $\rho = f_1$ or $\rho = f_2$ makes $\xi_{t,n}$ nonnegative. If yes, then the checked $t$ value is feasible and we terminate the algorithm. If we proceed to Step 3, then we know that $\xi_{t,n}|_{\rho=f_1} < 0$ and $\xi_{t,n}|_{\rho=f_2} < 0$. In Step 3, we check whether $\frac{\mathrm{d}\xi_{t,n}}{\mathrm{d}\rho}|_{\rho=f_1}$ and $\frac{\mathrm{d}\xi_{t,n}}{\mathrm{d}\rho}|_{\rho=f_2}$ are both nonpositive or both nonnegative. If they are both nonpositive or both nonnegative, then $\xi_{t,n}$

[10]Note that since $t^\dagger$ is feasible, we do not need to check $t$ values lower than $t^\dagger$ in the outer bisection search.

**Algorithm 1:** Inner Bisection Search

**Input:** value of $t$ to be checked for feasibility, and two end points of the interval $\mathcal{F}$: $f_1$ and $f_2$

**Output:** Feasibility of value $t$, updated $f_1$ and $f_2$

1 **if** $\xi_{t,n}|_{\rho=f_1} \geq 0$ *or* $\xi_{t,n}|_{\rho=f_2} \geq 0$ **then**

2 $\quad$ $t$ is feasible. Terminate the algorithm;

3 **if** $\frac{\mathrm{d}\xi_{t,n}}{\mathrm{d}\rho}|_{\rho=f_1} \times \frac{\mathrm{d}\xi_{t,n}}{\mathrm{d}\rho}|_{\rho=f_2} \geq 0$ **then**

4 $\quad$ $t$ is infeasible. Terminate the algorithm;

5 $f_1^{\mathrm{BS}} \leftarrow f_1, f_2^{\mathrm{BS}} \leftarrow f_2$;

6 $f_1^{\mathrm{new}} \leftarrow f_1, f_2^{\mathrm{new}} \leftarrow f_2$;

7 **if** $|f_2^{BS} - f_1^{BS}| < \epsilon_\rho$ **then**

8 $\quad$ $t$ is infeasible. Terminate the algorithm;

9 $f_{\mathrm{mid}} \leftarrow (f_1^{\mathrm{BS}} + f_2^{\mathrm{BS}})/2$;

10 **if** $\xi_{t,n}|_{\rho=f_{mid}} \geq 0$ **then**

11 $\quad$ $t$ is feasible; $f_1 \leftarrow f_1^{\mathrm{new}}, f_2 \leftarrow f_2^{\mathrm{new}}$; Terminate the algorithm;

12 **if** $\frac{\mathrm{d}\xi_{t,n}}{\mathrm{d}\rho}|_{\rho=f_{mid}} = 0$ **then**

13 $\quad$ $t$ is infeasible. Terminate the algorithm;

14 **if** $\frac{\mathrm{d}\xi_{t,n}}{\mathrm{d}\rho}|_{\rho=f_{mid}} > 0$ **then**

15 $\quad$ $f_1^{\mathrm{BS}} \leftarrow f_{\mathrm{mid}}$; $f_1^{\mathrm{new}} \leftarrow f_{\mathrm{mid}}$;Go to Step 7;

16 **if** $\frac{\mathrm{d}\xi_{t,n}}{\mathrm{d}\rho}|_{\rho=f_{mid}} < 0$ **then**

17 $\quad$ $f_2^{\mathrm{BS}} \leftarrow f_{\mathrm{mid}}$; $f_2^{\mathrm{new}} \leftarrow f_{\mathrm{mid}}$;Go to Step 7;

is a decreasing or increasing function with respect to $\rho \in \mathcal{F}$, and thus, we can conclude that the checked $t$ value is infeasible. So when we proceed to Step 5, we should have $\frac{\mathrm{d}\xi_{t,n}}{\mathrm{d}\rho}|_{\rho=f_1} > 0$ and $\frac{\mathrm{d}\xi_{t,n}}{\mathrm{d}\rho}|_{\rho=f_2} < 0$. Then we try to search the maximal point of $\xi_{t,n}$ over $\rho \in [f_1, f_2]$, by using inner bisection search of $\frac{\mathrm{d}\xi_{t,n}}{\mathrm{d}\rho}$ until $\frac{\mathrm{d}\xi_{t,n}}{\mathrm{d}\rho} = 0$. In the inner bisection search, $[f_1^{\mathrm{BS}}, f_2^{\mathrm{BS}}]$ represents the subinterval after bisecting the original interval of $\rho$, and $[f_1^{\mathrm{new}}, f_2^{\mathrm{new}}]$ represents the updated interval $\mathcal{F}$. In the inner bisection search, if a searched $\rho$ value makes $\xi_{t,n} \geq 0$, then we know that the checked $t$ value is feasible, and we update $\mathcal{F}$ (we can see that the updated $\mathcal{F}$ satisfies $\mathcal{R}_{t,n} \subseteq \mathcal{F}$), and terminate the algorithm (Steps 10–11). If the subinterval $[f_1^{\mathrm{BS}}, f_2^{\mathrm{BS}}]$ is sufficiently small (i.e., less than a threshold

value $\epsilon_\rho$) and no searched $\rho$ value makes $\xi_{t,n} \geq 0$, then we know the checked $t$ value is infeasible, and we do not update $\mathcal{F}$ (Steps 7–8).

The detailed algorithm for the outer bisection search is straightforward, and thus, is omitted here, for presentational simplicity.

**Complexity:** According to [86], the computational complexity of a bisection search is $O(\log(\frac{1}{\epsilon}))$, where $\epsilon$ is the pre-defined tolerance for convergence. Thus, the complexity of the proposed two-level bisection search is expressed as $O\big(\log(\frac{1}{\epsilon_t})\log(\frac{1}{\epsilon_\rho})\big)$, in which $\epsilon_t$ and $\epsilon_\rho$ are pre-defined convergence tolerance for the outer bisection search over $t$ and the inner bisection search over $\rho$.

**Impact of parameters $\epsilon_t$ and $\epsilon_\rho$:** Denote $t^*$ as the maximal feasible $t$ value, and denote $\rho^*$ as the corresponding $\rho$ that achieves $t^*$. Denote $\hat{t}$ as the $t$ value found by our proposed algorithm.

For the outer bisection search over $t$, when it converges, we get a region of $t$, denoted as $[l, u]$ with $u - l < \epsilon_t$. Then $\hat{t} = l$ is the $t$ value found by our algorithm.

If the inner bisection search (which does feasibility check for a specific $t$ value) is always accurate, then when the outer bisection search converges, $t = l$ is feasible, $t = u$ is infeasible, and $t^*$ falls within $[l, u]$. Thus, the gap between $t^*$ and $\hat{t}(= l)$ is less than $\epsilon_t$.

However, when the inner bisection search checks the feasibility of a value, say $t^\dagger$, close to $t^*$, it may not be accurate. It is possible that the inner bisection search may claim that $t^\dagger$ is infeasible, but actually $t^\dagger$ is feasible. If this happens, then when the outer bisection search converges at a region of $t$ denoted as $[l, u]$, actually $t = l$ and $t = u$ are both feasible, and we have $l < u < t^*$ (in other words, $t^*$ does not fall within $[l, u]$). Recall that our objective function $R_{ss,n}$ is a quasiconcave function, i.e., when the first order derivative is 0, the second order derivative is nonpositive. Thus, we can treat the quasiconcave function $R_{ss,n}$

as a concave function at the neighborhood of $\rho^*$. Based on this, $|t^* - u|$ is less than $\left|\frac{\mathrm{d}R_{ss,n}}{\mathrm{d}\rho}|_{\rho=\rho^*-\epsilon_\rho}\right|\epsilon_\rho$. Accordingly, the gap between $t^*$ and $\hat{t}(=l)$ is less than $\Delta \triangleq \epsilon_t + \left|\frac{\mathrm{d}R_{ss,n}}{\mathrm{d}\rho}|_{\rho=\rho^*-\epsilon_\rho}\right|\epsilon_\rho$.

For $R_{ss,n}$, its first-order derivative at $\rho = \rho^*$ is zero, i.e., $\frac{\mathrm{d}R_{ss,n}}{\mathrm{d}\rho}|_{\rho=\rho^*} = 0$. Since $R_{ss,n}$ can be viewed as a concave function at the neighborhood of $\rho^*$ and $\epsilon_\rho$ is small, we can see that $\left|\frac{\mathrm{d}R_{ss,n}}{\mathrm{d}\rho}|_{\rho=\rho^*-\epsilon_\rho}\right|$ is close to zero. Thus, $\Delta$ is small for small values of $\epsilon_t$ and $\epsilon_\rho$.

### 3.2.6 Further Discussion: When Primary Information is Sent during the First Phase

In the first phase, the wireless RF signals can actually be information signals of the PT for the PR. In other words, in the first phase, from the PT's signals, the ST tries to harvest energy while the PR tries to decode information. Thus, the primary system has an additional throughput expressed as $\rho\log(1+\frac{P_p g_{pp}}{\sigma^2})$. It also means that the target throughput of the primary system during the second and third phase is $\gamma^T - \rho\log(1+\frac{P_p g_{pp}}{\sigma^2})$. Therefore, in Problem P1, we should replace $\gamma^T$ with $\gamma^T - \rho\log(1+\frac{P_p g_{pp}}{\sigma^2})$, and accordingly, we have the following revised Problem P1:

**Revised Problem P1:**

$$\max_{\alpha,\rho} \quad R_{ss} = \frac{1-\rho}{2}\log\left(1+\frac{(1-\alpha)P_e g_{ss}}{\sigma^2}\right) \tag{3.43a}$$

$$\text{s.t.} \quad \rho \in \tilde{\mathcal{A}}_1; 0 \le \alpha \le 1 \tag{3.43b}$$

$$\min\{R_{pp}, R_{ps}\} \ge \gamma^T - \rho\log(1+\frac{P_p g_{pp}}{\sigma^2}) \tag{3.43c}$$

in which $\tilde{\mathcal{A}}_1 \triangleq \left[\max\{\frac{E_c - E_0}{\eta P_p g_{tt}}, 0\}, 1 - \frac{2\left(\gamma^T - \log(1+\frac{P_p g_{pp}}{\sigma^2})\right)}{\log(1+\frac{P_p g_{tt}}{\sigma^2}) - 2\log(1+\frac{P_p g_{pp}}{\sigma^2})}\right]$.

Similar to Lemma 1, we should have either $R_{pp} = \gamma^T - \rho\log(1+\frac{P_p g_{pp}}{\sigma^2})$ or $R_{ps} = \gamma^T - \rho\log(1+\frac{P_p g_{pp}}{\sigma^2})$ at optimality of the revised Problem P1. Accordingly, when $R_{pn} = \gamma^T - \rho\log(1+\frac{P_p g_{pp}}{\sigma^2})$, $n \in \{p, s\}$, we can see that $\alpha$ can be expressed in

terms of $\rho$ as $\alpha = \tilde{F}_n(\rho) \triangleq \frac{\tilde{\mu}_n(P_e g_{sn}+\sigma^2)-P_p g_{pn}}{(\tilde{\mu}_n+1)P_e g_{sn}}$ with $\tilde{\mu}_n \triangleq (1+\frac{P_p g_{pp}}{\sigma^2})^2 2^{\frac{2\tilde{\gamma}^T}{1-\rho}} - \frac{P_p g_{pn}}{\sigma^2} - 1$, in which $\tilde{\gamma}^T = \gamma^T - \log(1+\frac{P_p g_{pp}}{\sigma^2})$.

Afterwards, for each of the four cases defined in Section 3.2.1∼3.2.4, the revised Problem P1 is equivalent to maximizing

$$R_{ss}|_{\alpha=\tilde{F}_n(\rho)} = \frac{1-\rho}{2}\log\big(1+\frac{(P_e g_{sn}-\tilde{\mu}_n\sigma^2+P_p g_{pn})g_{sn}}{(\tilde{\mu}_n+1)g_{sn}\sigma^2}\big) \tag{3.44}$$

over closed intervals.

Then similar to Theorem 1, we can still prove that $R_{ss}|_{\alpha=\tilde{F}_n(\rho)}$ is quasiconcave over each closed interval, and thus, a two-level bisection search can be used to find the optimal solution.

For presentation simplicity, in the sequel, we consider that the PT does not send information to the PR during the first phase of each slot in the cooperative transmission mode.

## 3.3 Optimal Solution for Problem P2

Similar to Problem P1, when Problem P2 achieves the optimality, the constraint $R_{pp} \geq \gamma^T$ should take equality, which means $\alpha = F_p(\rho)$, as given in (3.9). Accordingly, Problem P2 is equivalent to

$$\max_{\rho} \quad R_{ss}^{w/o}|_{\alpha=F_p(\rho)} \tag{3.45a}$$

$$\text{s.t.} \quad \rho \in \mathcal{A}_1 \cap \mathcal{A}_2 \tag{3.45b}$$

with $R_{ss}^{w/o}|_{\alpha=F_p(\rho)} = \frac{1-\rho}{2}\log\lambda^{w/o}$, where

$$\lambda^{w/o} = 1+(P_e g_{sp}-\mu_p\sigma^2+P_p g_{pp})g_{ss}\Big\{\big[\mu_p(P_e g_{sp}+\sigma^2)- P_p g_{pp}\big]g_{ss}+(P_p g_{ps}+\sigma^2)(\mu_p+1)g_{sp}\Big\}^{-1}. \tag{3.46}$$

We have the following theorem for the objective function of Problem (3.45).

**Theorem 4.** *The objective function* $R_{ss}^{w/o}|_{\alpha=F_p(\rho)}$ *is quasiconcave with respect to* $\rho \in [0,1]$.

*Proof.* See Appendix 3.6.4. □

Since $R_{ss}^{w/o}|_{\alpha=F_p(\rho)}$ is quasiconcave, similar to Theorem 2, for any $t \geq 0$, inequality $R_{ss}^{w/o}|_{\alpha=F_p(\rho)} \geq t$ is equivalent to $\xi_t^{w/o} \geq 0$, with

$$\xi_t^{w/o} \triangleq (\lambda^{w/o} - 2^{\frac{2t}{1-\rho}})(1-\rho)\Big\{\big[\mu_p(P_e g_{sp} + \sigma^2) - P_p g_{pp}\big] g_{ss} + (P_p g_{ps} + \sigma^2)(\mu_p + 1) g_{sp}\Big\}. \quad (3.47)$$

The following theorem gives a feature of $\xi_t^{w/o}$.

**Theorem 5.** *For a given nonnegative value* $t$*, the function* $\xi_t^{w/o}$ *is concave with respect to* $\rho \in [0,1]$.

*Proof.* See Appendix 3.6.5. □

Therefore, a two-level bisection search similar to that in Section 3.2.5 can be used to find the optimal solution for Problem P2. The details are omitted here.

Overall, Fig. 3.4 shows the procedure for finding optimal solution of the considered system.

**Remark:** Interestingly, we have an observation that the maximal secondary throughput of Problem P1 may not guarantee to be larger than that of Problem P2. The reason is as follows. For specific $\alpha$ and $\rho$, the objective function value of Problem P1 is indeed larger than that of Problem P2. However, compared to Problem P2, Problem P1 has one more constraint $R_{ps} \geq \gamma^T$, which makes the feasible region of Problem P1 be a subset of the feasible region of Problem P2. Thus, in a larger feasible region, it is possible that the maximal secondary throughput of Problem P2 is larger than that of Problem P1.

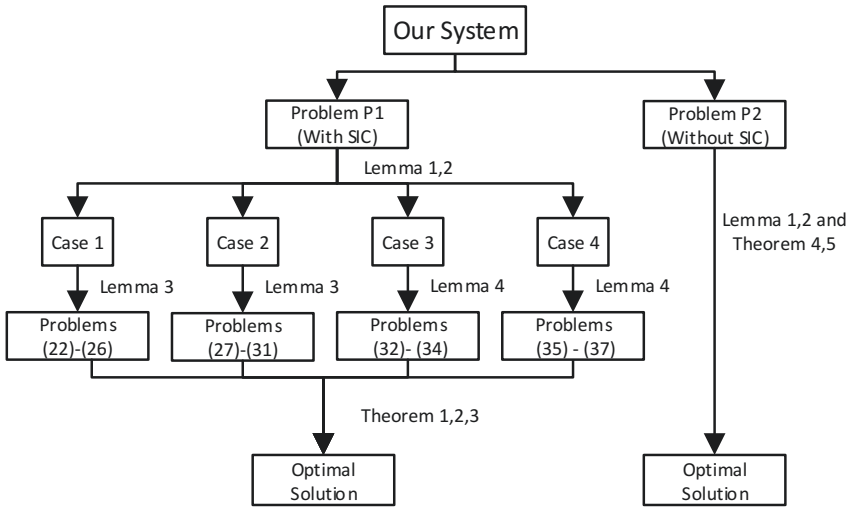


Figure 3.4: Flow chart of the procedure for finding optimal solution of the considered system.

A numerical example is also given here, which has the following parameter setting as: $g_{tt} = 7.15 \times 10^{-3}$, $g_{pp} = 2.69 \times 10^{-5}$, $g_{ps} = 2.65 \times 10^{-6}$, $g_{sp} = 1.1 \times 10^{-1}$, $g_{ss} = 2.88 \times 10^{-2}$, $P_p = 15$ dBm, $E_0 = 3.41 \times 10^{-5}$ J, $E_c = 1.5 \times 10^{-6}$ J, $\sigma^2 = -25$ dBm, and $\gamma^T = 0.5$ bps/Hz. In this specific example, the optimal solution of Problem P2 is 0.1448 bps/Hz, which is larger than the optimal solution of Problem P1, 0.0321 bps/Hz.

## 3.4 Numerical Results

We use Matlab simulation to evaluate the performance of our proposed algorithm[11]. Similar to [19], the channel power gain $g_i$ is further represented as $g_i = \frac{\tilde{g}_i}{1+d_i^{\kappa_i}}$, where $i \in \mathcal{M} = \{tt, pp, ps, sp, ss\}$, $\tilde{g}_i$ is exponentially distributed with parameter 1, $d_i$ is the distance of link $i$, and $\kappa_i$ is the path loss exponent of link $i$. The distance values are: $d_{pp} = 12$ m, $d_{tt} = d_{ps} = d_{sp} = d_{ss} = 8$ m. The

[11]In the sequel, by "our proposed algorithm," we mean the algorithm that takes the better solution of Problem P1 and Problem P2 if both problems are feasible, and takes the solution of Problem P2 if only Problem P2 is feasible. Note that if Problem P2 is infeasible, then Problem P1 should also be infeasible.

background noise variance is $\sigma^2 = -25$dBm and the energy conversion efficiency is $\eta = 0.5$. The energy expenditure in a time slot due to circuit operation and channel estimation is $E_c = 1.5 \times 10^{-6}$ J. In our simulation, a minimum throughput requirement 0.15 bps/Hz is set up at the ST. If the ST cannot achieve this throughput at a slot, our system works in direct primary transmission mode.

First we evaluate the chance of ST to access the channel. Three events, $D_1$, $D_2$ and $D_3$, are considered. Specifically, event $D_1$ is defined as $g_{pp} < (2^{\gamma^T} - 1)\sigma^2/P_p$, which means that the PT needs help. Event $D_2$ is defined as $g_{tt} \geq (2^{2\gamma^T} - 1)\sigma^2/P_p$, which means that it is possible to set up a $\rho$ such that $R_{tt} \geq \gamma^T$ (i.e., the ST is able to decode information from the PT in the second phase). Event $D_3$ is defined as the event that the PT needs help (i.e., $g_{pp} < (2^{\gamma^T} - 1)\sigma^2/P_p$) and at least one of Problems P1 and P2 is feasible[12]. Clearly, when event $D_3$ happens, events $D_1$ and $D_2$ should also happen. And the probability of event $D_3$ is exactly the probability of the ST to access the channel. By setting $\gamma^T = 0.25$ bps/Hz and 0.5 bps/Hz, $\kappa_{pp} = 4$, $\kappa_i = 2$, $i \in \mathcal{M}\backslash\{pp\}$ and varying $P_p$ from 0 dBm to 30 dBm, the occurrence probabilities of three events, $P(D_1), P(D_2)$, and $P(D_3)$, are shown in Fig. 3.5. Probabilities $P(D_1)$ and $P(D_2)$ are decreasing and increasing functions, respectively, of $P_p$, which is intuitive. Moreover, we get higher $P(D_1)$ and lower $P(D_2)$ through increasing $\gamma^T$ from 0.25 bps/Hz to 0.5 bps/Hz. This is because a higher target rate $\gamma^T$ means that the PT needs more help and the ST needs better channel gain $g_{tt}$ to decode information from the PT. At low $P_p$, $P(D_1)$ is close to 1 (i.e., the PT almost always needs help from the ST), and thus, the curve of $P(D_3)$ follows the trend of the curve of $P(D_2)$, i.e., increases when $P_p$ increases or $\gamma^T$ decreases. At high $P_p$, $P(D_2)$ is close to 1, and thus, the curve of

[12]Note that in cooperative transmission mode, when Problem P1 is feasible, Problem P2 is always feasible. Thus, "at least one of Problems P1 and P2 is feasible" is equivalent to "Problem P2 is feasible."

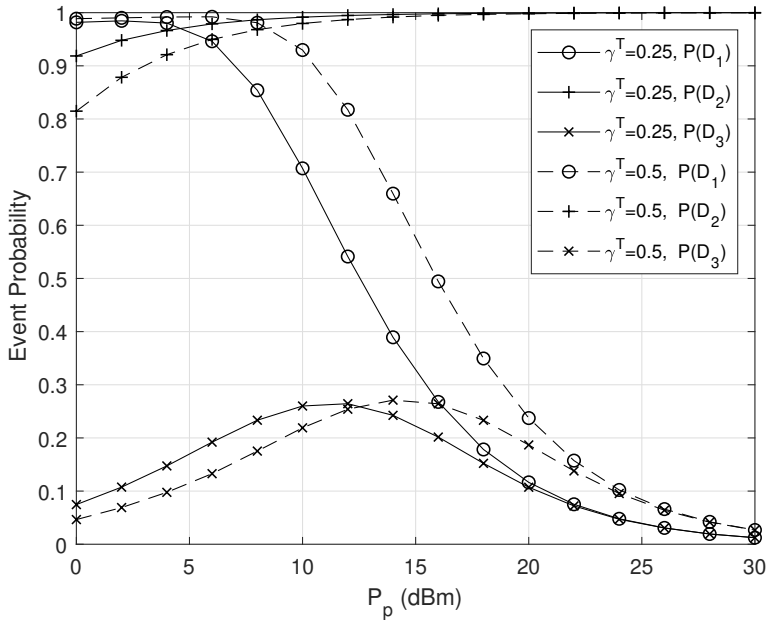


Figure 3.5: The probabilities of three events $D_1, D_2$, and $D_3$.

$P(D_3)$ follows the trend of the curve of $P(D_1)$, i.e., decreases when $P_p$ increases or $\gamma^T$ decreases.

Next we show by how much chance the performance of Problem P2 is better than that of Problem P1 (i.e., the maximal secondary throughput without SIC is higher than that with SIC). We set $\gamma^T = 0.1, 0.25, 0.5, 0.75$, and 1 bps/Hz, and $P_p = 0$ dBm and 10 dBm. For each $(\gamma^T, P_p)$ pair, we run simulations for $10^6$ time slots. In Table 3.2, the numbers after slash are numbers of time slots in which both Problems P1 and P2 are feasible, while the numbers before slash are numbers of time slots when the maximal secondary throughput of Problem P2 is larger than that of Problem P1. It can be seen that, in most time slots when both problems are feasible, Problem P1 has better performance. However, it is still possible (with a small probability) that Problem P2 performs better. Therefore, when both problems are feasible, if we directly take the solution of Problem P1, we have a very large chance to get the overall optimal solution, to

be verified below.

We compare our proposed algorithm with its two variants: an `SIC-if-possible` algorithm that takes the solution of Problem P1 when both Problem P1 and Problem P2 are feasible, and a `Never-SIC` algorithm that always takes the solution of Problem P2 even if both Problem P1 and Problem P2 are feasible. Fig. 3.6 shows secondary throughput performance of our proposed algorithm and the two variants for $\gamma^T = 0.25$ bps/Hz and 0.5 bps/Hz. It can be seen that the throughput of our proposed algorithm has similar trend as the channel access probability (the curve of $P(D_3)$ as shown in Fig. 3.5). By comparing Fig. 3.5 and Fig. 3.6, when $P_p$ increases beyond 20 dBm, the channel access probability and throughput of the secondary system in the proposed algorithm both decrease, but the decrease rate of the channel access probability is higher, explained as follows. When $P_p$ is high, the channel access probability is low, which means the ST has more chance to accumulate energy. Thus, at a slot, when the system works in cooperative transmission mode, the energy level of the ST is high, leading to high throughput at the slot. Thus, when $P_p$ increases beyond 20 dBm, the decrease rate of secondary system throughput is not as high as that of the channel access probability. From Fig. 3.6, the `SIC-if-possible` algorithm achieves almost the same performance as that of our proposed algorithm. This verifies our statement that when both Problem P1 and Problem P2 are feasible, if we directly take the solution of Problem P1, we have a very large chance to get the overall optimal solution. From Fig. 3.6, it can also be seen that there is a gap between the performance of the `Never-SIC` algorithm and that of our proposed algorithm. This is because it is with a very large probability (for example, more than 90% based on simulation results in Table 3.2) that the case with SIC performs better than the case without SIC.

Table 3.2: The number of time slots in which the maximal secondary throughput of Problem P2 is larger than that of Problem P1, and the number of time slots when both problems are feasible.

| | $P_p = 0$ dBm | $P_p = 10$ dBm |
|---|---|---|
| $\gamma^T = 0.1$ | 134/111690 | 20/219865 |
| $\gamma^T = 0.25$ | 150/74603 | 79/260055 |
| $\gamma^T = 0.5$ | 57/46421 | 89/218943 |
| $\gamma^T = 0.75$ | 5/31032 | 25/171037 |
| $\gamma^T = 1$ | 0/21085 | 1/132606 |

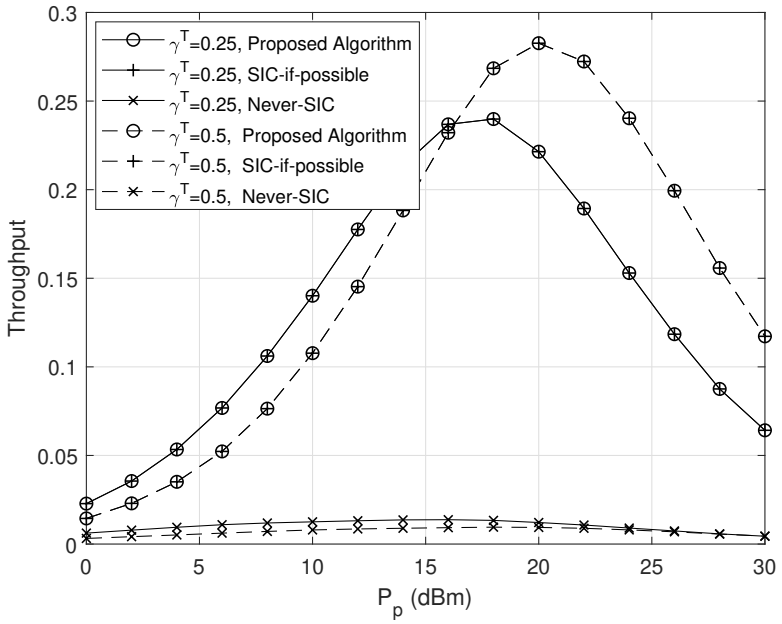


Figure 3.6: Secondary throughput of the proposed algorithm, the `SIC-if-possible` algorithm, and the `Never-SIC` algorithm.

**Remark**: The above observations do not mean that our Problem P2 is useless. This is because it is possible that Problem P1 is infeasible but Problem P2 is feasible, in which scenario we have to take the solution of Problem P2.

In our proposed algorithm, we use two levels of bisection search. In the inner bisection search, we keep shrinking the feasible region as shown in Algorithm 2.[13]

[13]Algorithm 2 is for the case with performing SIC. For the case without performing SIC, we also keep shrinking the feasible region in the inner bisection search.

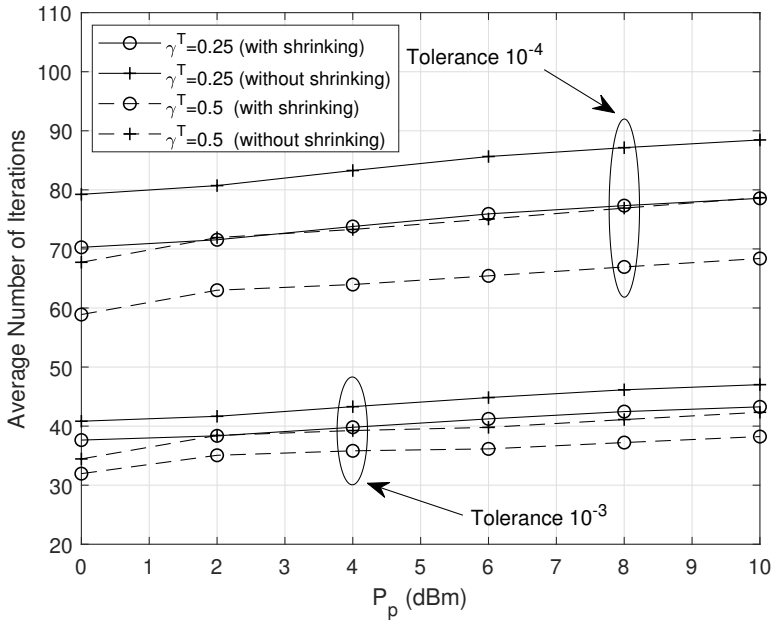


Figure 3.7: The average number of inner-bisecting iterations with and without shrinking.

To show the benefit of this, we compare two scenarios: our proposed algorithm is implemented with and without shrinking the feasible region in inner bisection search. Recall that the bisecting in the inner bisection search may not be implemented in Algorithm 1 (for example, when $\xi_{t,n}|_{\rho=f_1} \geq 0$ or $\xi_{t,n}|_{\rho=f_2} \geq 0$, Algorithm 2 terminates at Step 2, and thus, the bisecting is not implemented). Thus, in the comparison, we only consider the time slots when the bisecting in the inner bisection search is carried out (e.g., Algorithm 2 proceeds to Step 5). The average number of inner-bisecting iterations in a two-level bisection search algorithm is shown in Fig. 3.7, with the tolerance of convergence for bisection search being $\epsilon_t = \epsilon_\rho = 10^{-3}$ and $\epsilon_t = \epsilon_\rho = 10^{-4}$. It can be seen that shrinking feasible region in inner bisection search reduces the number of iterations in the inner bisection search by around 10%.

Now we try to compare our proposed algorithm with other algorithms. Since

no existing work in the literature considers overlay cognitive NOMA enhanced with TS-based SWIPT, here we compare with two algorithms: an OMA algorithm that partitions one time slot into one harvesting phase and three equal-length information transmission phases for links PT→ST&PR, ST→PR, and ST→SR, respectively, and an equal power allocation (EPA) algorithm that allocates equal amount of energy for transmitting the PT's signal and the ST's signal in the third phase of a time slot. Fig. 3.8 shows secondary throughput of our proposed algorithm, and the OMA and EPA algorithms. Clearly, our proposed algorithm outperforms the EPA and OMA algorithms in terms of higher secondary throughput. Moreover, performance gap of our algorithm with the EPA and OMA algorithms shrink at high $P_p$, explained as follows. At high $P_p$, the probability that the PT needs help is low (as observed in Fig. 3.5). So at time slots when the PT does not need help, the ST will only accumulate energy. Thus, at a time slot when the PT needs help, the ST has a large chance to have high energy, leading to high signal-to-noise ratio (SNR) at the SR. The throughput is a logarithm function of the SNR. The logarithm function is a concave function, i.e., at high SNR, increase of SNR does not lead to much increase in throughput. Thus, the throughput gap of our algorithm with the EPA and OMA algorithms shrink at high $P_p$. When $P_p$ is small, our algorithm, OMA and EPA algorithms have similar performances. This is because, as indicated in [11], compared to OMA, NOMA has performance loss when the SNR is low.

Distance plays a critical role in SWIPT-based systems, since the amount of harvested energy is largely determined by the distance from the RF transmitter. For the network topology considered in our simulation, we move the ST along the line segment of PT–ST, and fix the locations of other nodes. The secondary throughput is evaluated and illustrated in Fig. 3.9 for $P_p = 20$ dBm. It can be

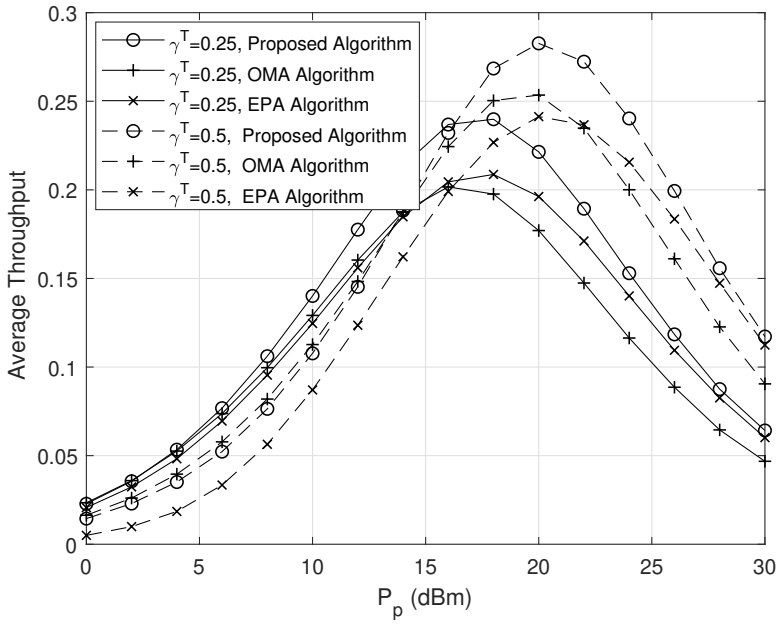


Figure 3.8: Secondary throughput of our proposed algorithm, the OMA and the EPA algorithms.

seen that the secondary throughout decreases with the increase of $d_{tt}$ (distance from the PT to the ST), due to the decay of harvested energy amount at the ST.

## 3.5 Conclusion and Further Discussion

### 3.5.1 Conclusion

We have investigated the secondary throughput maximization problem for an overlay cognitive NOMA network aided by SWIPT. For the research problems with and without SIC at the SR, we have transformed the problems to equivalent problems, the objective functions of which are proved to be quasiconcave. Optimal solutions for the equivalent problems have been found by two-level bisection search, and a method has been developed to reduce the number of iterations in the inner bisection search. Interestingly, the non-SIC case is possible to achieve a better secondary performance than the SIC case. Since this happens with a

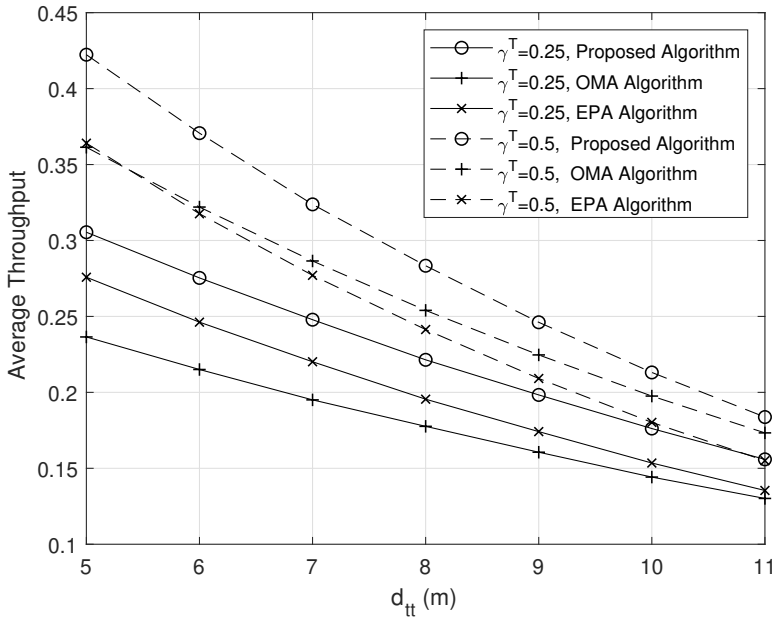


Figure 3.9: The impact of distance on secondary throughput of our proposed algorithm, the OMA and the EPA algorithms.

small probability as shown in our simulation results, if the ST just picks up the solution of the SIC case for a slot when both cases are feasible, it has a very large chance to achieve the optimal performance at the slot. By this method, the ST does not have to solve two optimization problems at the slot. On the other hand, at a slot when the non-SIC case is feasible but the SIC case is infeasible, the ST needs to take the solution of the non-SIC case.

Our numerical evaluation leads to the following observations. 1) When the transmit power of the PT increases, the ST's channel access probability and throughput first increase and then decease. The first increase is because when the PT's transmit power increases, the ST has a higher chance to decode the PT's signal and a higher chance to harvest more energy. The subsequent decrease of the ST's channel access probability and throughput is because a high transmit power of the PT increases the probability that the PT does not need help from

the ST. 2) Our proposed method can reduce the number of inner-bisection-search iterations by around 10%. 3) The distance between the PT and ST has a big effect on the secondary throughput.

### 3.5.2 Further Discussion

In our work, the ST harvests energy during the whole time slot under the direct primary transmission mode. Information transmission is not performed at the ST in this mode. Thus, the harvested energy will be stored into the battery. When our system works in the cooperative transmission mode, the ST uses up all the energy stored in the battery in a greedy manner if the ST is able to help the PT. A further research direction is to further consider another energy management strategy at the ST, which is different from the current greedy strategy. For such a consideration, the ST may transmit information by using only part of its energy stored in the battery. To achieve this goal, the dynamic programming technique can be adopted [87, 88]. Since the channel coefficients in future fading blocks are unknown, the modeling of the problem will become quite involved and challenging to solve. Then, approximations may be used to solve the problem.

## 3.6 Appendix

### 3.6.1 Derivation of Expression of Set $\mathcal{A}_2$

By expanding $P_e$ and $\mu_p$, the inequality $P_e g_{sp} - \mu_p \sigma^2 + P_p g_{pp} \geq 0$ is equivalent to $\frac{2(\eta P_p g_{tt} + E_0 - E_c) g_{sp}}{(1-\rho)\sigma^2} - \frac{2\eta P_p g_{tt} g_{sp}}{\sigma^2} + \frac{2 P_p g_{pp}}{\sigma^2} + 1 \geq 2^{\frac{2\gamma^T}{1-\rho}}$, which can be expressed in a compact form

$$\beta x + \theta \geq e^{\nu x}, \tag{3.48}$$

where $x = \frac{1}{1-\rho}$, $\beta = \frac{2(\eta P_p g_{tt} + E_0 - E_c) g_{sp}}{\sigma^2}$, $\theta = -\frac{2\eta P_p g_{tt} g_{sp}}{\sigma^2} + \frac{2 P_p g_{pp}}{\sigma^2} + 1$ and $\nu = 2(\ln 2)\gamma^T$.

From the geometric perspective, (3.48) can be seen as the portion of a straight line above an exponential line. If the equation (3.48) is feasible, this indicates that the two lines have intersection points. Whether there exist intersections between the two lines depends on whether equation

$$\beta x + \theta = e^{\nu x} \tag{3.49}$$

has roots. Multiplying both sides of (3.49) by $-\frac{\nu}{\beta}e^{-\nu x-\frac{\nu\theta}{\beta}}$, we have

$$-\frac{\nu(\beta x+\theta)}{\beta}e^{-\frac{\nu(\beta x+\theta)}{\beta}} = -\frac{\nu}{\beta}e^{-\frac{\nu\theta}{\beta}}. \tag{3.50}$$

Equation (3.50) has the format of $ae^a = b$, where $a$ is an unknown variable to be solved and $b < 0$ is a constant. According to [89, page 330, (1.5)], the Lambert W function $W_m(b)$, $m \in \{-1, 0\}$ can be used to represent the roots of the equation $ae^a = b$. There are three possible cases for the roots [89, page 331, Fig. 1].

- If $-e^{-1} < b < 0$, the equation has two roots denoted by $a_1 = W_{-1}(b)$ and $a_2 = W_0(b)$, where $W_{-1}(b)$ and $W_0(b)$ stand for the two real branches of Lambert W function $W_m(b)$.
- If $b = -e^{-1}$, the equation has only one root $a_1 = W_{-1}(-e^{-1}) = W_0(-e^{-1})$.
- If $b < -e^{-1}$, the equation has no root.

Accordingly, we have the following for equation (3.50) and for expression of interval $\mathcal{A}_2$.

- If $e^{-\frac{\nu\theta}{\beta}} < \frac{\beta}{\nu}e^{-1}$, the equation (3.50) has two roots, which can be obtained from

$$-\frac{\nu(\beta x+\theta)}{\beta} = W_m(-\frac{\nu}{\beta}e^{-\frac{\nu\theta}{\beta}}), m = -1, 0. \tag{3.51}$$

The two roots for $x$ are expressed as $x_1 = -\left(\frac{W_{-1}(-\frac{\nu}{\beta}e^{-\frac{\nu\theta}{\beta}})}{\nu} + \frac{\theta}{\beta}\right)$ and $x_2 = -\left(\frac{W_0(-\frac{\nu}{\beta}e^{-\frac{\nu\theta}{\beta}})}{\nu} + \frac{\theta}{\beta}\right)$. The corresponding roots for $\rho$ are given by $\rho_{r,i} = 1 - \frac{1}{x_i}, i \in \{1, 2\}$.

According to [89, page 331, Fig. 1], we have $W_0(-\frac{\nu}{\beta}e^{-\frac{\nu\theta}{\beta}}) > W_{-1}(-\frac{\nu}{\beta}e^{-\frac{\nu\theta}{\beta}})$ and thus, we have $x_1 > x_2$. Note that the values of $\rho$ should be within $[0, 1)$.

- If $x_1 > x_2 > 0$, we have $\mathcal{A}_2 = [\rho_{r,1}, \rho_{r,2}] \cap [0, 1)$.
- if $0 > x_1 > x_2$, we have $\mathcal{A}_2 = \emptyset$.
- if $x_1 > 0 > x_2$, we have $\mathcal{A}_2 = [-\infty, \rho_{r,1}] \cap [0, 1)$.

- If $e^{-\frac{\nu\theta}{\beta}} = \frac{\beta}{\nu}e^{-1}$, the equation (3.50) has one root, which is expressed as $\rho_r = 1 - \frac{1}{x_2}$. Thus, we have $\mathcal{A}_2 = \left\{1 - \frac{1}{x_2}\right\} \cap [0, 1)$.
- If $e^{-\frac{\nu\theta}{\beta}} > \frac{\beta}{\nu}e^{-1}$, the equation (3.50) has no root, and thus, $\mathcal{A}_2 = \emptyset$.

This completes the proof.

### 3.6.2 The Proof of Theorem 1

Define $\lambda_n = 1 + \frac{(P_e g_{sn} - \mu_n\sigma^2 + P_p g_{pn})g_{ss}}{(\mu_n+1)g_{sn}\sigma^2}$. The first and second order derivatives of objective function $R_{ss,n}$ are derived as

$$\begin{cases} \frac{\mathrm{d}R_{ss,n}}{\mathrm{d}\rho} = \frac{-1}{2}\log(\lambda_n) + \frac{1-\rho}{2(\ln 2)\lambda_n}\frac{\mathrm{d}\lambda_n}{\mathrm{d}\rho}, \\ \frac{\mathrm{d}^2R_{ss,n}}{\mathrm{d}\rho^2} = \frac{-1}{(\ln 2)\lambda_n}\frac{\mathrm{d}\lambda_n}{\mathrm{d}\rho} + \frac{1-\rho}{2(\ln 2)\lambda_n}\left(\frac{-1}{\lambda_n}(\frac{\mathrm{d}\lambda_n}{\mathrm{d}\rho})^2 + \frac{\mathrm{d}^2\lambda_n}{\mathrm{d}\rho^2}\right). \end{cases} \tag{3.52}$$

The expression of $\lambda_n$ can be rewritten as $\lambda_n = 1 + \frac{\lambda_a}{\lambda_b}$, where $\lambda_a \triangleq (P_e g_{sn} - \mu_n\sigma^2 + P_p g_{pn})g_{ss} \geq 0$ and $\lambda_b \triangleq (\mu_n + 1)g_{sn}\sigma^2 > 0$.[14] Then the first and second

[14]From (3.4), an equivalent form of $\lambda_n$ is $\lambda_n = 1 + \frac{(1-\alpha)P_e g_{ss}}{\sigma^2}$, which is always not less than 1. Since $\lambda_n = 1 + \frac{\lambda_a}{\lambda_b}$ and $\lambda_b \triangleq (\mu_n + 1)g_{sp}\sigma^2 > 0$ (noting that for $\rho \in \mathcal{B}$, we always have $\mu_n > 0$), we have $\lambda_a \geq 0$.

order derivatives of $\lambda_n$ are given by

$$\begin{cases} \frac{\mathrm{d}\lambda_n}{\mathrm{d}\rho} = \frac{1}{\lambda_b}\left(\frac{\mathrm{d}\lambda_a}{\mathrm{d}\rho} - \frac{\lambda_a}{\lambda_b}\frac{\mathrm{d}\lambda_b}{\mathrm{d}\rho}\right), \\ \frac{\mathrm{d}^2\lambda_n}{\mathrm{d}\rho^2} = \frac{-2\frac{\mathrm{d}\lambda_b}{\mathrm{d}\rho}\frac{\mathrm{d}\lambda_n}{\mathrm{d}\rho}}{\lambda_b} + \frac{\lambda_b\frac{\mathrm{d}^2\lambda_a}{\mathrm{d}\rho^2} - \lambda_a\frac{\mathrm{d}^2\lambda_b}{\mathrm{d}\rho^2}}{\lambda_b^2}, \end{cases} \tag{3.53}$$

where

$$\begin{cases} \frac{\mathrm{d}\lambda_a}{\mathrm{d}\rho} &= \left(g_{sn}\frac{\mathrm{d}P_e}{\mathrm{d}\rho} - \sigma^2\frac{\mathrm{d}\mu_n}{\mathrm{d}\rho}\right)g_{ss}, \\ \frac{\mathrm{d}^2\lambda_a}{\mathrm{d}\rho^2} &= \left(g_{sn}\frac{\mathrm{d}^2P_e}{\mathrm{d}\rho^2} - \sigma^2\frac{\mathrm{d}^2\mu_n}{\mathrm{d}\rho^2}\right)g_{ss}, \\ \frac{\mathrm{d}\lambda_b}{\mathrm{d}\rho} &= g_{sn}\sigma^2\frac{\mathrm{d}\mu_n}{\mathrm{d}\rho}, \\ \frac{\mathrm{d}^2\lambda_b}{\mathrm{d}\rho^2} &= g_{sn}\sigma^2\frac{\mathrm{d}^2\mu_n}{\mathrm{d}\rho^2}, \\ \frac{\mathrm{d}\mu_n}{\mathrm{d}\rho} &= \frac{2(\ln 2)\gamma^T}{(1-\rho)^2}2^{\frac{2\gamma^T}{1-\rho}}, \\ \frac{\mathrm{d}^2\mu_n}{\mathrm{d}\rho^2} &= \left(\frac{2(\ln 2)\gamma^T}{(1-\rho)^2}\right)^2 2^{\frac{2\gamma^T}{1-\rho}} + \frac{4(\ln 2)\gamma^T}{(1-\rho)^3}2^{\frac{2\gamma^T}{1-\rho}}, \end{cases} \tag{3.54}$$

with $\frac{\mathrm{d}P_e}{\mathrm{d}\rho}$ and $\frac{\mathrm{d}^2P_e}{\mathrm{d}\rho^2}$ given in (3.19).

According to [85, page 101], for a function over an interval, if its second order derivative is nonpositive when its first order derivative is 0, then the function is quasiconcave over the interval. Thus, next, we will show $R_{ss,n}$ is strictly quasiconcave, that is, $\frac{\mathrm{d}^2R_{ss,n}}{\mathrm{d}\rho^2} < 0$ when $\frac{\mathrm{d}R_{ss,n}}{\mathrm{d}\rho} = 0$. So in the rest of this proof, we only consider what happens when $\frac{\mathrm{d}R_{ss,n}}{\mathrm{d}\rho} = 0$.

Based on the first equation of (3.52), $\frac{\mathrm{d}R_{ss,n}}{\mathrm{d}\rho} = 0$ is equivalent to

$$-\lambda_n\log(\lambda_n) + \frac{1-\rho}{(\ln 2)}\frac{\mathrm{d}\lambda_n}{\mathrm{d}\rho} = 0. \tag{3.55}$$

As $\lambda_n$ is always not less than 1, $\lambda_n\log(\lambda_n)$ is nonnegative. Together with (3.55), we have $\frac{\mathrm{d}\lambda_n}{\mathrm{d}\rho} \geq 0$. From the second equation of (3.53), we have $\frac{\mathrm{d}^2\lambda_n}{\mathrm{d}\rho^2} = \frac{-2\frac{\mathrm{d}\lambda_b}{\mathrm{d}\rho}\frac{\mathrm{d}\lambda_n}{\mathrm{d}\rho}}{\lambda_b} + \omega \leq \omega$, where $\omega = \frac{\lambda_b\frac{\mathrm{d}^2\lambda_a}{\mathrm{d}\rho^2} - \lambda_a\frac{\mathrm{d}^2\lambda_b}{\mathrm{d}\rho^2}}{\lambda_b^2}$. Here the inequality is because $\frac{\mathrm{d}\lambda_b}{\mathrm{d}\rho} > 0$ (from (3.54)), $\frac{\mathrm{d}\lambda_n}{\mathrm{d}\rho} \geq 0$, and $\lambda_b > 0$ (from definition of $\lambda_b$).

Using $\frac{\mathrm{d}^2\lambda_n}{\mathrm{d}\rho^2} \leq \omega$,, we can obtain the following for the second order derivative of $R_{ss,n}$

$$\begin{aligned} \frac{\mathrm{d}^2R_{ss,n}}{\mathrm{d}\rho^2} &= \frac{-(1-\rho)\left(\frac{\mathrm{d}\lambda_n}{\mathrm{d}\rho}\right)^2}{2(\ln 2)(\lambda_n)^2} + \frac{(1-\rho)\frac{\mathrm{d}^2\lambda_n}{\mathrm{d}\rho^2} - 2\frac{\mathrm{d}\lambda_n}{\mathrm{d}\rho}}{2(\ln 2)\lambda_n} \\ &\leq \frac{-(1-\rho)\left(\frac{\mathrm{d}\lambda_n}{\mathrm{d}\rho}\right)^2}{2(\ln 2)(\lambda_n)^2} + \frac{(1-\rho)\omega - 2\frac{\mathrm{d}\lambda_n}{\mathrm{d}\rho}}{2(\ln 2)\lambda_n}, \end{aligned} \tag{3.56}$$

in which the first equality is from (3.52). Apparently, for the right hand side of the inequality in (3.56), the first term is nonpositive. Next we show that the second term is negative. The numerator of the second term can be rewritten as

$$(1-\rho)\omega - 2\frac{\mathrm{d}\lambda_n}{\mathrm{d}\rho} = \frac{\left((1-\rho)\frac{\mathrm{d}^2\lambda_a}{\mathrm{d}\rho^2} - 2\frac{\mathrm{d}\lambda_a}{\mathrm{d}\rho}\right)\lambda_b}{\lambda_b^2} - \frac{\left((1-\rho)\frac{\mathrm{d}^2\lambda_b}{\mathrm{d}\rho^2} - 2\frac{\mathrm{d}\lambda_b}{\mathrm{d}\rho}\right)\lambda_a}{\lambda_b^2}. \tag{3.57}$$

For the two terms on the right hand-side of (3.57), we have

$$\begin{cases} (1-\rho)\frac{\mathrm{d}^2\lambda_a}{\mathrm{d}\rho^2} - 2\frac{\mathrm{d}\lambda_a}{\mathrm{d}\rho} & = (1-\rho)(g_{sn}\frac{\mathrm{d}^2P_e}{\mathrm{d}\rho^2} - \sigma^2\frac{\mathrm{d}^2\mu_n}{\mathrm{d}\rho^2})g_{ss} \\ & \quad -2(g_{sn}\frac{\mathrm{d}P_e}{\mathrm{d}\rho} - \sigma^2\frac{\mathrm{d}\mu_n}{\mathrm{d}\rho})g_{ss} \\ & = -\left((1-\rho)\frac{\mathrm{d}^2\mu_n}{\mathrm{d}\rho^2} - 2\frac{\mathrm{d}\mu_n}{\mathrm{d}\rho}\right)\sigma^2 g_{ss} \\ & \overset{\text{(iv)}}{<} 0 \\ (1-\rho)\frac{\mathrm{d}^2\lambda_b}{\mathrm{d}\rho^2} - 2\frac{\mathrm{d}\lambda_b}{\mathrm{d}\rho} & = \left((1-\rho)\frac{\mathrm{d}^2\mu_n}{\mathrm{d}\rho^2} - 2\frac{\mathrm{d}\mu_n}{\mathrm{d}\rho}\right)g_{sn}\sigma^2 \\ & \overset{\text{(v)}}{>} 0, \end{cases} \tag{3.58}$$

in which steps (iv) and (v) come from the fact that

$$(1-\rho)\frac{\mathrm{d}^2\mu_n}{\mathrm{d}\rho^2} - 2\frac{\mathrm{d}\mu_n}{\mathrm{d}\rho} \overset{\text{(vi)}}{=} \frac{\left(2(\ln 2)\gamma^T\right)^2}{(1-\rho)^3}2^{\frac{2\gamma^T}{1-\rho}} > 0 \tag{3.59}$$

with step (vi) from (3.54).

Thus, the numerator of the second term on the right hand-side of the inequality in (3.56) is negative, and accordingly, we have $\frac{\mathrm{d}^2R_{ss,n}}{\mathrm{d}\rho^2} < 0$ when $\frac{\mathrm{d}R_{ss,n}}{\mathrm{d}\rho} = 0$. Therefore, $R_{ss,n}$ is a quasiconcave function. This completes the proof.

### 3.6.3 The Proof of Theorem 3

The function $\xi_{t,n}$ in (3.39) can be rewritten as

$$\xi_{t,n} = (1-\rho)(\mu_n+1) + (1-\rho)(P_e g_{sn} - \mu_n\sigma^2 + P_p g_{pn})\frac{g_{ss}}{g_{sn}\sigma^2} - (1-\rho)(\mu_n+1)2^{\frac{2t}{1-\rho}}. \tag{3.60}$$

The first order derivative of $\xi_{t,n}$ is given by (3.61), which is shown at the top

of the next page.

$$\begin{aligned}\frac{\mathrm{d}\xi_{t,n}}{\mathrm{d}\rho} =& -\mu_n - 1 + (1-\rho)\frac{\mathrm{d}\mu_n}{\mathrm{d}\rho} + \frac{2\eta P_p g_{tt} g_{ss}}{\sigma^2} + \\ & \frac{g_{ss}}{g_{sn}}\mu_n - (1-\rho)\frac{g_{ss}}{g_{sn}}\frac{\mathrm{d}\mu_n}{\mathrm{d}\rho} + (\mu_n+1)2^{\frac{2t}{1-\rho}} - \\ & (1-\rho)\frac{\mathrm{d}\mu_n}{\mathrm{d}\rho}2^{\frac{2t}{1-\rho}} - (\mu_n+1)\frac{2(\ln 2)t}{1-\rho}2^{\frac{2t}{1-\rho}} \\ =& (\frac{g_{ss}}{g_{sn}} - 1)\big(\mu_n - (1-\rho)\frac{\mathrm{d}\mu_n}{\mathrm{d}\rho}\big) + \frac{2\eta P_p g_{tt} g_{ss}}{\sigma^2} - 1 \\ & - \Big((\mu_n+1)\big(\frac{2(\ln 2)t}{1-\rho} - 1\big) + (1-\rho)\frac{\mathrm{d}\mu_n}{\mathrm{d}\rho}\Big)2^{\frac{2t}{1-\rho}}.\end{aligned} \tag{3.61}$$

Define a function $G(y)$ over $y \geq 0$ as

$$G(y) = \frac{\big(2(\ln 2)y\big)^2}{(1-\rho)^3}. \tag{3.62}$$

We have

$$G(\gamma^T + t) = G(\gamma^T) + G(t) + \frac{8(\ln 2)^2\gamma^T t}{(1-\rho)^3} \geq G(\gamma^T) + G(t). \tag{3.63}$$

The second order derivative of $(1-\rho)2^{\frac{2y}{1-\rho}}$ can be expressed as $\frac{\mathrm{d}^2\left((1-\rho)2^{\frac{2y}{1-\rho}}\right)}{\mathrm{d}\rho^2} = G(y)2^{\frac{2y}{1-\rho}}$. Based on this, the second order derivative of $\xi_{t,n}$ in (3.60) is given by

$$\frac{\mathrm{d}^2\xi_{t,n}}{\mathrm{d}\rho^2} = (1 - \frac{g_{ss}}{g_{sn}})G(\gamma^T)2^{\frac{2\gamma^T}{1-\rho}} + \frac{P_p g_{pn}}{\sigma^2}G(t)2^{\frac{2t}{1-\rho}} - G(\gamma^T + t)2^{\frac{2(t+\gamma^T)}{1-\rho}}, \tag{3.64}$$

which, by using inequality (3.73), leads to

$$\frac{\mathrm{d}^2\xi_{t,n}}{\mathrm{d}\rho^2} \leq (1 - \frac{g_{ss}}{g_{sn}} - 2^{\frac{2t}{1-\rho}})G(\gamma^T)2^{\frac{2\gamma^T}{1-\rho}} + (\frac{P_p g_{pn}}{\sigma^2} - 2^{\frac{2\gamma^T}{1-\rho}})G(t)2^{\frac{2t}{1-\rho}} \leq 0, \tag{3.65}$$

in which the second inequality comes from $1 - \frac{g_{ss}}{g_{sn}} - 2^{\frac{2t}{1-\rho}} \leq 1 - 2^{\frac{2t}{1-\rho}} \leq 0$ and $\frac{P_p g_{pn}}{\sigma^2} - 2^{\frac{2\gamma^T}{1-\rho}} = -(\mu_n + 1) < 0$.

This completes the proof.

### 3.6.4 The Proof of Theorem 4

Denote $\lambda^{w/o} = 1 + \frac{\lambda_a|_{n=p}}{\lambda_c}$, where $\lambda_a|_{n=p}$ and its first and second order derivatives are given in Appendix 3.6.2, and $\lambda_c$ and its first and second order derivatives are expressed as

$$\begin{cases} \lambda_c & = [\mu_p(P_e g_{sp} + \sigma^2) - P_p g_{pp}] g_{ss} \\ & \quad + (P_p g_{ps} + \sigma^2)(\mu_p + 1) g_{sp}, \\ \frac{\mathrm{d}\lambda_c}{\mathrm{d}\rho} & = (P_e g_{sp} + \sigma^2) g_{ss} \frac{\mathrm{d}\mu_p}{\mathrm{d}\rho} + \mu_p g_{sp} g_{ss} \frac{\mathrm{d}P_e}{\mathrm{d}\rho} \\ & \quad + (P_p g_{ps} + \sigma^2) g_{sp} \frac{\mathrm{d}\mu_p}{\mathrm{d}\rho}, \\ \frac{\mathrm{d}^2\lambda_c}{\mathrm{d}\rho^2} & = (P_e g_{sp} + \sigma^2) g_{ss} \frac{\mathrm{d}^2\mu_p}{\mathrm{d}\rho^2} + 2 g_{sp} g_{ss} \frac{\mathrm{d}\mu_p}{\mathrm{d}\rho} \frac{\mathrm{d}P_e}{\mathrm{d}\rho} \\ & \quad + \mu_p g_{sp} g_{ss} \frac{\mathrm{d}^2 P_e}{\mathrm{d}\rho^2} + (P_p g_{ps} + \sigma^2) g_{sp} \frac{\mathrm{d}^2\mu_p}{\mathrm{d}\rho^2}, \end{cases} \tag{3.66}$$

with $\frac{\mathrm{d}\mu_p}{\mathrm{d}\rho}$ and $\frac{\mathrm{d}^2\mu_p}{\mathrm{d}\rho^2}$ given in (3.54), and $\frac{\mathrm{d}P_e}{\mathrm{d}\rho}$ and $\frac{\mathrm{d}^2 P_e}{\mathrm{d}\rho^2}$ given in (3.19).

The proof for quasiconcavity of $R_{ss}^{w/o}$ is similar to that in Appendix 3.6.2 if we replace $\lambda_b$ in Appendix 3.6.2 by $\lambda_c$. The only difference is that we need to prove $(1-\rho)\frac{\mathrm{d}^2\lambda_c}{\mathrm{d}\rho^2} - 2\frac{\mathrm{d}\lambda_c}{\mathrm{d}\rho} > 0$ instead of the second equation of (3.58) in Appendix 3.6.2. Base on (3.66), we have

$$\begin{aligned} (1-\rho)\frac{\mathrm{d}^2\lambda_c}{\mathrm{d}\rho^2} - 2\frac{\mathrm{d}\lambda_c}{\mathrm{d}\rho} &\overset{\text{(vii)}}{=} \Big((1-\rho)\frac{\mathrm{d}^2\mu_p}{\mathrm{d}\rho^2} - 2\frac{\mathrm{d}\mu_p}{\mathrm{d}\rho}\Big) \\ &\quad \times \Big((P_e g_{sp} + \sigma^2) g_{ss} + (P_p g_{ps} + \sigma^2) g_{sp}\Big) + 2(1-\rho) g_{sp} g_{ss} \frac{\mathrm{d}\mu_p}{\mathrm{d}\rho} \frac{\mathrm{d}P_e}{\mathrm{d}\rho} \overset{\text{(viii)}}{>} 0, \end{aligned} \tag{3.67}$$

in which step (vii) uses (3.66) and $\frac{\mathrm{d}^2 P_e}{\mathrm{d}\rho^2} = \frac{2}{1-\rho}\frac{\mathrm{d}P_e}{\mathrm{d}\rho}$, and step (viii) uses (3.59), $\frac{\mathrm{d}\mu_p}{\mathrm{d}\rho} > 0$ from (3.54), and $\frac{\mathrm{d}P_e}{\mathrm{d}\rho} > 0$ from (3.19).

### 3.6.5 The Proof of Theorem 5

$\xi_t^{w/o}$ given in (3.47) can be rewritten as

$$\begin{aligned} \xi_t^{w/o} = (1-\rho)(\mu_p + 1)(P_e g_{ss} + P_p g_{ps} + \sigma^2) g_{sp} - \\ (1-\rho)\big\{[\mu_p(P_e g_{sp} + \sigma^2) - P_p g_{pp}] g_{ss} + \\ (P_p g_{ps} + \sigma^2)(\mu_p + 1) g_{sp}\big\} 2^{\frac{2t}{1-\rho}}. \end{aligned}$$

Defining $\chi \triangleq 2(\eta P_p g_{tt} + E_0 - E_c)$ and $\psi \triangleq 2\eta P_p g_{tt}$, $P_e$ given in (3.1) can be represented as

$$P_e = \frac{1}{(1-\rho)}\big(\chi - (1-\rho)\psi\big). \tag{3.68}$$

Using (3.68) and applying some math manipulations, $\xi_t^{w/o}$ can be expressed as

$$\xi_t^{w/o} = \phi_a + \phi_b - \phi_c - \phi_d - \phi_e, \tag{3.69}$$

in which

$$\begin{cases} \phi_a &= \big(\chi - (1-\rho)\psi\big)(2^{\frac{2\gamma^T}{1-\rho}} - \frac{P_p g_{pp}}{\sigma^2})g_{ss}g_{sp}, \\ \phi_b &= (1-\rho)(2^{\frac{2\gamma^T}{1-\rho}} - \frac{P_p g_{pp}}{\sigma^2})(P_p g_{ps} + \sigma^2)g_{sp}, \\ \phi_c &= \big(\chi - (1-\rho)\psi\big)(2^{\frac{2\gamma^T}{1-\rho}} - \frac{P_p g_{pp}}{\sigma^2} - 1)g_{ss}g_{sp}2^{\frac{2t}{1-\rho}}, \\ \phi_d &= (1-\rho)(2^{\frac{2\gamma^T}{1-\rho}} - \frac{2P_p g_{pp}}{\sigma^2} - 1)g_{ss}\sigma^2 2^{\frac{2t}{1-\rho}}, \\ \phi_e &= (1-\rho)(2^{\frac{2\gamma^T}{1-\rho}} - \frac{P_p g_{pp}}{\sigma^2})(P_p g_{ps} + \sigma^2)g_{sp}2^{\frac{2t}{1-\rho}}. \end{cases} \tag{3.70}$$

The first order derivative of $\xi_t^{w/o}$ is expressed by

$$\frac{\mathrm{d}\xi_t^{w/o}}{\mathrm{d}\rho} = \frac{\mathrm{d}\phi_a}{\mathrm{d}\rho} + \frac{\mathrm{d}\phi_b}{\mathrm{d}\rho} - \frac{\mathrm{d}\phi_c}{\mathrm{d}\rho} - \frac{\mathrm{d}\phi_d}{\mathrm{d}\rho} - \frac{\mathrm{d}\phi_e}{\mathrm{d}\rho}, \tag{3.71}$$

where

$$\begin{cases} \frac{\mathrm{d}\phi_a}{\mathrm{d}\rho} &= \big(\psi(\mu_p+1) + (1-\rho)P_e\frac{\mathrm{d}\mu_p}{\mathrm{d}\rho}\big)g_{ss}g_{sp}, \\ \frac{\mathrm{d}\phi_b}{\mathrm{d}\rho} &= \big(-\mu_p - 1 + (1-\rho)\frac{\mathrm{d}\mu_p}{\mathrm{d}\rho}\big)(P_p g_{ps} + \sigma^2)g_{sp}, \\ \frac{\mathrm{d}\phi_c}{\mathrm{d}\rho} &= \Big(\psi\mu_p + (1-\rho)P_e\big(\frac{\mathrm{d}\mu_p}{\mathrm{d}\rho} + \mu_p\frac{2(\ln 2)t}{(1-\rho)^2}\big)\Big)g_{ss}g_{sp}2^{\frac{2t}{1-\rho}}, \\ \frac{\mathrm{d}\phi_d}{\mathrm{d}\rho} &= \Big((1-\rho)\frac{\mathrm{d}\mu_p}{\mathrm{d}\rho} + (\mu_p - \frac{P_p g_{pp}}{\sigma^2})\big(\frac{2(\ln 2)t}{1-\rho} - 1\big)\Big)g_{ss}\sigma^2 2^{\frac{2t}{1-\rho}}, \\ \frac{\mathrm{d}\phi_e}{\mathrm{d}\rho} &= \Big((1-\rho)\frac{\mathrm{d}\mu_p}{\mathrm{d}\rho} + (\mu_p+1)\big(\frac{2(\ln 2)t}{1-\rho} - 1\big)\Big)(P_p g_{ps} + \\ & \quad \sigma^2)g_{sp}2^{\frac{2t}{1-\rho}}. \end{cases} \tag{3.72}$$

Define two functions $G(y)$ and $K(y)$ over $y \geq 0$ as $G(y) = \frac{\big(2(\ln 2)y\big)^2}{(1-\rho)^3}$ and $K(y) = \frac{4(\ln 2)y}{(1-\rho)^3} + \frac{\big(2(\ln 2)y\big)^2}{(1-\rho)^4}$, respectively. We have

$$G(\gamma^T + t) = G(\gamma^T) + G(t) + \frac{8(\ln 2)^2\gamma^T t}{(1-\rho)^3} \geq G(\gamma^T) + G(t), \tag{3.73}$$

$$K(\gamma^T+t)=K(\gamma^T)+K(t)+\frac{8(\ln 2)^2\gamma^T t}{(1-\rho)^4}\geq K(\gamma^T)+K(t). \tag{3.74}$$

Then using $G(y)$ and $K(y)$, the second order derivatives of $(1-\rho)2^{\frac{2y}{1-\rho}}$ and $2^{\frac{2y}{1-\rho}}$ are written as $\frac{\mathrm{d}^2((1-\rho)2^{\frac{2y}{1-\rho}})}{\mathrm{d}\rho^2}=G(y)2^{\frac{2y}{1-\rho}}$ and $\frac{\mathrm{d}^2(2^{\frac{2y}{1-\rho}})}{\mathrm{d}\rho^2}=K(y)2^{\frac{2y}{1-\rho}}$. Using this, we have

$$\begin{cases} \frac{\mathrm{d}^2\phi_a}{\mathrm{d}\rho^2} & =\big(\chi K(\gamma^T)-\psi G(\gamma^T)\big)g_{ss}g_{sp}2^{\frac{2\gamma^T}{1-\rho}}, \\ \frac{\mathrm{d}^2\phi_b}{\mathrm{d}\rho^2} & =G(\gamma^T)(P_pg_{ps}+\sigma^2)g_{sp}2^{\frac{2\gamma^T}{1-\rho}}, \\ \frac{\mathrm{d}^2\phi_c}{\mathrm{d}\rho^2} & =\Big(\big(\chi K(\gamma^T+t)-\psi G(\gamma^T+t)\big)2^{\frac{2(\gamma^T+t)}{1-\rho}} \\ & \quad -\big(\chi K(t)-\psi G(t)\big)(\frac{P_pg_{pp}}{\sigma^2}+1)2^{\frac{2t}{1-\rho}}\Big)g_{ss}g_{sp}, \\ \frac{\mathrm{d}^2\phi_d}{\mathrm{d}\rho^2} & =G(\gamma^T+t)g_{ss}\sigma^2 2^{\frac{2(\gamma^T+t)}{1-\rho}} \\ & \quad -G(t)(\frac{2P_pg_{pp}}{\sigma^2}+1)g_{ss}\sigma^2 2^{\frac{2t}{1-\rho}}, \\ \frac{\mathrm{d}^2\phi_e}{\mathrm{d}\rho^2} & =G(\gamma^T+t)(P_pg_{ps}+\sigma^2)g_{sp}2^{\frac{2(\gamma^T+t)}{1-\rho}} \\ & \quad -G(t)\frac{P_pg_{pp}}{\sigma^2}(P_pg_{ps}+\sigma^2)g_{sp}2^{\frac{2t}{1-\rho}}. \end{cases} \tag{3.75}$$

In the expressions for $\frac{\mathrm{d}^2\phi_a}{\mathrm{d}\rho^2}$ and $\frac{\mathrm{d}^2\phi_c}{\mathrm{d}\rho^2}$, both of them contain the item $\chi K(y)-\psi G(y)$, where $y$ takes the value $\gamma^T$, $t$, or $(\gamma^T+t)$. By checking $\chi K(y)-\psi G(y)$, it can be represented as the following

$$\begin{aligned} \chi K(y)-\psi G(y) &= \chi\big(\frac{4(\ln 2)y}{(1-\rho)^3}+\frac{\big(2(\ln 2)y\big)^2}{(1-\rho)^4}\big)-\psi\frac{\big(2(\ln 2)y\big)^2}{(1-\rho)^3} \\ &= \frac{4(\ln 2)y}{(1-\rho)^3}\big(\chi+(\ln 2)yP_e\big), \end{aligned} \tag{3.76}$$

in which the last equality uses (3.68).

Then $\frac{\mathrm{d}^2\phi_a}{\mathrm{d}\rho^2} - \frac{\mathrm{d}^2\phi_c}{\mathrm{d}\rho^2}$ is expressed as

$$\begin{aligned}
\frac{\mathrm{d}^2\phi_a}{\mathrm{d}\rho^2} - \frac{\mathrm{d}^2\phi_c}{\mathrm{d}\rho^2} &= \big(\chi K(\gamma^T) - \psi G(\gamma^T)\big) g_{ss} g_{sp} 2^{\frac{2\gamma^T}{1-\rho}} \\
&\quad - \Big( \big(\chi K(\gamma^T + t) - \psi G(\gamma^T + t)\big) 2^{\frac{2(\gamma^T + t)}{1-\rho}} \\
&\quad - \big(\chi K(t) - \psi G(t)\big) (\frac{P_p g_{pp}}{\sigma^2} + 1) 2^{\frac{2t}{1-\rho}} \Big) g_{ss} g_{sp} \\
&= -\Big( \frac{4(\ln 2)\gamma^T}{(1-\rho)^3} \big(\chi + (\ln 2)\gamma^T P_e\big) (2^{\frac{2t}{1-\rho}} - 1) 2^{\frac{2\gamma^T}{1-\rho}} \\
&\quad + \frac{4(\ln 2)t}{(1-\rho)^3} \big(\chi + (\ln 2) t P_e\big) \mu_p 2^{\frac{2t}{1-\rho}} \\
&\quad + \frac{8(\ln 2)^2 \gamma^T t}{(1-\rho)^3} P_e 2^{\frac{2(\gamma^T + t)}{1-\rho}} \Big) g_{ss} g_{sp} \leq 0, \quad (3.77)
\end{aligned}$$

in which the first equality is from (3.75), and the second equality is from the first equality of (3.73), the first equality of (3.74), (3.10), (3.76), and (3.68).

Moreover, we have

$$\begin{aligned}
\tfrac{\mathrm{d}^2\phi_b}{\mathrm{d}\rho^2} - \tfrac{\mathrm{d}^2\phi_e}{\mathrm{d}\rho^2} &\overset{\text{(ix)}}{=} -\Big( G(\gamma^T + t) 2^{\frac{2(\gamma^T + t)}{1-\rho}} - G(\gamma^T) 2^{\frac{2\gamma^T}{1-\rho}} \\
&\quad - G(t) \tfrac{P_p g_{pp}}{\sigma^2} 2^{\frac{2t}{1-\rho}} \Big) (P_p g_{ps} + \sigma^2) g_{sp} \\
&\overset{\text{(x)}}{\leq} -\Big( G(\gamma^T) (2^{\frac{2t}{1-\rho}} - 1) 2^{\frac{2\gamma^T}{1-\rho}} \\
&\quad + G(t)(\mu_p + 1) 2^{\frac{2t}{1-\rho}} \Big) (P_p g_{ps} + \sigma^2) g_{sp} \leq 0,
\end{aligned} \quad (3.78)$$

in which (ix) is from (3.75), and (x) is from $G(\gamma^T + t) \geq G(\gamma^T) + G(t)$ and (3.10).

From (3.75) and $G(\gamma^T + t) \geq G(\gamma^T) + G(t)$, we have

$$\begin{aligned}
\frac{\mathrm{d}^2\phi_d}{\mathrm{d}\rho^2} &\geq \big(G(\gamma^T) + G(t)\big) g_{ss} \sigma^2 2^{\frac{2(\gamma^T + t)}{1-\rho}} - G(t) \big(\frac{2P_p g_{pp}}{\sigma^2} + 1\big) g_{ss} \sigma^2 2^{\frac{2t}{1-\rho}} \\
&= G(\gamma^T) g_{ss} \sigma^2 2^{\frac{2(\gamma^T + t)}{1-\rho}} + G(t)(\mu_p - \frac{P_p g_{pp}}{\sigma^2}) g_{ss} \sigma^2 2^{\frac{2t}{1-\rho}} \quad (3.79) \\
&> 0.
\end{aligned}$$

Combining (3.69), (3.77), (3.78), and (3.79), it can be seen that $\frac{\mathrm{d}^2\xi_t^{w/o}}{\mathrm{d}\rho^2} < 0$, namely, $\xi_t^{w/o}$ is a strictly concave function.

# Chapter 4

# Optimal Resource Allocation in Downlink Non-orthogonal Multiple Access Networks

Since mobile users are usually deemed as individually distributed entities, they may only care about their own demand of resources, which yields the inapplicability of the centralized method. To overcome this drawback, game theory [43,44] is usually resorted to tackle the efficient distribution of radio resources. In OMA systems, various modeling of games have been adopted to address the resource allocation. In [90], two sellers, constrained by their own spectrum budget, dynamically compete to lease the spectrum to users over multiple stages. The optimal equilibrium solution to the amount of spectrum to lease for each seller at each stage is provided. To address the power allocation for multiple users in a multi-channel scenario with interferences, a Nash bargaining cooperative game is adopted in [91]. In [92], with the aim of enhancing user's achievable rate, each user purchases the power resource from the relay. The optimal pricing strategy at the relay and the power amount to purchase at each user are investigated. The work in [93] considers an underlay cognitive network, in which the interference power, incurred from the femtocell users, is sold by the macrocell BS. The

optimal solutions to the prices and the amount of purchased interference power are derived. The work in [94] investigates one cooperative multicast scenario, in which the relaying services, provided by the successful users, are purchased by the unsuccessful users. Then the pricing strategy is optimized under the framework of evolutionary and Stackelberg game.

When game theoretical models are leveraged in NOMA systems, the wireless system is envisioned to be not only spectrum-efficient, but also economically efficient [23,24,81,95,96]. The work in [95] studies a multi-carrier NOMA system, in which a matching game is designed to pair users and perform power allocation for users. By considering a CR-inspired NOMA system with a group of primary and secondary users, a matching game is exploited to pair each primary user with one secondary user, and allocate power for each user pair in [81]. For a small cell NOMA network, the problem of BS association and minimization of power consumption is conducted by using a coalition game in [96]. Under the Stackelberg game framework, sub-optimal solutions are provided to address the power allocation for downlink NOMA systems in [23] and [24], respectively. In specific, one iterative algorithm based on the interior point method is given in [23]. One optimal solution for the two-user case, and one sub-optimal heuristic algorithm for the multi-user case are investigated in [24].

In this chapter, we investigate the optimal solutions to the power allocation for the multi-user downlink NOMA networks by using the Stackelberg game. The contributions of our work are summarized as follows.

1) A novel game formulation is considered. Different from the adoption of fixed total allocated transmit power to users in [23] and [24], we consider a variable total allocated transmit power to users in our work. Also, a novel seller-level utility is adopted, which stands for the profit per unit power. The profit characterizes the

revenue from users' payments and the cost of providing transmit power.

2) The optimal solution is obtained for the formulated problems. Based on backward induction, the optimal solution to the buyer-level game is obtained first. Although the optimization problem at the seller-level game is non-convex, by using the inherent layered structure, a two-stage method is devised to tackle it. Specifically, in stage 1, we show there exists a closed-form solution for the three-user case. For the multi-user case, we provide an approach to transform the original optimization problem into a tractable form. Then an efficient iterative algorithm is also designed to identify the optimal solution to the transformed problem, in which one efficient search method and one user admission strategy are proposed. In stage 2, based on the concavity of the solution in stage 1, the utility function in this stage is proved to be quasiconcave, and thus, the optimal solution can be efficiently reached.

The rest of this chapter is organized as follows. In Section 4.1, the system model is outlined. For the considered problems, the optimal solution to the buyer-level game is offered in Section 4.2. Then at the seller-level game, the optimal solutions in stage 1 and stage 2 are provided in Section 4.3 and Section 4.4, respectively. In Section 4.5, simulation results are presented. At last, conclusion is given in Section 4.6. The symbols used in Chapter 4 are listed in Table 4.1.

# 4.1 System Model

## 4.1.1 Network Model

We consider a multi-user downlink NOMA network scenario, in which one BS serves $N$ users, forming the set $\mathcal{N} = \{1, 2, \ldots, N\}$. Time is partitioned into identical slots with unit length. The channel coefficient from the BS to user $i$ is denoted as $h_i$, $i \in \mathcal{N}$. We assume the channel is block faded, which indicates that

| Symbol | Meaning |
|---|---|
| $p_i$ | The transmit power for user $i$ |
| $h_i$ | The channel coefficient from the BS to user $i$ |
| $g_i$ | The channel power gain from the BS to user $i$ |
| $x_i$ | The information signal for user $i$ |
| $R_i$ | User $i$'s achievable rate |
| $P_0$ | Circuit power consumption at the BS |
| $n_i$ | AWGN noise at user $i$ |
| $\zeta_i$ | The price for the transmit power for user $i$ |
| $N$ | User number in the system |
| $Q$ | The total transmit power allocated to users |
| $U_s$ | The utility function at the BS |
| $C_0$ | The coefficients of cost for at the BS |
| $C_u$ | The gain per unit rate at the user side |

Table 4.1: The notations used in Chapter 4

the channel coefficient is fixed in one slot and varies independently in another different slot. Without loss of generality, the channel power gain, denoted as $g_i = |h_i|^2$, is ordered as: $g_1 \leq g_2 \leq \ldots \leq g_N$. The power consumption at the BS is divided into two parts, including the transmit power and circuit power consumption. The transmit power is constrained by the maximal value $P_t$, while the circuit power consumption is a constant $P_0$. At each time slot, the BS broadcasts a superimposed signal $\sum_{i=1}^{N} \sqrt{p_i} x_i$ to all users with the total allocated transmit power $\sum_{i=1}^{N} p_i = Q$, in which $p_i$ is the power allocated to user $i$ and $x_i$ is the information signal intended to user $i$.

User $i$ receives the signal of $y_i = \sum_{j=1}^{N} \sqrt{p_j} x_j h_i + n_i$, where $n_i$ is the background AWGN at user $i$, distributed as $n_i \sim \mathcal{CN}(0, \sigma^2)$. With the aim of decoding information, the SIC technique is leveraged to remove the interferences. In other words, the signal component from user $j$, $\forall j < i$, will be detected and subtracted.

Then user $i$'s achievable rate can be represented by

$$R_i = \log\left(1 + \frac{p_i g_i}{\sum_{j=i+1}^{N} p_j g_i + \sigma^2}\right). \tag{4.1}$$

### 4.1.2 Game Formulation

To perform the power allocation, a Stackelberg game model is adopted. In our game, the BS plays the role of the seller. The users play the role of the buyers. Then we can formulate the two levels of games.

**1) Seller-level Game**

As the seller, the BS decides the price $\xi_i$ of unit received power for user $i$. If the allocated power amount for user $i$ is $p_i$, the BS gains the revenue of $\sum_{i=1}^{N} \xi_i p_i g_i$ from all users' payments. Besides the revenue, the BS has the cost of $C_0 Q$ for providing total allocated transmit power $Q$ to users with the coefficient of $C_0$. Thus, the profit at the BS is denoted as $\sum_{i=1}^{N} \xi_i p_i g_i - C_0 Q$, which characterizes the revenue and cost. Afterwards, with the aim of maximizing the profit per unit consumed power, the utility function at the BS is defined as $U_s(\boldsymbol{\xi}, Q) = \frac{\sum_{i=1}^{N} \xi_i p_i g_i - C_0 Q}{P_0 + Q}$, in which $\boldsymbol{\xi} = [\xi_1, \xi_2, \ldots, \xi_N]^T$. Note that $P_0 + Q$ stands for the consumed power from the total allocated transmit power $Q$ and the circuit power $P_0$. Accordingly, we formulate the seller-level game into the following optimization problem.

*Problem P1:*

$$\max_{\boldsymbol{\xi}, Q} \quad U_s(\boldsymbol{\xi}, Q) = \frac{\sum_{i=1}^{N} \xi_i p_i g_i - C_0 Q}{P_0 + Q} \tag{4.2a}$$

$$\text{s.t.} \quad \sum_{i=1}^{N} p_i = Q \tag{4.2b}$$

$$Q \leq P_t. \tag{4.2c}$$

**2) Buyer-level Game**

The achievable rate $R_i$ is treated as the revenue at user $i$. Under the total allocated transmit power $Q$, the variable decided at user $i$ is the power $p_i$, which yields the cost of payment $\xi_i p_i g_i$. Thus, to maximize the profit, user $i$'s utility function is represented as $U_i(p_i, \boldsymbol{p}_{-i}) = C_u R_i - \xi_i p_i g_i$, where $C_u$ is the gain of per unit rate for each user, and $\boldsymbol{p}_{-i}$ stands for the power allocation for all other users except user $i$. Accordingly, we formulate the buyer-level game into an optimization problem as

*Problem P2:*

$$\max_{p_i} \quad U_i(p_i, \boldsymbol{p}_{-i}) = C_u R_i - \xi_i p_i g_i \tag{4.3a}$$

$$\text{s.t.} \quad 0 \leq p_i \leq Q. \tag{4.3b}$$

In the sequel, we solve the optimal solution to the formulated game.

## 4.2 Optimal Solution to the Buyer-level Game

Based on backward induction, to obtain the solution of Problem P2, by following a similar approach as [23], we observe the first order optimality.

Then under given $Q$ and $\boldsymbol{\xi}$, we take the first order derivative of $U_i(p_i, \boldsymbol{p}_{-i})$ with $p_i$, which is given as $\frac{\mathrm{d}U_i(p_i, \boldsymbol{p}_{-i})}{\mathrm{d}p_i} = \frac{C_u g_i}{\sum_{j=i}^{N} p_j g_i + \sigma^2} - \xi_i g_i$. After setting $\frac{\mathrm{d}U_i(p_i, \boldsymbol{p}_{-i})}{\mathrm{d}p_i} = 0$, the optimal solution $p_i^*$ at user $i$ can be written into a function of $\boldsymbol{\xi}$ as

$$p_i^* = \frac{C_u}{\xi_i g_i} - \frac{C_u}{\xi_{i+1} g_{i+1}} + \frac{\sigma^2}{g_{i+1}} - \frac{\sigma^2}{g_i}, \forall i \in \mathcal{N}, \tag{4.4}$$

in which $\frac{\sigma^2}{g_{N+1}} = 0$ and $\frac{1}{\xi_{N+1}} = 0$ are assumed.

*Remark*: Based on (4.4), we proceed to solve Problem P1 at the seller-level game. Due to its inherent layered structure, we decompose Problem P1 into two stages to obtain the optimal solution. To be specific, in stage 1, with given $Q$,

maximizing $U_s(\boldsymbol{\xi}, Q)$ is equivalent to maximizing $\sum_{i=1}^{N} \xi_i p_i g_i$. In stage 2, we will show that maximizing Problem P1 boils down to maximizing function $U_s(Q)$ with $Q$, and thus, we will get the optimal $Q$. In next section, the optimal solution in stage 1 is provided.

## 4.3 Optimal Solution to the Seller-level Game in Stage 1

At the seller-level game, for any given feasible $Q \in [0, P_t]$, one can check that maximizing Problem P1 in stage 1 is equivalent to maximizing

*Problem P3:*

$$\max_{\boldsymbol{\xi}} \quad H_s(\boldsymbol{\xi}) = \sum_{i=1}^{N} \xi_i p_i g_i \tag{4.5a}$$

$$\text{s.t.} \quad \sum_{i=1}^{N} p_i \leq Q. \tag{4.5b}$$

By using the optimal solution of Problem P2, we proceed to identify the equivalent representations of the objective and constraint functions in Problem P3.

### 4.3.1 Equivalent Representations in Problem P3

To facilitate the subsequent analysis, by denoting $\frac{1}{\zeta_i} = \frac{C_u}{\xi_i g_i}$, we further define $G_s(\boldsymbol{\zeta})$ as

$$G_s(\boldsymbol{\zeta}) = \sum_{j=1}^{N} (\frac{1}{\zeta_i} - \frac{1}{\zeta_{i+1}} + \frac{\sigma^2}{g_{i+1}} - \frac{\sigma^2}{g_i})\zeta_i, \tag{4.6}$$

where $\boldsymbol{\zeta} = [\zeta_1, \zeta_2, \ldots, \zeta_N]^T$.

As for the objective function (4.5a) in Problem P3, we have $H_s(\boldsymbol{\xi}) = C_u G_s(\boldsymbol{\zeta})$. Also, it can be observed that maximizing $H_s(\boldsymbol{\xi})$ is equivalent to maximizing $G_s(\boldsymbol{\zeta})$.

As for the constraint function (4.5b) in Problem P3, by checking $\frac{\mathrm{d}U_i(p_i,\boldsymbol{p}_{-i})}{\mathrm{d}p_i}$, (4.5b) can be equivalently written as

$$\frac{1}{\zeta_1} - \frac{\sigma^2}{g_1} \leq Q. \tag{4.7}$$

As for the feasible condition $p_i^* \geq 0$, from (4.4), it is equivalent to $\frac{1}{\zeta_i} - \frac{1}{\zeta_{i+1}} + \frac{\sigma^2}{g_{i+1}} - \frac{\sigma^2}{g_i} \geq 0$. In Problem P3, when the optimality is achieved, the constraint function (4.5b) should be active, which indicates $\frac{1}{\zeta_1} - \frac{\sigma^2}{g_1} = Q$. This can be readily observed from the equivalent Problem P4, to be presented in Section 4.3.3.

*Remark:* One can find that the equivalent objective function (4.6) is non-convex. However, through conducting some mathematical manipulations, we provide an efficient approach to solve the optimal solution of Problem P3. Specifically, we first show there exists a closed-form solution for the scenario with three users. For the general scenario with multiple users, we provide a method to efficiently obtain the optimal solution.

### 4.3.2 The Existence of Closed-form Solution to Problem P3 with Three Users

According to Section 4.3.1, when the user number $N = 3$, we equivalently solve

$$G_s(\boldsymbol{\zeta}) = (Q - \frac{1}{\zeta_2} + \frac{\sigma^2}{g_2})\frac{1}{Q + \frac{\sigma^2}{g_1}} + (\frac{1}{\zeta_2} - \frac{1}{\zeta_3} + \frac{\sigma^2}{g_3} - \frac{\sigma^2}{g_2})\zeta_2 + (\frac{1}{\zeta_3} - \frac{\sigma^2}{g_3})\zeta_3. \tag{4.8}$$

To obtain the optimal solutions, by taking the first order derivatives of $G_s(\boldsymbol{\zeta})$ with $\zeta_2$ and $\zeta_3$, we have

$$\begin{cases} \dfrac{\partial G_s(\boldsymbol{\zeta})}{\partial \zeta_2} = \dfrac{1}{\zeta_2^2}\dfrac{1}{Q + \frac{\sigma^2}{g_1}} - \dfrac{1}{\zeta_3} - \dfrac{\sigma^2}{g_2} + \dfrac{\sigma^2}{g_3} \\ \dfrac{\partial G_s(\boldsymbol{\zeta})}{\partial \zeta_3} = \dfrac{\zeta_2}{\zeta_3^2} - \dfrac{\sigma^2}{g_3}. \end{cases} \tag{4.9}$$

After setting $\frac{\partial G_s(\boldsymbol{\zeta})}{\partial \zeta_2} = 0$ and $\frac{\partial G_s(\boldsymbol{\zeta})}{\partial \zeta_3} = 0$, we have $\zeta_2 = \frac{\sigma^2}{g_3}\zeta_3^2$, and we also have a univariate quartic equation of $\zeta_3$, which is given as

$$(\frac{\sigma^2}{g_2} - \frac{\sigma^2}{g_3})\zeta_3^4 + \zeta_3^3 - \frac{g_3^2}{\sigma^4}\frac{1}{Q + \frac{\sigma^2}{g_1}} = 0. \tag{4.10}$$

It is known that quartic equation has a closed-form solution [97]. Thus, there are four possible solutions $\zeta_{3,n}, n \in \{1, 2, 3, 4\}$ for equation (4.10). The expressions for $\zeta_{3,n}$ are lengthy, and thus, they are omitted here.

For each real and positive $\zeta_{3,n}$, we denote $\boldsymbol{\zeta}_n = [\zeta_1, \zeta_{2,n}, \zeta_{3,n}]^T$, in which $\zeta_{2,n} = \frac{\sigma^2}{g_3}\zeta_{3,n}^2$ and $\zeta_1 = \frac{1}{Q+\frac{\sigma^2}{g_1}}$. Then we verify the feasibility and optimality of each $\boldsymbol{\zeta}_n$. As for the feasibility, the condition $\frac{1}{\zeta_i} - \frac{1}{\zeta_{i+1}} + \frac{\sigma^2}{g_{i+1}} - \frac{\sigma^2}{g_i} \geq 0$ should be satisfied. Among all the feasible $\boldsymbol{\zeta}_n$, the optimal one is $\boldsymbol{\zeta}^*$, which should maximize the objective function (4.8). Based on $\boldsymbol{\zeta}^*$ and (4.4), we can also obtain the optimal $\{\boldsymbol{\xi}^*, \boldsymbol{p}^*\}$, which constitutes the closed-form solution to the three-user case of Problem P3.

Since the root for an equation with a power higher than four does not generally have closed-form solution, an algorithm is devised to optimally solve the general scenario with multiple users.

### 4.3.3 Optimal Solution to Problem P3 with Multiple Users

For the general multi-user case of Problem P3, based on the equivalent representations in Section 4.3.1, we first conduct two transformations to yield a tractable form. Then we perform the dual analysis, based on which some useful features are identified. Subsequently, with the aid of these features, we design an iterative method to obtain the optimal solution.

**1) Problem Transformations**

Based on (4.6), we perform the first transformation by conducting a variable replacement, which is given as

$$t_i = (\frac{1}{\zeta_i} - \frac{1}{\zeta_{i+1}} + \frac{\sigma^2}{g_{i+1}} - \frac{\sigma^2}{g_i})\zeta_i, \forall i \in \mathcal{N}. \tag{4.11}$$

Note that for $t_i$, the condition $t_i < 1$ is always satisfied [1]. Based on the replacement in (4.11), our aim is to represent the equivalent objective function (4.6) and constraint function (4.7) by $\boldsymbol{t}$, where $\boldsymbol{t} = [t_1, t_2, \ldots, t_N]^T$. To this end, we first show how to represent $\boldsymbol{\zeta}$ by $\boldsymbol{t}$. Then we have the following Lemma.

**Lemma 5.** *The variable $\zeta_i$ can be represented as a function of $\boldsymbol{t}$, which is given by*

$$\zeta_i = \frac{1}{\sum_{k=i}^{N}(\prod_{n=i}^{k}\frac{1}{1-t_n})(\frac{\sigma^2}{g_k} - \frac{\sigma^2}{g_{k+1}})}, \forall i \in \mathcal{N}. \tag{4.12}$$

*Proof.* We prove this lemma by induction. When $i = N$, we have $t_N = (\frac{1}{\zeta_N} - \frac{\sigma^2}{g_N})\zeta_N$, and thus, we have $\zeta_N = (1 - t_N)\frac{g_N}{\sigma^2}$. When $i = m + 1$, we assume that $\zeta_{m+1} = \frac{1}{\sum_{k=m+1}^{N}(\prod_{n=m+1}^{k}\frac{1}{1-t_n})(\frac{\sigma^2}{g_k} - \frac{\sigma^2}{g_{k+1}})}$ holds. Afterwards, when $i = m$, we have $t_m = (\frac{1}{\zeta_m} - \frac{1}{\zeta_{m+1}} + \frac{\sigma^2}{g_{m+1}} - \frac{\sigma^2}{g_m})\zeta_m$. Then the variable $\zeta_m$ is given as

$$\begin{aligned}
\zeta_m &= \frac{1 - t_m}{\frac{1}{\zeta_{m+1}} + \frac{\sigma^2}{g_m} - \frac{\sigma^2}{g_{m+1}}} \\
&\overset{\text{(ii)}}{=} \frac{1 - t_m}{\sum_{k=m+1}^{N}(\prod_{n=m+1}^{k}\frac{1}{1-t_n})(\frac{\sigma^2}{g_k} - \frac{\sigma^2}{g_{k+1}}) + \frac{\sigma^2}{g_m} - \frac{\sigma^2}{g_{m+1}}} \\
&= \frac{1}{\sum_{k=m}^{N}(\prod_{n=m}^{k}\frac{1}{1-t_n})(\frac{\sigma^2}{g_k} - \frac{\sigma^2}{g_{k+1}})},
\end{aligned} \tag{4.13}$$

in which the assumption of $\zeta_{m+1}$ is used in (ii).

Therefore, the statement in (4.12) holds. □

[1] Since we have $\frac{1}{\zeta_{i+1}} + \frac{\sigma^2}{g_i} - \frac{\sigma^2}{g_{i+1}} > 0$, then we have $t_i = 1 - (\frac{1}{\zeta_{i+1}} + \frac{\sigma^2}{g_i} - \frac{\sigma^2}{g_{i+1}})\zeta_i < 1$.

*Remark:* With the aid of variable replacement, we are able to transform the equivalent objective function $G_s(\boldsymbol{\zeta})$ into $G_s(\boldsymbol{t}) = \sum_{i=1}^{N} t_i$. Moreover, based on Lemma 5, we are also able to convert the equivalent constraint function $\frac{1}{\zeta_1} - \frac{\sigma^2}{g_1} \leq Q$ into $\sum_{i=1}^{N}(\prod_{n=1}^{i} \frac{1}{1-t_n})(\frac{\sigma^2}{g_i} - \frac{\sigma^2}{g_{i+1}}) - \frac{\sigma^2}{g_1} \leq Q$.

Afterwards, we conduct a second transformation by introducing auxiliary variables in $\boldsymbol{s} = [s_1, s_2, \ldots, s_N]^T$. Accordingly, it yields the following problem as

*Problem P4:*

$$\max_{\boldsymbol{t},\boldsymbol{s}} \quad G_s(\boldsymbol{t}) = \sum_{i=1}^{N} t_i \tag{4.14a}$$

$$\text{s.t.} \quad \prod_{n=1}^{i} \frac{1}{1-t_n}(\frac{\sigma^2}{g_i} - \frac{\sigma^2}{g_{i+1}}) \leq s_i, \forall i \in \mathcal{N} \tag{4.14b}$$

$$\sum_{i=1}^{N} s_i - \frac{\sigma^2}{g_1} \leq Q \tag{4.14c}$$

$$t_i \geq 0, s_i \geq 0, \forall i \in \mathcal{N}. \tag{4.14d}$$

Note that $t_i \geq 0$ is equivalent to $\frac{1}{\zeta_i} - \frac{1}{\zeta_{i+1}} + \frac{\sigma^2}{g_{i+1}} - \frac{\sigma^2}{g_i} \geq 0$. Moreover, all constraint functions in (4.14b) and (4.14c) should be active at the optimality of Problem P4, which means maximizing Problem P4 is equivalent to maximizing Problem P3.

By observing Problem P4, we have two useful features, which are given in the following two Lemmas.

**Lemma 6.** *The constraint function (4.14b) is quasi-convex with* $\boldsymbol{t}$ *and* $\boldsymbol{s}$.

*Proof.* Since $s_i > 0$ and $0 \leq t_i < 1$, $\forall i \in \mathcal{N}$, inspecting (4.14b) is equivalent to inspecting $\omega_i(\boldsymbol{t}, \boldsymbol{s}) = \prod_{n=1}^{i} \frac{1}{1-t_n}(\frac{\sigma^2}{g_i} - \frac{\sigma^2}{g_{i+1}})\frac{1}{s_i}$. According to [85], for a fixed non-negative number $y$, if the sub-level set $\{(\boldsymbol{t}, \boldsymbol{s})|\omega_i(\boldsymbol{t}, \boldsymbol{s}) \leq y\}$ is a convex set, the function $\omega_i(\boldsymbol{t}, \boldsymbol{s})$ is quasi-convex. As taking logarithm does not impact set $\{(\boldsymbol{t}, \boldsymbol{s})|\omega_i(\boldsymbol{t}, \boldsymbol{s}) \leq y\}$, it subsequently leads to $\{(\boldsymbol{t}, \boldsymbol{s})|\omega_i(\boldsymbol{t}, \boldsymbol{s}) \leq y\} =$

$\{(\boldsymbol{t},\boldsymbol{s})|\sum_{n=1}^{i}\log(\frac{1-t_n}{\frac{\sigma^2}{g_i}-\frac{\sigma^2}{g_{i+1}}})+\log(s_i)\geq-\log(y)\}$, and thus, $\{(\boldsymbol{t},\boldsymbol{s})|\omega_i(\boldsymbol{t},\boldsymbol{s})\leq y\}$ is a convex set.

Therefore, the constraint function (4.14b) is quasi-convex. □

**Lemma 7.** *When the optimality is achieved, we have* $t_1 \leq t_2 \leq \ldots \leq t_N$.

*Proof.* See Appendix 4.7.1 □

Note that Lemma 7 can be treated as a constraint function for Problem P4, which is leveraged in the subsequent analysis.

**2) Dual Analysis**

In Problem P4, the objective function is linear, and the constraint function is quasi-convex. This indicates Problem P4 is a quasi-convex program. Hence, the Karush–Kuhn–Tucker (KKT) condition is sufficient in terms of optimality [98,99]. Accordingly, the Lagrangian function is given as

$$\mathcal{L}=\sum_{i=1}^{N}t_i-\sum_{i=1}^{N}\lambda_i\Big\{\prod_{n=1}^{i}\frac{1}{1-t_n}(\frac{\sigma^2}{g_i}-\frac{\sigma^2}{g_{i+1}})-s_i\Big\}- \mu(\sum_{i=1}^{N}s_i-\frac{\sigma^2}{g_1}-Q)+\sum_{i=1}^{N}\chi_i t_i, \quad (4.15)$$

where $\mu$, $\lambda_i$, $\chi_i$ and $\psi_i$, $i\in\mathcal{N}$, are Lagrangian multipliers associated with the constraint functions. Meanwhile, the KKT conditions are expressed as

$$\frac{\partial\mathcal{L}}{\partial t_i}=1-\sum_{k=i}^{N}\lambda_k\prod_{n=1}^{k}\frac{1}{1-t_n}(\frac{\sigma^2}{g_k}-\frac{\sigma^2}{g_{k+1}})\frac{1}{1-t_i}+\chi_i=0,\forall i\in\mathcal{N} \quad (4.16a)$$

$$\frac{\partial\mathcal{L}}{\partial s_i}=\lambda_i-\mu=0,\forall i\in\mathcal{N} \quad (4.16b)$$

$$\lambda_i\Big\{\prod_{n=1}^{i}\frac{1}{1-t_n}(\frac{\sigma^2}{g_i}-\frac{\sigma^2}{g_{i+1}})-s_i\Big\}=0,\forall i\in\mathcal{N} \quad (4.16c)$$

$$\mu(\sum_{i=1}^{N}s_i-\frac{\sigma^2}{g_1}-Q)=0 \quad (4.16d)$$

$$\chi_i t_i=0,\forall i\in\mathcal{N}. \quad (4.16e)$$

For the KKT conditions in (4.16a)-(4.16e), we have the observations as follows.

- We have $\lambda_i = \mu$, $\forall i \in \mathcal{N}$, which can be obtained from (4.16b). We have $\mu > 0$, which can be verified from $\lambda_N > 0$.

- When (4.15) is maximized for a fixed $\mu$, there exists a user (say $j^\dagger$), satisfying conditions $t_i > 0$, $\forall i \in \mathcal{F} = \{j^\dagger, \ldots, N\}$ and $t_i = 0$, $\forall i \in \mathcal{N} \backslash \mathcal{F}$. This feature is due to the aforementioned increasing property of $t_i$ in Lemma 7. Since we do not know which user is $j^\dagger$, to identify the solution to $t_i$, we will treat one feasible user as $j^\dagger$, and call it a possible last-admitted user. When (4.15) is maximized, the possible last-admitted user is called the optimal last-admitted user.

- We have $\chi_i = 0$, $\forall i \in \mathcal{F}$ and $\chi_i > 0$, $\forall i \in \mathcal{N} \backslash \mathcal{F}$.

- We have $t_N > 0$. If we assume $t_N = 0$, we must have $t_i = 0$, $\forall i \in \mathcal{N}$, which is obviously not optimal.

*Remark:* Based on Lemma 7, there exists a maximal number of feasible users under given $\mu$. Thus, we should find the maximal number of feasible users, and solve the optimal $\boldsymbol{t}^*$ for the feasible users. Since we do not know which user is feasible, we first assume one user is feasible, and we treat it as the possible last-admitted user $j^\dagger$. Although it can be seen from the KKT equations that the variables in $\boldsymbol{t}$ are coupled together, we provide a method to efficiently solve $\boldsymbol{t}$. Subsequently, we can design a user admission strategy to find the maximal number of feasible users under given $\mu$. Also, we identify the $\boldsymbol{t}^*$ that maximizes (4.15). Afterwards, we update $\mu$. In such a way, the optimal solution to Problem P4 can be found. Accordingly, the overall solving procedure to solve Problem P4 is provided in Algorithm 3.

Then if one user is assumed to be feasible under fixed $\mu$, we show how to solve $\boldsymbol{t}$.

**3) Solving $\boldsymbol{t}$ under Given $\mu$ and $j^\dagger$**

For a given $\mu$, we assume one user is feasible, and it is set as the possible last-admitted user $j^\dagger$. Then we have $t_i > 0$, $\forall i \in \mathcal{F}$ and $t_i = 0$, $\forall i \in \mathcal{N}\backslash\mathcal{F}$. To obtain the solution to $t_i$, $\forall i \in \mathcal{F}$, we have one useful feature, which is given as follows.

**Theorem 6.** *For a given $\mu$, the optimization variable $t_i$, $i \in \mathcal{F}\backslash j^\dagger$, can be recursively represented by $t_{j^\dagger}$, based on the relationship of*

$$t_i = t_{i-1} + \mu \prod_{n=j^\dagger}^{i-1} \frac{1}{1-t_n}\left(\frac{\sigma^2}{g_{i-1}} - \frac{\sigma^2}{g_i}\right). \tag{4.17}$$

*Proof.* By observing the KKT condition, if we multiply the both sides of (4.16a) by $1 - t_i$, we have

$$1 - t_i = \mu \sum_{k=i}^{N}\left(\prod_{n=j^\dagger}^{k} \frac{1}{1-t_n}\right)\left(\frac{\sigma^2}{g_k} - \frac{\sigma^2}{g_{k+1}}\right). \tag{4.18}$$

Similarly, from (4.16a), we have

$$1 - t_{i-1} = \mu \sum_{k=i-1}^{N}\left(\prod_{n=j^\dagger}^{k} \frac{1}{1-t_n}\right)\left(\frac{\sigma^2}{g_k} - \frac{\sigma^2}{g_{k+1}}\right). \tag{4.19}$$

By subtracting (4.18) from (4.19), we can obtain (4.17).

This completes the proof. □

*Remark:* According to Theorem 6, it can be seen that $t_i$ is a function of $t_k$, $j^\dagger \leq k \leq i-1$. Also, based on (4.17), by further iteratively expanding $t_{i-1}$ backward until $t_{j^\dagger}$, we have another equivalent form of $t_i$ as $t_i = t_{j^\dagger} + \mu \sum_{k=j^\dagger}^{i-1}(\prod_{n=j^\dagger}^{k} \frac{1}{1-t_n})(\frac{\sigma^2}{g_k} - \frac{\sigma^2}{g_{k+1}})$. From this expression, if we check $i$ from $j^\dagger + 1$ to $N$, we can find that each $t_i$ can be uniquely determined by $t_{j^\dagger}$. Consequently,

due to the *one-to-one* mapping, $t_i$ is a *univariate* function of $t_{j^\dagger}$. Indeed, we can treat (4.17) as a *semi-closed form* solution for $t_i$.

Accordingly, when $t_{j^\dagger} = x$, the value of $t_i$, $i \in \mathcal{F}$, can be determined by $x$, which is denoted as $t_i(j^\dagger, x)$. [2] Moreover, finding the solution to KKT condition (4.16a) is equivalent to finding the zero point of $w_i(j^\dagger, x) = 1 - t_i(j^\dagger, x) - \mu \sum_{k=i}^{N} (\prod_{n=j^\dagger}^{k} \frac{1}{1-t_n(j^\dagger,x)})(\frac{\sigma^2}{g_k} - \frac{\sigma^2}{g_{k+1}})$. Note that for any $i \in \mathcal{F}$, if we substitute $t_i(j^\dagger, x)$ into $w_i(j^\dagger, x)$, we can obtain the same equation. Therefore, to obtain the solution of $t_{j^\dagger}$, we can efficiently search the root of $w_i(j^\dagger, x) = 0$ for any $i \in \mathcal{F}$, which is denoted as $x^*$. Since $w_i(j^\dagger, x)$ is a univariate and decreasing function of $x$, $x^*$ can be identified by existing numerical methods, such as bisection. The solution to $t_i$ can also be obtained as $t_i(j^\dagger, x^*)$.

**4) User Admission Strategy, Determining Optimal $\boldsymbol{t}^*$ for Given $\mu$ and Updating $\mu$**

Then we design a user admission strategy to determine the user admission set $\mathcal{F}_a$, as shown in Algorithm 2. The set $\mathcal{F}_a$ has the maximal number of feasible users, in which each feasible user $i$, $i \in \mathcal{F}_a$, has a nonzero $t_i$ satisfying the KKT condition (4.16a).

In Algorithm 2, we denote $\mathcal{F}_c$ as the set that includes the current admitted users. Since user $N$ should always be admitted, $\mathcal{F}_c$ is initialized as $\mathcal{F}_c = \{N\}$. Moreover, due to the increasing property of $\boldsymbol{t}$ from Lemma 7, users having larger channel gains should be admitted first. Users should be sequentially determined whether to be admitted into $\mathcal{F}_c$ backward from $N-1$ to 1.

We show how to admit a new user $u_c$. We suppose users who have larger channel gains than user $u_c$ have been successfully admitted, and thus, we set $\mathcal{F}_c = \{u_c + 1, \ldots, N\}$. Then user $u_c$ is tentatively treated as a possible last-

[2] When $i = j^\dagger$, we have $t_{j^\dagger}(j^\dagger, x) = x$.

admitted user $j^{\dagger}$. Consequently, based on KKT condition (4.16a) and Theorem 6, the feasibilities of the already admitted users in $\mathcal{F}_c$ will be impacted if user $u_c$ is admitted. The impacts are given in the two facts as follows.

- **Fact 1:** the minimal feasible value of $t_i$, $i \in \mathcal{F}_c$, will increase when a new user $u_c$ is admitted. User $u_c$ should not be admitted if $t_i(u_c, 0) \geq 1$ happens for any user $i$ in $\mathcal{F}_c$.

  Prior to admitting user $u_c$, user $u_c + 1$ is the smallest feasible user. The minimal feasible value of $t_{u_c+1}$ is 0. For user $i$ in $\mathcal{F}_c$, the minimal feasible value of $t_i$ is $\min\{t_i\} = t_i(u_c + 1, 0)$ [3]. After admitting user $u_c$, the minimal feasible value of $t_{u_c}$ is 0. Moreover, due to the recursive form of $t_i(j^{\dagger}, x)$, for user $i$ in $\mathcal{F}_c$, the minimal feasible $t_i$ changes from $t_i(u_c + 1, 0)$ to $t_i(u_c, 0)$. It can be observed that $t_i(u_c, 0) > t_i(u_c + 1, 0)$, which can be readily verified that $\min\{t_{u_c+1}\} = t_{u_c+1}(u_c, 0) > t_{u_c+1}(u_c + 1, 0) = 0$. Thus, the minimal feasible value of $t_i$ will increase.

  According to Lemma 7, any user in $\mathcal{F}_c$ yields a higher $t_i$ than user $u_c$. It means user $u_c$ should not be admitted if any user $i$ in $\mathcal{F}_c$ becomes infeasible. Recall that a feasible $t_i$ is constrained by $0 \leq t_i < 1$. When user $u_c$ is admitted, it is possible that $t_i(u_c, 0) \geq 1$ may happen and user $i$ may become infeasible. In this case, user $u_c$ should not be admitted.

- **Fact 2:** the root of $w_i(u_c, x) = 0$ exists when $w_i(u_c, 0) > 0$ is satisfied.

  As aforementioned, the optimal solution to $t_{u_c}$ can be found by searching the root of $w_i(u_c, x) = 0$. We know that function $w_i(u_c, x)$ is continuous and monotonically decreasing with $x$. Also, as $t_N \to 1$, we have $w_i(u_c, x) \to -\infty$. Thus, the root exists when $w_i(u_c, 0) > 0$ is satisfied. Otherwise, when

[3] Here we have $t_{u_c+1}(u_c + 1, 0) = 0$.

$w_i(u_c, 0) < 0$ happens, it indicates that KKT conditions cannot be satisfied for users in $\mathcal{F}_c$, which indicates user $u_c$ cannot be admitted.

Based on the above two facts, user $u_c$ should be successfully admitted only when two feasibility conditions are satisfied, which include $t_i(u_c, 0) < 1$, $\forall i \in \mathcal{F}_c$ and $w_i(u_c, 0) > 0$, for any $i \in \mathcal{F}_c$. Thus, by using Algorithm 2, each feasible user will be admitted in a one-by-one manner. In such a way, the user admission set $\mathcal{F}_a$ can be determined.

After obtaining the user admission set $\mathcal{F}_a$, we treat each user in $\mathcal{F}_a$ as a possible last-admitted user $j^\dagger$, and then identify the solution to $\boldsymbol{t}$ by using one bisection. For fixed $\mu$, we search all the feasible users in $\mathcal{F}_a$. The optimal solution $\boldsymbol{t}^*$ to (4.15) is identified under the possible last-admitted user that maximizes (4.15). This user is also the optimal last-admitted user.

To update the multiplier $\mu$, the sub-gradient method [85, 100] is exploited. A sub-gradient to update the Lagrangian multiplier $\mu$ is given by $d(\mu) = Q + \frac{\sigma^2}{g_1} - \sum_{i=1}^{N} s_i$, in which $s_i$ is calculated when constraint functions (4.14b) and (4.14c) are active.

**5) Iterative Algorithm to Solve Problem P4**

Based on the aforementioned analysis, we can design an iterative algorithm to obtain the optimal solution to our Problem P4, as shown in Algorithm 3. The overall solving process is described as follows. For a fixed multiplier $\mu_n$ in the $n$-th iteration, the user admission set $\mathcal{F}_a$ can be determined by Algorithm 2. Subsequently, for each possible last-admitted user, we determine the solution to $\boldsymbol{t}$. Under fixed $\mu_n$, the optimal solution $\boldsymbol{t}^*$ is found when function (4.15) is maximized under the optimal last-admitted user. Afterwards, we use the sub-gradient method to calculate a new sub-gradient. Our algorithm continues to

**Algorithm 2:** User Admission Strategy

**Input:** The power budget $Q$ and channel power gains for $N$ users
**Output:** The user admission set $\mathcal{F}_a$

```
Initialize the set F_c as F_c = {N};
for u_c = N − 1 : −1 : 1 do
    flag=1;
    for i = u_c + 1 : 1 : N do
        Calculate t_i(u_c, 0);
        if t_i(u_c, 0) > 1 then
            flag=0; Break;
    if flag==1 then
        Calculate w_i(u_c, 0) for any u_c + 1 ≤ i ≤ N;
        if w_i(u_c, 0) > 0 then
            F_c = F_c ∪ {u_c};
        else
            F_a = F_c; Break;
    else
        F_a = F_c; Break;
```

update $\mu_n$ until $n$ reaches the maximal iteration number $M_\epsilon$, which is a predefined number for convergence. When our iterative algorithm converges, we can obtain the overall optimal $\boldsymbol{t}^*$. Then from (4.12), the optimal $\boldsymbol{\zeta}^*$ and the optimal $\boldsymbol{\xi}^*$ to Problem P3 can also be found.

## 4.4 Optimal Solution to the Seller-level Game in Stage 2

We denote the maximal value of $G_s(\boldsymbol{\zeta})$ in stage 1 as $F(Q) = \max_{\boldsymbol{\zeta}} G_s(\boldsymbol{\zeta})$. In stage 2, by using $F(Q)$, our Problem P1 boils down to the following optimization problem.

**Algorithm 3:** Iterative Algorithm to Solve Problem P4

**Input:** The transmit power $Q$, channel gain $g_i$ and noise variance $\sigma^2$

**Output:** The optimal objective value of $G_s(\boldsymbol{t}^*)$, and the optimal solutions to $\boldsymbol{t}^*$, $\boldsymbol{\zeta}^*$ and $\boldsymbol{p}^*$

1 Set $n = 0$, and an initial value of $\mu_0$;
2 For a fixed $\mu_n$, perform Algorithm 2 to obtain the user admission set $\mathcal{F}_a$;
3 **if** $|\mathcal{F}_a| > 1$ **then**
4  $q = 0$, $L_0 = 0$;
5  **for** $i = N - |\mathcal{F}_a| + 1 : 1 : N$ **do**
6  Set user $i$ as user $j^\dagger$; Calculate $\boldsymbol{t}$ by using bisection; Obtain the value of $\mathcal{L}$ in (4.15);
7  **if** $\mathcal{L} > L_0$ **then**
8  $q = i$, $L_0 = \mathcal{L}$, $\boldsymbol{t}^*$=$\boldsymbol{t}$;
9  Obtain $G_s(\boldsymbol{t}^*) = \sum_{i=j^\dagger}^{N} t_i^*$;
10 **else**
11  Calculate $t_N^*$ by $t_N^* = 1 - \sqrt{\frac{\mu_n \sigma^2}{g_N}}$; Obtain $G_s(\boldsymbol{t}^*) = t_N^*$;
12 Set $n = n + 1$; Calculate $\mu_n$ by using the sub-gradient method;
13 **if** $n \leq M_\epsilon$ **then**
14  Go back to Line 2;
15 **else**
16  Calculate the optimal $\boldsymbol{\zeta}^*$ and powers $\boldsymbol{p}^*$ by (4.12) and (4.4).
17  Terminate the algorithm.

*Problem P5:*

$$\max_{Q} \ U_s(Q) = \frac{C_u F(Q) - C_0 Q}{P_0 + Q} \tag{4.20a}$$

$$\text{s.t.} \ \ Q \leq P_t \tag{4.20b}$$

One can check that Problem P5 is non-convex. However, we show it can be efficiently solved by leveraging $F(Q)$. For $F(Q)$, we have a useful feature, as stated below.

**Theorem 7.** *Function $F(Q)$ is monotonically increasing and concave with $Q$.*

*Proof.* First we show the monotonicity of $F(Q)$. Given any feasible $Q_a$ and $Q_b$ satisfying $0 \leq Q_a \leq Q_b \leq P_t$, we assume the associated optimal solutions

for Problem P4 are $\{t_{m,i}\}$ and $\{s_{m,i}\}$, $\forall i \in \mathcal{N}$, $m \in \{a,b\}$. Then we have $\prod_{n=1}^{i} \frac{1}{1-t_{m,n}}(\frac{\sigma^2}{g_i} - \frac{\sigma^2}{g_{i+1}}) = s_{m,i}$, $\forall i \in \mathcal{N}$ and $\sum_{i=1}^{N} s_{m,i} - \frac{\sigma^2}{g_1} = Q_m$. We construct another set of feasible solution $\{t_{c,i}\}$ and $\{s_{c,i}\}$ with objective value $\bar{F}(Q_b)$, satisfying $\sum_{i=1}^{N} s_{c,i} - \frac{\sigma^2}{g_1} = Q_b$, $s_{c,i} = s_{a,i}$ and $t_{c,i} = t_{a,i}$, $\forall i \in \mathcal{N}\backslash N$. Since $Q_a \leq Q_b$, we have $s_{a,N} \leq s_{c,N}$ and $t_{a,N} \leq t_{c,N}$.

Then we have

$$F(Q_a) \overset{\text{(iii)}}{\leq} \bar{F}(Q_b) \overset{\text{(iv)}}{\leq} F(Q_b), \tag{4.21}$$

in which (iii) is due to $t_{a,N} \leq t_{c,N}$, and (iv) is due to the optimality of $F(Q_b)$. Therefore, $F(Q)$ is a monotonically increasing function of $Q$.

Next we show the concavity of $F(Q)$. In specific, we should prove $F(\theta Q_a + (1-\theta)Q_b) \geq \theta F(Q_a) + (1-\theta)F(Q_b)$ for any $\theta \in [0,1]$. In Problem P4, by replacing $Q$ with $\theta Q_a + (1-\theta)Q_b$, we have $\theta \sum_{i=1}^{N} s_{a,i} + (1-\theta)\sum_{i=1}^{N} s_{b,i} - \frac{\sigma^2}{g_1} = \theta Q_a + (1-\theta)Q_b$ when (4.14c) is active. From (4.14b), as for the item $\theta s_{a,i} + (1-\theta)s_{b,i}$, $\forall i \in \mathcal{N}$, we have

$$\begin{aligned}
&\log\Big(\theta s_{a,i} + (1-\theta)s_{b,i}\Big) \\
&\geq \theta \log(s_{a,i}) + (1-\theta)\log(s_{b,i}) \\
&= \theta\Big\{\log(\frac{\sigma^2}{g_i} - \frac{\sigma^2}{g_{i+1}}) - \sum_{n=1}^{i}\log(1-t_{a,n})\Big\} + \\
&(1-\theta)\Big\{\log(\frac{\sigma^2}{g_i} - \frac{\sigma^2}{g_{i+1}}) - \sum_{n=1}^{i}\log(1-t_{b,n})\Big\} \\
&\geq \log\Big(\frac{\sigma^2}{g_i} - \frac{\sigma^2}{g_{i+1}}\Big) - \sum_{n=1}^{i}\log\Big(1-\theta t_{a,n} - (1-\theta)t_{b,n}\Big).
\end{aligned} \tag{4.22}$$

Consequently, we take the exponential operation in (4.22), and then, we can obtain $\prod_{n=1}^{i} \frac{1}{1-\theta t_{a,n} - (1-\theta)t_{b,n}}(\frac{\sigma^2}{g_i} - \frac{\sigma^2}{g_{i+1}}) \leq \theta s_{a,i} + (1-\theta)s_{b,i}$, $\forall i \in \mathcal{N}$. This means $\theta t_{a,i} + (1-\theta)t_{b,i}$, is feasible under the power amount $\theta Q_a + (1-\theta)Q_b$.

Since the objective function is $G_s(\boldsymbol{t}) = \sum_{i=1}^{N} t_i$, the objective value associated with $\theta t_{a,i} + (1-\theta)t_{b,i}$, $\forall i \in \mathcal{N}$, is $\theta F(Q_a) + (1-\theta)F(Q_b)$. This indicates $\theta F(Q_a) +$

$(1-\theta)F(Q_b)$ is feasible under the power $\theta Q_a + (1-\theta)Q_b$. Since $F(\theta Q_a + (1-\theta)Q_b)$ is the optimal objective value under the power $\theta Q_a + (1-\theta)Q_b$, we have $F(\theta Q_a + (1-\theta)Q_b) \geq \theta F(Q_a) + (1-\theta)F(Q_b)$.

Therefore, $F(Q)$ is a concave function of $Q$.

This completes the proof.

□

For the objective function $U_s(Q)$, we also have a useful feature, which is given as follows.

**Theorem 8.** *Function $U_s(Q)$ is quasiconcave with respect to $Q$.*

*Proof.* See Appendix 4.7.2. □

Based on the quasi-concavity of $U_s(Q)$, we can use a bisection based two-level method to identify the optimal solution of $Q^*$ [85], in which the outer level is solved by bisection, and the inner level is solved by golden section search. Thus, the optimal solution to Problem P1 can also be found. Then the optimal set of $\{Q^*, \boldsymbol{\xi}^*\}$ forms the optimal solution to Problem P1. Accordingly, the optimal solution $\{Q^*, \boldsymbol{\xi}^*, \boldsymbol{p}^*\}$ is the Stackelberg Equilibrium to our formulated game.

In this chapter, we divide the formulated problem into two stages to solve it. In terms of iteration number, the complexity of our proposed algorithm is given as follows. In stage 1, we use bisection for certain times under a fixed Lagrange multiplier. In the worst case, user number $N$ is the running times of bisection. It yields the complexity of $NK_1$, where $K_1$ is the iteration number of bisection in stage 1. Then we update the Lagrange multiplier for a fixed iteration times of $M_\epsilon$. So the complexity in stage 1 is $NM_\epsilon K_1$. In stage 2, the problem is quasiconcave, which is solved by the bisection based two-level method. The outer level bisection is solved with $K_2$ iterations. The inner level golden section

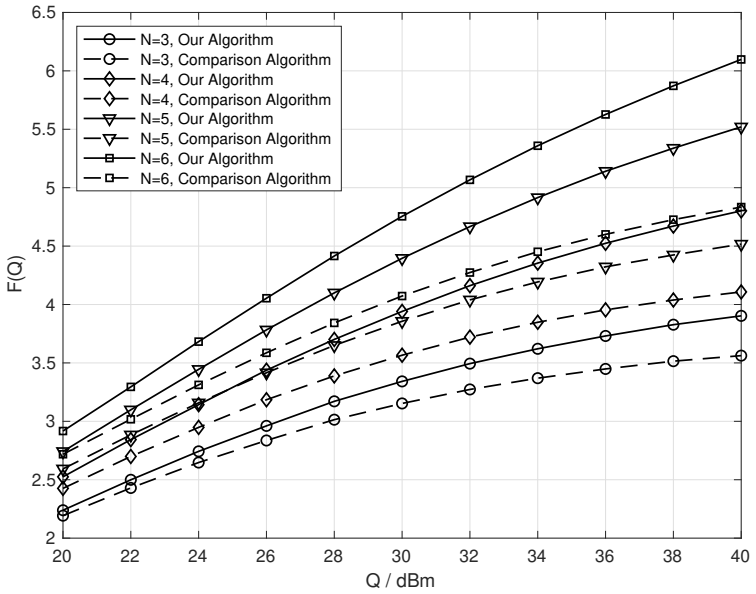


Figure 4.1: The solution $F(Q)$ in stage 1 at the BS versus transmit power $Q$.

search is solved with $K_3$ iterations. Thus, the overall complexity of the proposed algorithm is $NM_\epsilon K_1 K_2 K_3$ iterations.

## 4.5 Numerical Results

To verify the performance of our proposed algorithm, simulations are designed. The channel coefficient from the BS to user $i$, $i \in \mathcal{N}$, is further modeled as $h_i = \tilde{h}_i/\sqrt{d_i^\alpha}$, in which $\tilde{h}_i$ is a circular symmetric complex Gaussian random variable distributed as $\mathcal{CN} \sim (0, 1)$, $d_i$ is the distance from the BS to user $i$, and $\alpha$ means the path loss exponent.

We first evaluate the solution $F(Q)$ in stage 1 at the BS, [4] as demonstrated in Fig. 4.1. The used parameters are given as follows. The distance $d_i$ is chosen as $d_i = 100$ m, $\forall i \in \mathcal{N}$. The path loss exponent is fixed as $\alpha = 2$. The variance

[4]Here we call $F(Q)$ the solution in stage 1. Because the constant $C_u$ does not impact the maximization of $H(\boldsymbol{\xi})$.

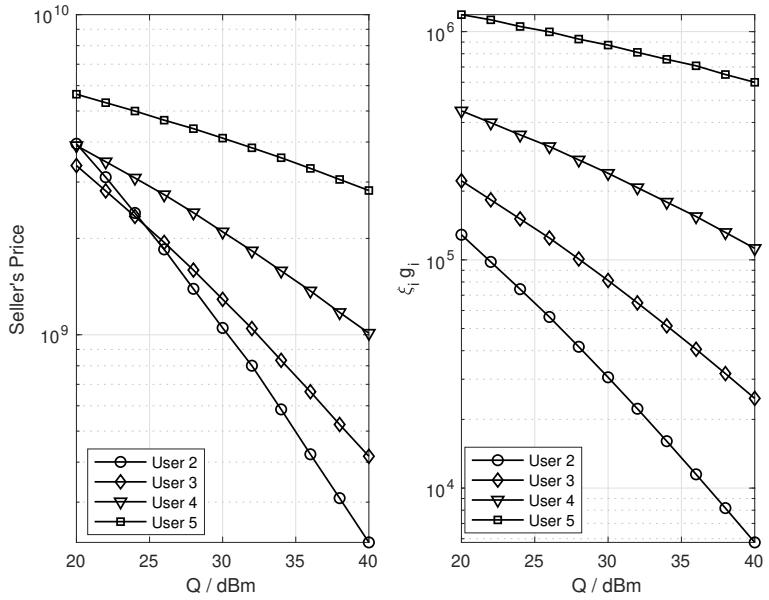


Figure 4.2: The price and variable $\xi_i g_i$ for each user in stage 1 solution.

of the background noise is $\sigma^2 = -30$ dBm. We set the user numbers to $N = 3$, 4, 5 and 6, and vary the total allocated transmit power $Q$ from 20 dBm to 40 dBm. Observed from Fig. 4.1, as the increase of transmit power $Q$, the value of $F(Q)$ increases, which is intuitive. Moreover, for a fixed $Q$, as the increase of user number $N$, the value of $F(Q)$ becomes larger. For example, at 40 dBm, the value of $F(Q)$ for the 6-user case is 1.5 times larger than the value for the 3-user case. The reason comes from the fact that the increase of user number leads to the increase of the dimensionality of the feasible region. What is more, we compare our algorithm with the power allocation strategy proposed in [24]. Clearly, our algorithm outperforms the comparison algorithm in [24].

As shown in Fig. 4.2, the price of the received power for each user is illustrated under the 5-user case. The price is evaluated when $Q$ is changing and $F(Q)$ is achieved. Observed from Fig. 4.2, as the increase of user $i$, the price follows an overall increasing trend under fixed $Q$. When $Q$ is high, the price for one stronger

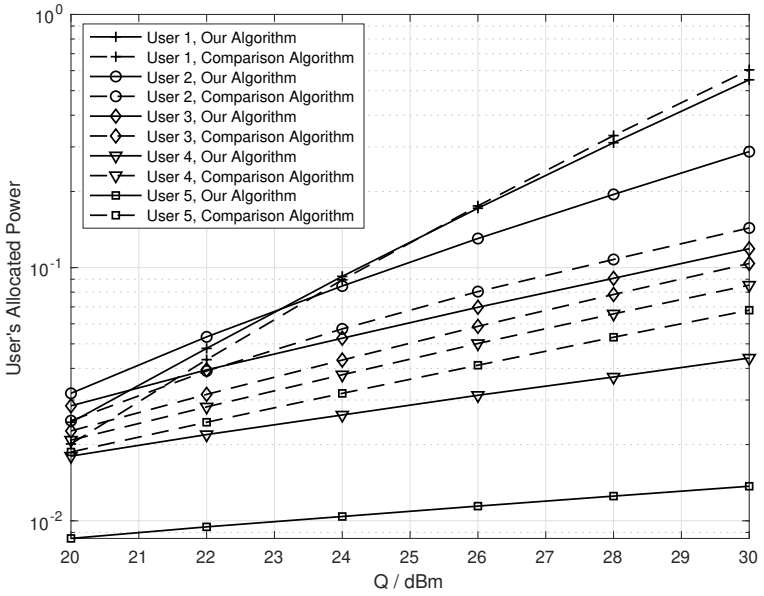


Figure 4.3: The allocated power at the user side in stage 1 solution.

user will be much higher than the price for one weaker user [5]. To identify the reason, we can inspect equation (4.4). To guarantee a feasible and nonnegative power allocation at the buyer side, the BS should adopt a pricing strategy such that the variable $\xi_i g_i$ for a stronger user should be higher than that for a weaker user, which is also illustrated in Fig. 4.2.

As shown in Fig. 4.3, the optimal amount of allocated power for each user is evaluated under the solution $F(Q)$. It can be seen that as the increase of transmit power $Q$, the allocated power for each user increases. It can also be noted that the slope of a weaker user is larger than that of a stronger user, which indicates that the allocated power at a weaker user increases faster than a stronger user. The reason for this can be found by observing Fig. 4.2. Because as the increase of Q, the decreasing rate of the price for the stronger user is smaller than that

[5]For two users, the stronger user means the user with a larger channel gain. The weaker user means the user with a smaller channel gain.

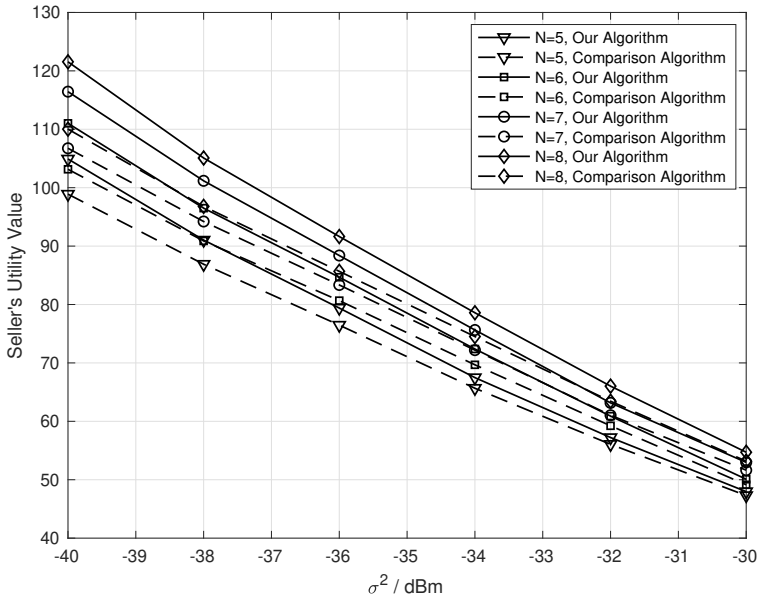


Figure 4.4: The BS's utility $U_s(\boldsymbol{\xi}, Q)$ versus $\sigma^2$.

of the weaker user. Compared with the algorithm in [24], it can be seen that the algorithm in [24] allocates a higher power to the strongest user than our algorithm. Since as shown in Fig. 4.1, our algorithm achieves a higher utility, it means our algorithm concentrates on the overall revenue from users. This also indicates that the algorithm in [24] allocates too much power to the strongest user.

As shown in Fig. 4.4, the BS's utility value $U_s(\boldsymbol{\xi}, Q)$ is demonstrated. The parameters used for evaluation are given as follows. The distance from the BS to each user is set as $d_i = 80$ m. The transmit power budget is fixed as $P_t = 40$ dBm. The noise variance $\sigma^2$ varies from $-40$ dBm to $-30$ dBm. The circuit power consumption $P_0$, the coefficients $C_0$ and $C_u$ are chosen as $P_0 = 0.02$ W, $C_0 = 0.001$ and $C_u = 1$. It can be observed that the utility value declines with the increase of noise variance $\sigma^2$. The reason is because the increase of noise variance will decrease the SINR for each user to decode information. As a result,

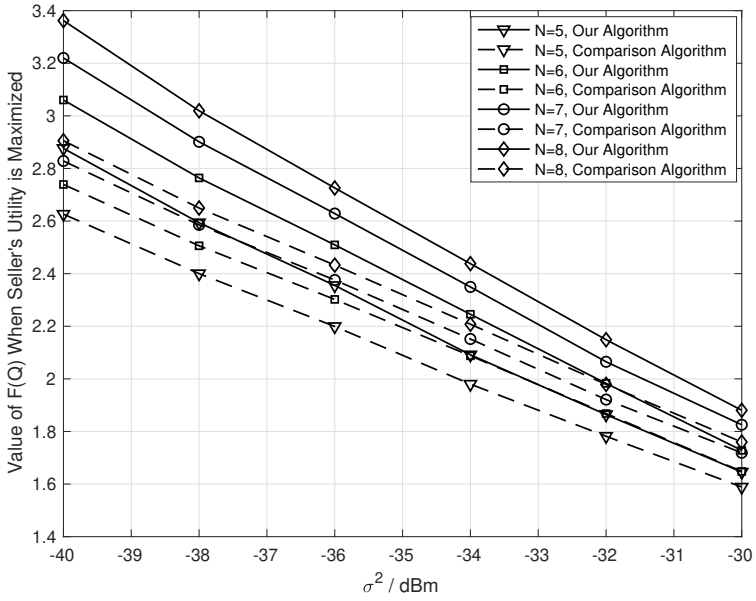


Figure 4.5: The value of $F(Q)$ versus $\sigma^2$ when $U_s(\boldsymbol{\xi}, Q)$ is maximized.

the revenue for the seller will decrease, which yields the decline of seller's utility $U_s(\boldsymbol{\xi}, Q)$. When compared with the the comparison algorithm in [24], we replace the power allocation strategy for calculating $F(Q)$ in our algorithm by the method in [24]. Obviously, our algorithm achieves a higher utility than the comparison algorithm. We also evaluate the value of function $F(Q)$ when the seller's utility value is maximized, as depicted in Fig. 4.5. It can be seen that $F(Q)$ exhibits a similar trend as $U_s(\boldsymbol{\xi}, Q)$.

Since the full power allocation scheme is a widely adopted strategy, we compare it with our algorithm. At the seller side, the ratio between our utility and the utility of full power allocation scheme are evaluated, as illustrated in Fig. 4.6. We use the parameters $d_i = 80$ m and $P_t = 30$ dBm. It can be seen that our strategy can realize a utility at least 10 times larger than that of the full power allocation scheme. The reason is because allocating all the power to users may not achieve the maximal point of $U_s(\boldsymbol{\xi}, Q)$.

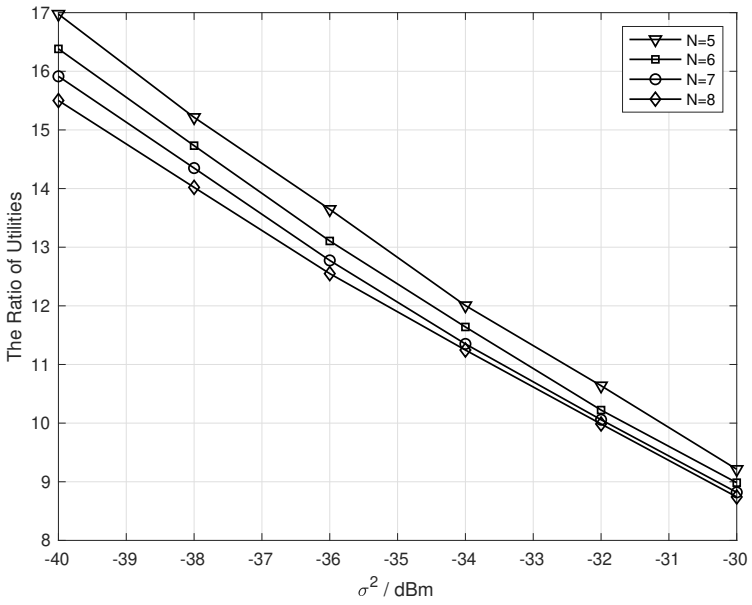


Figure 4.6: The ratio between our utility and the utility of full power allocation scheme.

## 4.6 Conclusion

In this chapter, we investigate the Stackelberg game aided power allocation in downlink NOMA system, in which two levels of games are formulated. To maximize the utility of profit per unit power, the BS determines the price and the total power. Each user maximizes its own profit by determining the power. The optimal solutions are derived. To be more specific, by using the solution at the buyer side, we have a non-convex optimization problem at the seller side. Thus, we design two stages to solve the optimization problem for the seller. An efficient iterative algorithm is designed in the first stage. Then the solution in the first stage is utilized to reach the optimal solution in the second stage.

## 4.7 Appendix

### 4.7.1 The Proof of Lemma 7

*Proof.* This lemma is proved by using contradiction. For two adjacent users, $i^\dagger$ and $i^\dagger + 1$, we assume the inequality $t_{i^\dagger} > t_{i^\dagger+1}$ is satisfied when the optimality is achieved.

From the definition, we have $\zeta_k = \frac{g_k}{\sum_{j=k}^{N} p_j g_k + \sigma^2}$ and $t_k = \frac{p_k g_k}{\sum_{j=k}^{N} p_j g_k + \sigma^2}$, and thus, we have $G_s = \sum_{k=1}^{N} t_k = \sum_{k=1}^{N} \frac{p_k g_k}{\sum_{j=k}^{N} p_j g_k + \sigma^2}$.

By examining the first order derivatives of $G_s$ with $p_{i^\dagger}$ and $p_{i^\dagger+1}$, one can obtain

$$\frac{\partial G_s}{\partial p_{i^\dagger}} = \frac{1}{\sum_{j=i^\dagger}^{N} p_j + \frac{\sigma^2}{g_{i^\dagger}}} - \sum_{k=1}^{i^\dagger} \frac{p_k}{(\sum_{j=k}^{N} p_j + \frac{\sigma^2}{g_k})^2} \tag{4.23}$$

and

$$\frac{\partial G_s}{\partial p_{i^\dagger+1}} = \frac{1}{\sum_{j=i^\dagger+1}^{N} p_j + \frac{\sigma^2}{g_{i^\dagger+1}}} - \sum_{k=1}^{i^\dagger+1} \frac{p_k}{(\sum_{j=k}^{N} p_j + \frac{\sigma^2}{g_k})^2}. \tag{4.24}$$

To compare $\frac{\partial G_s}{\partial p_{i^\dagger}}$ and $\frac{\partial G_s}{\partial p_{i^\dagger+1}}$, we have

$$\frac{\partial G_s}{\partial p_{i^\dagger+1}} - \frac{\partial G_s}{\partial p_{i^\dagger}} = \frac{\sum_{j=i^\dagger+2}^{N} p_j + \frac{\sigma^2}{g_{i^\dagger+1}}}{(\sum_{j=i^\dagger+1}^{N} p_j + \frac{\sigma^2}{g_{i^\dagger+1}})^2} - \frac{1}{\sum_{j=i^\dagger}^{N} p_j + \frac{\sigma^2}{g_{i^\dagger}}}. \tag{4.25}$$

Since $t_{i^\dagger} > t_{i^\dagger+1}$ is assumed, inequality $1 - t_{i^\dagger} < 1 - t_{i^\dagger+1}$ holds, which indicates

$$\frac{\sum_{j=i^\dagger+1}^{N} p_j + \frac{\sigma^2}{g_{i^\dagger}}}{\sum_{j=i^\dagger}^{N} p_j + \frac{\sigma^2}{g_{i^\dagger}}} < \frac{\sum_{j=i^\dagger+2}^{N} p_j + \frac{\sigma^2}{g_{i^\dagger+1}}}{\sum_{j=i^\dagger+1}^{N} p_j + \frac{\sigma^2}{g_{i^\dagger+1}}}. \tag{4.26}$$

By observing (4.26), we have

$$\begin{aligned} \frac{1}{\sum_{j=i^\dagger}^{N} p_j + \frac{\sigma^2}{g_{i^\dagger}}} &< \frac{\sum_{j=i^\dagger+2}^{N} p_j + \frac{\sigma^2}{g_{i^\dagger+1}}}{\sum_{j=i^\dagger+1}^{N} p_j + \frac{\sigma^2}{g_{i^\dagger+1}}} \frac{1}{\sum_{j=i^\dagger+1}^{N} p_j + \frac{\sigma^2}{g_{i^\dagger}}} \\ &\overset{\text{(v)}}{\leq} \frac{\sum_{j=i^\dagger+2}^{N} p_j + \frac{\sigma^2}{g_{i^\dagger+1}}}{(\sum_{j=i^\dagger+1}^{N} p_j + \frac{\sigma^2}{g_{i^\dagger+1}})^2}, \end{aligned} \tag{4.27}$$

in which the fact $\frac{\sigma^2}{g_{i^\dagger+1}} \leq \frac{\sigma^2}{g_{i^\dagger}}$ is used in (v).

Combining (4.25) with (4.27), we have $\frac{\partial G_s}{\partial p_{i^\dagger}} < \frac{\partial G_s}{\partial p_{i^\dagger+1}}$. By fixing the power allocation for all users in $\mathcal{N}\backslash\{i^\dagger, i^\dagger+1\}$, one can check that $t_k$ for each user in $\mathcal{N}\backslash\{i^\dagger, i^\dagger+1\}$ will not change. We also fix $p_{i^\dagger} + p_{i^\dagger+1}$. Then a small amount of power, which does not violate $\frac{\partial G_s}{\partial p_{i^\dagger}} < \frac{\partial G_s}{\partial p_{i^\dagger+1}}$, can always be transferred from $p_{i^\dagger}$ to $p_{i^\dagger+1}$. Accordingly, the item $t_{i^\dagger} + t_{i^\dagger+1}$ will increase, and thus, we can have a larger overall objective value $G_s$. This indeed contradicts with the optimality of $t_{i^\dagger} > t_{i^\dagger+1}$.

As a result, for the two adjacent users $i^\dagger$ and $i^\dagger + 1$, whenever the weak user has a higher value of $t_{i^\dagger}$, power can be transferred to the strong user such that $t_{i^\dagger+1} \geq t_{i^\dagger}$ is satisfied.

Therefore, when the optimality is achieved, we have $t_1 \leq t_2 \ldots \leq t_{N-1} \leq t_N$.

This completes the proof. □

### 4.7.2 The Proof of Theorem 8

*Proof.* For any $0 \leq \theta \leq 1$, we define $Q_c = \theta Q_a + (1-\theta)Q_b$. To prove the quasiconcavity of function $U_s(Q)$, we should prove that $U_s(Q_c) \geq \min\{U_s(Q_a), U_s(Q_b)\}$ holds.

Based on (4.20a), we have

$$\begin{aligned} U_s(Q_c) &= \frac{C_u F(\theta Q_a + (1-\theta)Q_b) - C_0(\theta Q_a + (1-\theta)Q_b)}{P_0 + \theta Q_a + (1-\theta)Q_b} \\ &\overset{\text{(vi)}}{\geq} \frac{\theta(C_u F(Q_a) - C_0 Q_a)}{P_0 + \theta Q_a + (1-\theta)Q_b} + \frac{(1-\theta)(C_u F(Q_b) - C_0 Q_b)}{P_0 + \theta Q_a + (1-\theta)Q_b} \\ &= \eta \frac{C_u F(Q_a) - C_0 Q_a}{P_0 + Q_a} + (1-\eta)\frac{C_u F(Q_b) - C_0 Q_b}{P_0 + Q_b} \\ &\overset{\text{(vii)}}{\geq} \min\{U_s(Q_a), U_s(Q_b)\}, \end{aligned} \tag{4.28}$$

where $\eta = \frac{\theta(P_0+Q_a)}{\theta(P_0+Q_a)+(1-\theta)(P_0+Q_b)}$ and $1-\eta = \frac{(1-\theta)(P_0+Q_b)}{\theta(P_0+Q_a)+(1-\theta)(P_0+Q_b)}$. The inequality (vi) uses the fact that $F(Q) - C_0 Q$ is a concave function of $Q$. The inequality (vii) uses the fact that any point on the segment connecting two points has a

larger value than the minimum value of the two points.

Therefore, $U_s(Q)$ is a quasi-concave function of $Q$.

This completes the proof.

□

# Chapter 5

# Optimal Resource Allocation in Energy-aware Non-orthogonal Multiple Access Networks with Multi-access Edge Computing

Since NOMA can improve the spectrum efficiency and MEC offloading can reduce the energy consumption and latency, the information transmission will be even more efficient in NOMA MEC networks. The work in [101] investigates the minimization of latency by considering different constraint conditions from power or energy in NOMA MEC network. By utilizing NOMA MEC transmission in one massive IoT network, the maximization of energy efficiency is studied under the guarantee of target delay in [102]. The work in [103] studies one two-user uplink NOMA system, in which user cooperation is carried out in the process of data offloading. With the aim of minimizing energy consumption or maximizing data transmission, the related resources are optimized, which include time, data amount and power. When the information offloading of a two-user NOMA system is threatened by one eavesdropper, one optimization problem to enhance the physical layer security is investigated in [104]. In [105], NOMA MEC transmission is conducted in the network scenario with IoT. The decoding order

for SIC, together with the allocation of resource for computing are optimized.

By leveraging game theoretical models in MEC networks [43, 44] , efficient approaches of resource allocation are expected from the economic perspectives. In conventional OMA based MEC networks, many research works have been presented, such as [25, 106, 107]. The work in [106] studies the minimization of system overhead for information offloading, with the aid of the potential game. The work in [107] investigates one industrial IoT system, in which a double auction strategy is exploited to determine the pricing of the resource used for information computation. The work in [25] studies a Stackelberg game based network, in which data offloading is conducted through making payments, with the aim of saving energy. Recently, NOMA is further integrated with MEC by using game theoretical approaches. By treating each subcarrier as a coalition, a coalitional game is utilized to group users into each subcarrier for the multi-carrier NOMA MEC system in [108]. In [109], the association of users with edge servers and allocation of related radio resources are investigated by combining the matching game with coalitional game. The work in [26] investigates one Stackelberg game based NOMA MEC network, in which the leader performs the task and power allocation, while the follower conducts the allocation of sub-channel.

In this chapter, we investigate the optimal resource allocation in an energy-aware NOMA MEC network, by using a two-level Stackelberg game. The *major differences* from the Stackelberg game approach in Chapter 4 are described as follows.

1) Different problem formulations are adopted. In general, in our utility function, the profit consists of the revenue and the cost. As for the buyer-level game, in Chapter 4, to maximize the profit at each user, the achievable rate is

treated as the revenue, while the payment for purchasing is treated as the cost. In this chapter, each user minimizes the utility standing for the overall costs from the computation energy and the payment to purchase the interference. Indeed, this is equivalent to maximizing the profit by treating the energy saving for data computation as the revenue. As for the seller-level game, the payment from the user is the revenue. In Chapter 4, the cost of providing transmit power is considered in the profit. The profit per unit power is maximized at the BS. In this chapter, the BS maximizes the profit by treating the computational energy as the cost.

2) Different methodologies are used to solve the formulated problems in the two chapters. In Chapter 4, the buyer-level solution is found first. Then we develop a two-stage solution for the seller-level game. Specifically, by fixing the total allocated transmit power in stage 1, we offer an iterative method to optimally solve the optimization problem. Then we show the solution in stage 1 is concave with the power. Also, the quasiconcavity of the objective function is theoretically proved and then is used to solve the overall optimal solution. In this chapter, we use another approach to achieve the optimal resource allocation. After solving the buyer-level game, we intentionally add one more dimension for the time allocation in the seller-level optimization problem. Then by fixing the time allocation, we show existing method can be applied to solve the optimization variables. Afterwards, by varying the time allocation, we prove the optimization problem is monotone, and thus, the Polyblock method can be adopted to reach the optimal solution.

The contributions of this work are summarized as follows.

1) We provide a novel design of energy-aware resource allocation in NOMA MEC networks. In [25], with the aim of promoting energy saving, one payment-

based data offloading scheme is investigated in OMA MEC networks. When Stackelberg game is adopted in NOMA MEC, the sub-channel allocation is performed by using one game theoretical approach in [26]. However, to help to save energy with making payments, how to allocate resource within the same channel by using the game theoretical approach has not been investigated in NOMA MEC. Therefore, to fill the research gap, we study one Stackelberg game based data offloading, and conduct the related resource allocation in NOMA MEC networks.

2) We offer an optimal solution to the formulated problem. We first identify the optimal solution to the buyer-level game. As for the seller-level game, it yields a non-convex optimization problem. Accordingly, we devise an approach to optimally tackle it. To be specific, after adding one dimension in time, we show that the optimization problem is separable under fixed time allocation. The optimal solution can also be efficiently found by using existing methodology. Subsequently, the monotonicity with time is proved, based on which the global optima is obtained by employing the Polyblock algorithm.

The organization for the rest of this chapter is described as follows. In Section 5.1, we introduce the system model. In Section 5.2, how to identify the solution to the buyer-level game is provided. In Section 5.3, we show the approach to achieve the optimal solution to the seller-level game. The numerical results are offered in Section 5.4. Section 5.5 draws the conclusion. Table 5.1 describes the notations used in Chapter 5.

| Symbol | Meaning |
|---|---|
| $p_i$ | The transmit power for user $i$ |
| $h_i$ | The channel coefficient from user $i$ to the BS |
| $g_i$ | The channel power gain from user $i$ to the BS |
| $x_i$ | User $i$'s information signal |
| $R_i$ | User $i$'s achievable rate |
| $D_i$ | User $i$'s offloading data amount |
| $N_i$ | User $i$'s information bits in the task |
| $T$ | Time slot length |
| $\tau$ | Offloading time for users |
| $f_{l,i}$ | Local CPU frequency for computation at user $i$ |
| $P_{l,i}$ | Local power consumption for computation at user $i$ |
| $E_{l,i}$ | Local energy consumption for computation at user $i$ |
| $a_{0,i}$ | Number of CPU cycles used for computing one input bit at user $i$ |
| $K$ | User number in the system |
| $U_i$ | User $i$'s utility function |
| $U_b$ | The utility function at the BS |
| $C_b$ | The coefficient of cost for computing users' information at the BS |
| $C_u$ | The coefficient of cost for computing user $i$'s own information |

Table 5.1: The notations used in Chapter 5

# 5.1 System Model

## 5.1.1 Communication Model

An uplink NOMA scenario is considered in this chapter. In our system, there are one BS and a set of $K$ users. The user set is denoted as $\mathcal{K} = \{1, 2, \cdots, K\}$. There is an edge server integrated with the BS, which is equipped with powerful computational capacity to compute the offloaded information from users. Each user, who has limited computational capacity, resorts to the assistance from the BS for data offloading. We assume the time has a slotted structure, with the

same slot length of $T$. We denote the channel coefficient from user $i$ to the BS as $h_i$, $i \in \mathcal{K}$, which is associated with the channel power gain $g_i$. It is assumed that the channel fading is quasi-static. In other words, the values of the channel coefficients are fixed during one slot. But the values change independently during another different slot. The channel power gains are assumed to be ordered as: $g_1 \leq g_2 \leq \cdots \leq g_K$.

Each time slot is divided into two phases. The first phase has a length of $\tau$, during which all users offload their data information to the BS. The second phase has a length of $T - \tau$, during which the BS computes the offloaded data information from users. The time for the BS to send the computed results back to users is considered to be sufficiently small, and thus, it is negligible.

There is a task to be computed at user $i$, which consists of $N_i$ bits. Then user $i$ selects to partially offload $D_i$ bits to the BS during the first phase, by transmitting information signal $x_i$ to the BS with the transmit power $p_i$.

Accordingly, the received signal at the BS is represented as $y_b = \sum_{i=1}^{K} \sqrt{p_i} h_i x_i + n_b$, where $n_b$ is the background AWGN, distributed as $n_b \sim \mathcal{CN}(0, \sigma^2)$. Afterwards, to detect user $i$'s information, the BS employs SIC to eliminate the interference from user $j$, $i+1 \leq j \leq K$. Thus, the achievable rate for user $i$ is given as

$$R_i = \log\left(1 + \frac{p_i g_i}{\sum_{j=1}^{i-1} p_j g_j + \sigma^2}\right). \tag{5.1}$$

Then the offloaded data amount at user $i$ is given as $D_i = R_i \tau$.

### 5.1.2 Computation Model

According to [110], the power consumption for computation at user $i$ is expressed as $P_{l,i} = l_0 f_{l,i}^3$, where $l_0$ is a constant determined by the CPU architecture, and $f_{l,i}$ is user $i$'s CPU frequency for local computation.

Since $D_i$ bits are offloaded to the BS, there are still $N_i - D_i$ bits to be locally processed at user $i$. If the number of CPU cycles used to calculate each bit information are $a_{0,i}$, the total number of CPU cycles used to locally compute $N_i - D_i$ bits are $a_{0,i}(N_i - D_i)$. Since the whole time slot is used to perform local computation, we have $T = \frac{a_{0,i}(N_i - D_i)}{f_{l,i}}$. Then the energy consumption for local computation is expressed as

$$E_{l,i} = \frac{l_0 a_{0,i}^3 (N_i - D_i)^3}{T^2}. \tag{5.2}$$

### 5.1.3 Game Formulation

In our system, to promote the efficient usage of energy from the economic perspective, a two-level Stackelberg game is leveraged to model the process of data offloading in the NOMA MEC system. Specifically, the BS is deemed as the seller, while users are deemed as the buyers.

**1) Seller Level Game**

During the first phase, the BS decides the offloading time $\tau$ and the price $x_i$ to sell the interference per unit time for user $i$. Then the interference purchased by user $i$ is $p_i g_i$, and thus, the BS's revenue is the total payment $\sum_{i=1}^{K} p_i g_i x_i \tau$ earned from selling interferences during time $\tau$. After making a payment, user $i$ is allowed to offload a data amount of $D_i$. [1] During the second phase, due to the multiple CPU or multi-core architecture at the edge server, users' offloaded information is computed at the same time within time duration $T - \tau$. By following a similar derivation as the user side, the energy consumption for computing user $i$'s offloaded data amount $D_i$ is given as $\frac{l_0 a_{0,i}^3 D_i^3}{(T-\tau)^2}$. Then the cost of computing user $i$'s offloaded data is $\frac{C_b l_0 a_{0,i}^3 D_i^3}{(T-\tau)^2}$, in which $C_b$ is coefficient of the cost. Thus, the

[1] Note that given $\tau$ and other users' power strategies, $D_i$ can be determined by $p_i g_i$.

utility function at the BS is expressed as $U_b = \sum_{i=1}^{K}\{p_i g_i x_i \tau - \frac{C_b l_0 a_{0,i}^3 D_i^3}{(T-\tau)^2}\}$, which consists of the revenue and the cost. Accordingly, we formulate the seller-level game as the following optimization problem.

*Problem P1:*

$$\max_{\{x_i\},\tau} \quad U_b = \sum_{i=1}^{K}\left\{p_i g_i x_i \tau - \frac{C_b l_0 a_{0,i}^3 D_i^3}{(T-\tau)^2}\right\}, \tag{5.3a}$$

$$\text{s.t.} \quad 0 \le \tau \le T. \tag{5.3b}$$

**2) Buyer Level Game**

The computational energy without offloading at user $i$ is $\frac{l_0 a_{0,i}^3 N_i^3}{T^2}$. With the aid of data offloading, the energy saving can be written as $\frac{l_0 a_{0,i}^3 N_i^3}{T^2} - \frac{l_0 a_{0,i}^3 (N_i - D_i)^3}{T^2}$, which is deemed as user $i$'s revenue. User $i$ decides the transmit power $p_i$. Then the cost of payment is $p_i g_i x_i \tau$. Accordingly, the profit can be expressed as $C_u(\frac{l_0 a_{0,i}^3 N_i^3}{T^2} - \frac{l_0 a_{0,i}^3 (N_i - D_i)^3}{T^2}) - p_i g_i x_i \tau$, where $C_u$ is the coefficient of energy consumption. It can be observed that maximizing the profit is equivalent to minimizing the utility function as $U_i = \frac{C_u l_0 a_{0,i}^3 (N_i - D_i)^3}{T^2} + p_i g_i x_i \tau$. Indeed, utility $U_i$ can be regarded as the overall costs from computational energy and the payment. Thus, for user $i$, the buyer-level game is formulated into the following optimization problem.

*Problem P2:*

$$\min_{p_i} \quad U_i = \frac{C_u l_0 a_{0,i}^3 (N_i - D_i)^3}{T^2} + p_i g_i x_i \tau \tag{5.4a}$$

$$\text{s.t.} \quad 0 \le D_i \le N_i. \tag{5.4b}$$

In what follows, we use backward induction to solve the formulated problems in the two-level game.

## 5.2 Optimal Solution to Problem P2

To obtain the optimal solution to Problem P2, we observe the first order derivative of the objective function (5.4a), which can be expressed as

$$\frac{\mathrm{d}U_i}{\mathrm{d}p_i} = -\frac{3C_u l_0 a_{0,i}^3 (N_i - D_i)^2 g_i}{(\ln 2)(\sum_{j=1}^{i} p_j g_j + \sigma^2) T^2} \tau + g_i x_i \tau, \tag{5.5}$$

in which the fact $\frac{\mathrm{d}D_i}{\mathrm{d}p_i} = \frac{\mathrm{d}R_i}{\mathrm{d}p_i}\tau = \frac{1}{\ln 2}\frac{g_i}{\sum_{j=1}^{i} p_j g_j + \sigma^2}\tau$ is used.

After setting $\frac{\mathrm{d}U_i}{\mathrm{d}p_i} = 0$, the relationship between price $x_i$ and power $p_i$ is given by

$$x_i = h(p_i) \triangleq \frac{3C_u l_0 a_{0,i}^3 (N_i - D_i)^2}{(\ln 2)(\sum_{j=1}^{i} p_j g_j + \sigma^2) T^2}. \tag{5.6}$$

Then it can be checked that (5.6) is a decreasing function of $p_i$. Thus, based on the announced price $x_i$, the optimal solution $p_i$ to Problem P2 can be obtained as

$$p_i = h^{-1}(x_i). \tag{5.7}$$

## 5.3 Optimal Solution to Problem P1

By exploiting the expression in (5.6), the objective function $U_b$ in Problem P1 can be equivalently rewritten as

$$U_b = \sum_{i=1}^{K} \left\{ \frac{3C_u l_0 a_{0,i}^3 (N_i - D_i)^2 p_i g_i}{(\ln 2)(\sum_{j=1}^{i} p_j g_j + \sigma^2) T^2} \tau - \frac{C_b l_0 a_{0,i}^3 D_i^3}{(T - \tau)^2} \right\}. \tag{5.8}$$

It can be seen that $U_b$ is indeed a function of $\{p_i\}$ and $\tau$, which is non-convex. Thus, the optimal solution is generally hard to get. However, in this chapter, we can devise an approach to efficiently identify the optimal solution. To this end, we first have a useful lemma.

**Lemma 8.** *The item* $\frac{p_i g_i}{\sum_{j=1}^{i} p_j g_j + \sigma^2}$ *can be represented into a compact form as* $1 - 2^{-\frac{D_i}{\tau}}$.

*Proof.* Since the achievable rate is $R_i = \log(1 + \frac{p_i g_i}{\sum_{j=1}^{i-1} p_j g_j + \sigma^2})$, we have

$$\sum_{j=1}^{i-1} p_j g_j + \sigma^2 = \frac{p_i g_i}{2^{R_i} - 1}. \tag{5.9}$$

Subsequently, by using (5.9), we can obtain

$$\begin{aligned} \frac{p_i g_i}{\sum_{j=1}^{i=i} p_j g_j + \sigma^2} &= \frac{p_i g_i}{p_i g_i + \frac{p_i g_i}{2^{R_i}-1}} \\ &= 1 - 2^{-R_i} \\ &= 1 - 2^{-\frac{D_i}{\tau}}. \end{aligned} \tag{5.10}$$

□

For the objective function $U_b$, we add one more dimension in time allocation by replacing $T-\tau$ with $\omega$. Moreover, with the aid of Lemma 8, it can be rewritten as

$$U_b(\{D_i\}, \tau, \omega) = \sum_{i=1}^{K} \left\{ \frac{3C_u l_0 a_{0,i}^3 (N_i - D_i)^2}{(\ln 2) T^2} (1 - 2^{-\frac{D_i}{\tau}})\tau - \frac{C_b l_0 a_{0,i}^3 D_i^3}{\omega^2} \right\}. \tag{5.11}$$

Accordingly, the original Problem P1 can be converted into the following optimization problem.

*Problem P3:*

$$\max_{\{D_i\},\tau,\omega} \quad U_b(\{D_i\}, \tau, \omega) \tag{5.12a}$$

$$\text{s.t.} \quad 0 \leq \tau + \omega \leq T \tag{5.12b}$$

$$0 \leq \tau \leq T \tag{5.12c}$$

$$0 \leq \omega \leq T. \tag{5.12d}$$

In Problem P3, it can be seen that the objective function $U_b(\{D_i\}, \tau, \omega)$ is still non-convex. However, after a careful inspection, we find that there is an inherent layered structure in Problem P3. Thus, we can divide the solving procedure of Problem P3 into two steps. To be more specific, in the first step, for given $\tau$ and

$\omega$, the optimal solutions to $\{D_i\}$ can be identified. Then based on (5.1), (5.6) and (5.7), the solutions to $\{p_i\}$ and $\{x_i\}$ can be determined. In the second step, how to reach the optimal solutions of $\tau$ and $\omega$ will be provided. We will show solving Problem P3 is equivalent to solving Problem P1 in Section 5.3.2.

Then we proceed to obtain the optimal solution in the first step.

### 5.3.1 Solving Optimal Solutions to $\{D_i\}$ for Fixed $\tau$ and $\omega$

In the first step, for fixed $\tau$ and $\omega$, it can be observed that function $U_b$ in (5.11) is separable. Thus, it can be further written as $U_b = \sum_{i=1}^{K} U_{b,i}$, in which $U_{b,i} = \frac{3C_u l_0 a_{0,i}^3 (N_i - D_i)^2}{(\ln 2) T^2}(1 - 2^{-\frac{D_i}{\tau}})\tau - \frac{C_b l_0 a_{0,i}^3 D_i^3}{\omega^2}$. Then we have one useful feature for $U_{b,i}$, which is given as follows.

**Theorem 9.** *For fixed $\tau$ and $\omega$, $U_{b,i}$ is not concave. There is a unique root $D_i^*$ to $\frac{\mathrm{d}U_{b,i}}{\mathrm{d}D_i} = 0$. Also, $U_{b,i}$ is increasing over $[0, D_i^*)$, and decreasing over $[D_i^*, N_i]$.*

*Proof.* The first order derivative of $U_{b,i}$ with $D_i$ is given by

$$\frac{\mathrm{d}U_{b,i}}{\mathrm{d}D_i} = -\frac{6C_u l_0 a_{0,i}^3 (N_i - D_i)}{(\ln 2) T^2}(1 - 2^{-\frac{D_i}{\tau}})\tau + \frac{3C_u l_0 a_{0,i}^3 (N_i - D_i)^2}{T^2} 2^{-\frac{D_i}{\tau}} - \frac{3C_b l_0 a_{0,i}^3 D_i^2}{\omega^2}. \quad (5.13)$$

The second order derivative of $U_{b,i}$ with $D_i$ is given by

$$\frac{\mathrm{d}^2 U_{b,i}}{\mathrm{d}D_i^2} = \frac{6C_u l_0 a_{0,i}^3}{(\ln 2) T^2}(1 - 2^{-\frac{D_i}{\tau}})\tau - \frac{12C_u l_0 a_{0,i}^3 (N_i - D_i)}{T^2} 2^{-\frac{D_i}{\tau}} - \frac{3(\ln 2) C_u l_0 a_{0,i}^3 (N_i - D_i)^2}{T^2 \tau} 2^{-\frac{D_i}{\tau}} - \frac{6C_b l_0 a_{0,i}^3 D_i}{\omega^2}. \quad (5.14)$$

From (5.14), it can be seen that $U_{b,i}$ is not concave.

However, after a careful inspection, the first order derivative (5.13) can be

rewritten as

$$\frac{\mathrm{d}U_{b,i}}{\mathrm{d}D_i} = (N_i - D_i)^2 \Bigg\{ - \frac{6C_u l_0 a_{0,i}^3}{(\ln 2) T^2 (N_i - D_i)} (1 - 2^{-\frac{D_i}{\tau}})\tau + \frac{3C_u l_0 a_{0,i}^3}{T^2} 2^{-\frac{D_i}{\tau}} - \frac{3C_b l_0 a_{0,i}^3 D_i^2}{\omega^2 (N_i - D_i)^2} \Bigg\}. \quad (5.15)$$

We denote $H(D_i) = -\frac{6C_u l_0 a_{0,i}^3}{(\ln 2) T^2 (N_i - D_i)} (1 - 2^{-\frac{D_i}{\tau}})\tau + \frac{3C_u l_0 a_{0,i}^3}{T^2} 2^{-\frac{D_i}{\tau}} - \frac{3C_b l_0 a_{0,i}^3 D_i^2}{\omega^2 (N_i - D_i)^2}$. By observing the first order derivative of $H(D_i)$, we have $\frac{\mathrm{d}H(D_i)}{\mathrm{d}D_i} < 0$. Thus, $H(D_i)$ is decreasing with $D_i$. Moreover, when $D_i = 0$ and $D_i \to N_i$, we have

$$\begin{cases} H(D_i)|_{D_i=0} = \dfrac{3C_u l_0 a_{0,i}^3}{T^2} > 0 \\ H(D_i)|_{D_i \to N_i} = -\infty. \end{cases} \quad (5.16)$$

Since $(N_i - D_i)^2 \geq 0$ and $H(D_i)$ is decreasing with $D_i$, by combining (5.16), it indicates that we have one unique root $D_i^*$ for $\frac{\mathrm{d}U_{b,i}}{\mathrm{d}D_i} = 0$. It also means $\frac{\mathrm{d}U_{b,i}}{\mathrm{d}D_i} > 0$ over $[0, D_i^*)$, and $\frac{\mathrm{d}U_{b,i}}{\mathrm{d}D_i} \leq 0$ over $[D_i^*, N_i]$. Thus, $U_{b,i}$ is increasing over $[0, D_i^*)$, and decreasing over $[D_i^*, N_i]$.

This completes the proof. □

**Remark:** Since there is a unique root $D_i^*$ to $\frac{\mathrm{d}U_{b,i}}{\mathrm{d}D_i} = 0$, existing methodology can be employed to identify $D_i^*$ for $U_{b,i}$, $\forall i \in \mathcal{K}$, such as the golden section search method [111]. Recall that the objective function $U_b$ is separable under given $\tau$ and $\omega$. Thus, the maximization of $U_b$ is equivalent to the maximization of each $U_{b,i}$. In other words, for fixed $\tau$ and $\omega$, the optimal solutions to $\{D_i\}$ can be efficiently solved.

Subsequently, we proceed to solve Problem P3 in the second step.

### 5.3.2 Solving Optimal Solutions to $\tau$ and $\omega$

For fixed $\tau$ and $\omega$, we denote the optimal objective value in the first step as $G_b(\tau, \omega) = \max_{\{D_i\}} U_b(\{D_i\}, \tau, \omega)$. In the second step, with the aim of identifying

the optimal solutions to $\tau$ and $\omega$, solving Problem P3 boils down to the following optimization problem.

*Problem P4:*

$$\max_{\tau,\omega} \quad G_b(\tau,\omega) \tag{5.17a}$$

$$\text{s.t.} \quad 0 \le \tau + \omega \le T \tag{5.17b}$$

$$0 \le \tau \le T \tag{5.17c}$$

$$0 \le \omega \le T. \tag{5.17d}$$

For the objective function $G_b(\tau,\omega)$, we have the following lemma.

**Lemma 9.** *Function $G_b(\tau,\omega)$ is increasing with $\tau$ and $\omega$.*

*Proof.* Based on (5.11), to prove the monotonicity of $G_b(\tau,\omega)$ with $\tau$, it is equivalent to prove the monotonicity of $f(\tau) \triangleq (1-2^{-\frac{D_i}{\tau}})\tau$ with $\tau$. Then we take the first order derivative of $f(\tau)$, which is given by

$$\frac{\mathrm{d}f(\tau)}{\mathrm{d}\tau} = 1 - (1+(\ln 2)\frac{D_i}{\tau})2^{-\frac{D_i}{\tau}}. \tag{5.18}$$

Moreover, when $\tau \to 0$ and $\tau \to \infty$, we have

$$\begin{cases} \lim\limits_{\tau\to 0} \dfrac{\mathrm{d}f(\tau)}{\mathrm{d}\tau} = 1 - \lim\limits_{\tau\to 0} \dfrac{\frac{\mathrm{d}}{\mathrm{d}\tau}(1+(\ln 2)\frac{D_i}{\tau})}{\frac{\mathrm{d}}{\mathrm{d}\tau}(2^{\frac{D_i}{\tau}})} \\ \qquad\qquad \overset{\text{(i)}}{=} 1 - \lim\limits_{\tau\to 0} \dfrac{-(\ln 2)\frac{D_i}{\tau^2}}{2^{\frac{D_i}{\tau}}(\ln 2)(-\frac{D_i}{\tau^2})} = 1 \\ \lim\limits_{\tau\to\infty} \dfrac{\mathrm{d}f(\tau)}{\mathrm{d}\tau} = 0, \end{cases} \tag{5.19}$$

in which the L'Hopital's rule is used in (i).

The second order derivative of $f(\tau)$ is given by

$$\begin{aligned} \frac{\mathrm{d}^2 f(\tau)}{\mathrm{d}\tau^2} &= (\ln 2)\frac{D_i}{\tau^2}2^{-\frac{D_i}{\tau}} - (\ln 2)\frac{D_i}{\tau^2}(1+(\ln 2)\frac{D_i}{\tau})2^{-\frac{D_i}{\tau}} \\ &= -(\ln 2)^2\frac{D_i^2}{\tau^3}2^{-\frac{D_i}{\tau}} < 0. \end{aligned} \tag{5.20}$$

Since $\frac{\mathrm{d}^2 f(\tau)}{\mathrm{d}\tau^2} < 0$, it means $\frac{\mathrm{d}f(\tau)}{\mathrm{d}\tau}$ is decreasing with $\tau$. By further considering $\lim_{\tau\to 0} \frac{\mathrm{d}f(\tau)}{\mathrm{d}\tau} > 0$ and $\lim_{\tau\to\infty} \frac{\mathrm{d}f(\tau)}{\mathrm{d}\tau} = 0$, it indicates that $\frac{\mathrm{d}f(\tau)}{\mathrm{d}\tau} > 0$ for any $\tau \in (0, \infty)$. Thus, $f(\tau)$ is increasing with $\tau$, which also indicates that $G_b(\tau, \omega)$ is increasing with $\tau$.

For the monotonicity of $G_b(\tau, \omega)$ with $\omega$, it can be readily verified that (5.11) is increasing with $\omega$.

Afterwards, by assuming $\tau^\dagger \le \tau^\ddagger$ and $\omega^\dagger \le \omega^\ddagger$, we have

$$\begin{aligned}
&G_b(\tau^\dagger, \omega^\dagger) \\
&= \sum_{i=1}^{K} \left\{ \frac{3C_u l_0 a_{0,i}^3 (N_i - D_i^\dagger)^2}{(\ln 2) T^2} (1 - 2^{-\frac{D_i^\dagger}{\tau^\dagger}}) \tau^\dagger - \frac{C_b l_0 a_{0,i}^3 (D_i^\dagger)^3}{(\omega^\dagger)^2} \right\} \\
&\overset{\text{(ii)}}{\le} \sum_{i=1}^{K} \left\{ \frac{3C_u l_0 a_{0,i}^3 (N_i - D_i^\dagger)^2}{(\ln 2) T^2} (1 - 2^{-\frac{D_i^\dagger}{\tau^\ddagger}}) \tau^\ddagger - \frac{C_b l_0 a_{0,i}^3 (D_i^\dagger)^3}{(\omega^\ddagger)^2} \right\} \\
&\overset{\text{(iii)}}{\le} \sum_{i=1}^{K} \left\{ \frac{3C_u l_0 a_{0,i}^3 (N_i - D_i^\ddagger)^2}{(\ln 2) T^2} (1 - 2^{-\frac{D_i^\ddagger}{\tau^\ddagger}}) \tau^\ddagger - \frac{C_b l_0 a_{0,i}^3 (D_i^\ddagger)^3}{(\omega^\ddagger)^2} \right\} \\
&= G_b(\tau^\ddagger, \omega^\ddagger),
\end{aligned} \tag{5.21}$$

in which (ii) is from $\tau^\dagger \le \tau^\ddagger$ and $\omega^\dagger \le \omega^\ddagger$, and (iii) is from the optimality of $\{D_i^\ddagger\}$ in $U_b(\{D_i\}, \tau^\ddagger, \omega^\ddagger)$ under given $\tau^\ddagger$ and $\omega^\ddagger$.

Therefore, function $G_b(\tau, \omega)$ is increasing with $\tau$ and $\omega$. □

**Remark:** Since both $G_b(\tau, \omega)$ and the constraint function (5.17b) are increasing with $\tau$ and $\omega$, the constraint function (5.17b) should be active at the optimality. As a result, solving Problem P4 or Problem P3 is equivalent to solving Problem P1. Moreover, Problem P4 is a monotonic optimization problem. Thus, the Polyblock Algorithm [112,113] can be leveraged to solve the optimal solution, as shown in Algorithm 4. After solving Problem P4, we can obtain the optimal $\tau^*$, $\omega^*$ and $\{D_i^*\}$, $\forall i \in \mathcal{K}$. Then based on (5.1), (5.6) and (5.7), it indicates the Stackelberg Equilibrium solutions $\tau^*$, $\{x_i^*\}$, $\{p_i^*\}$ can also be reached.

Here we explain the complexity of the proposed algorithm. For fixed time

allocation, the golden section search is used, which has a linear convergence. To identify the optimal time allocation, the Polyblock algorithm is adopted, which does not have an expression for the complexity. However, since there are only two dimensions for the time allocation, the overall complexity is reasonable.

**Algorithm 4:** Polyblock Algorithm to Problem P4

**Input:** Function $G_b(\tau, \omega)$ and the tolerance $\epsilon$.
**Output:** The optimal $\tau^*$, $\omega^*$ and objective value $s^*$.

Initialize $\boldsymbol{v}_0 = [T, T]$, $\mathcal{V} = \{\boldsymbol{v}_0\}$ and $s^* = 0$.
**while** $|\mathcal{V}| \neq 0$ **do**
  **for** $i = 1 : 1 : |\mathcal{V}|$ **do**
    Find the index $i^\dagger = \arg\max_{1 \leq i \leq |\mathcal{V}|} G_b(\tau_i, \omega_i)$ and the associated vertex $\boldsymbol{v}_{i^\dagger} = [\tau_{i^\dagger}, \omega_{i^\dagger}]$.
    Set $\lambda_{i^\dagger} = T/(\tau_{i^\dagger} + \omega_{i^\dagger})$.
    **if** $G_b(\lambda_{i^\dagger}\tau_{i^\dagger}, \lambda_{i^\dagger}\omega_{i^\dagger}) > s^*$ **then**
      Set $\boldsymbol{y}^* = \lambda_{i^\dagger}\boldsymbol{v}_{i^\dagger}$ and $s^* = G_b(\lambda_{i^\dagger}\tau_{i^\dagger}, \lambda_{i^\dagger}\omega_{i^\dagger})$.
    Delete any vertex $\boldsymbol{v}_j \in \mathcal{V}, j \in \{1, 2, \ldots, |\mathcal{V}|\}$ satisfying $G_b(\tau_j, \omega_j) \leq G_b(\tau_{i^\dagger}, \omega_{i^\dagger}) + \epsilon$.
    Delete any vertex $\boldsymbol{v}_j$ satisfying $\boldsymbol{v}_j > \boldsymbol{v}_{i^\dagger}$.
    **if** $|\mathcal{V}| \neq 0$ **then**
      Generate two new vertexes $\boldsymbol{v}^{\sharp 1} = \boldsymbol{v}_{i^\dagger} + (\lambda_{i^\dagger}\boldsymbol{v}_{i^\dagger} - \boldsymbol{v}_{i^\dagger}) \circ (0, 1)$ and $\boldsymbol{v}^{\sharp 2} = \boldsymbol{v}_{i^\dagger} + (\lambda_{i^\dagger}\boldsymbol{v}_{i^\dagger} - \boldsymbol{v}_{i^\dagger}) \circ (1, 0)$.
      Delete $\boldsymbol{v}_{i^\dagger}$ from $\mathcal{V}$, and let $\mathcal{V} = \mathcal{V} \cup \{\boldsymbol{v}^{\sharp 1}, \boldsymbol{v}^{\sharp 2}\}$.
Output $\boldsymbol{y}^*$ as $[\tau^*, \omega^*]$ and $s^*$ before $|\mathcal{V}| = 0$

## 5.4 Numerical Results

Now we use simulations to evaluate the performance for our Stackelberg game based resource allocation algorithm. We further model the channel coefficient as $h_i = \tilde{h}_i/\sqrt{d_i^\kappa}$, $\forall i \in \mathcal{K}$, where $\tilde{h}_i$ is a circularly symmetric complex Gaussian random variable with zero mean and unit variance, $d_i$ is the distance between user $i$ and the BS, and $\kappa$ stands for the path loss exponent. We set the distances as $d_i = 100$ m, $\forall i \in \mathcal{K}$. The path loss exponent is fixed as $\kappa = 2$. The system

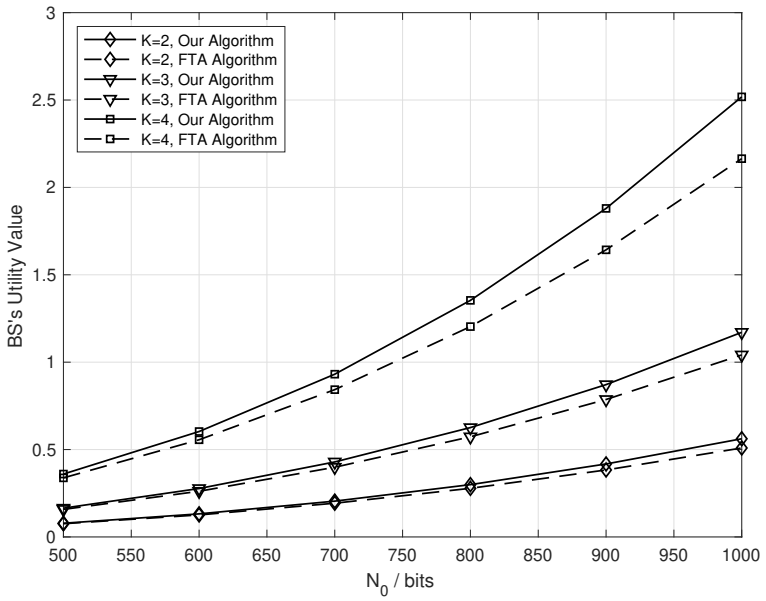


Figure 5.1: The BS's utility value in our algorithm.

bandwidth is 1 MHz. The noise variance is $\sigma^2 = -30$ dBm. The time slot length is $T = 1$ ms. The coefficients $C_u$ and $C_b$ are $C_u = 10^3$ and $C_b = 10^3$. The constant related to CPU architecture is $l_0 = 10^{-23}$. The number of CPU cycles to compute one bit data are $a_{0,i} = 40$, $\forall i \in \mathcal{K}$.

As shown in Fig. 5.1, the BS's utility value is evaluated. The user numbers are set to: $K = 2, 3, 4$. We assume each user has a different number of data bits $N_i$ to compute, and $N_i$ increase when $i$ increases. In specific, we set $N_1 = N_0$, $N_2 = 1.25N_0$, $N_3 = 1.5N_0$ and $N_4 = 2N_0$, where $N_0 = 500 : 100 : 1000$. Observed from Fig. 5.1, the utility value increases with the increase of $N_0$. This is because when $N_0$ becomes larger, more interferences should be purchased for data offloading at the user side. It results in the increase of revenue at the BS. The BS's utility also increases with the user number $K$. One conventional approach of offloading is the fixed time allocation (FTA) scheme. We compare our algorithm with one FTA scheme, in which the offloading time is set as $\tau = T/4$. It can be

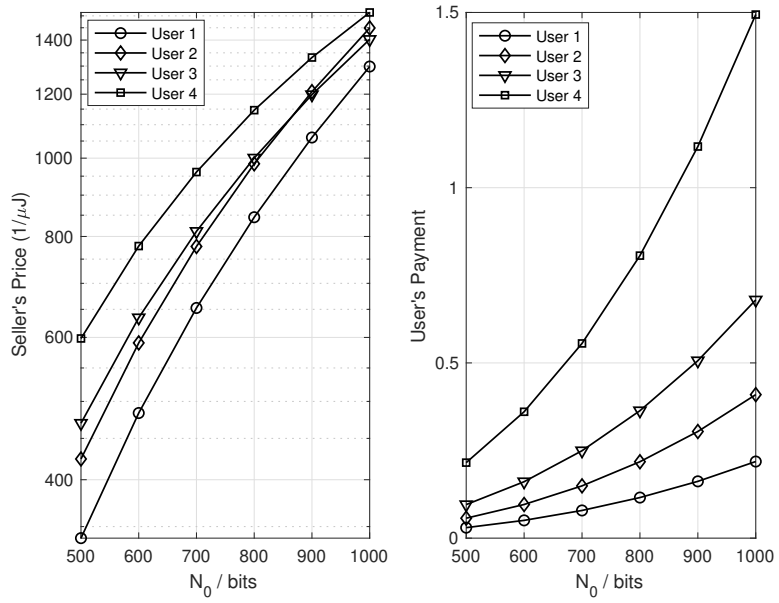


Figure 5.2: The price of the interference and user's payment in our algorithm.

seen that the gap between our algorithm and the FTA algorithm becomes larger with the increase of $N_0$.

The price of interference and user's payment are shown in Fig. 5.2. For a fixed number of data bits $N_0$, user's price follows an overall increasing trend when user $i$ increases. Moreover, observed from Fig. 5.2, a stronger user makes a higher payment than a weaker user. For example, user 4's payment is over 5 times larger than user 1's payment. This also means the BS can earn a higher revenue from a stronger user. The user's utility value is illustrated in Fig. 5.3. It can be seen from Fig. 5.3 that user's utility value has a similar trend as the payment made by the user. One reason is due to a larger number of data bits $N_i$ in the task of a stronger user. The other reason is due to a higher payment from a stronger user.

As illustrated in Fig. 5.4, the offloaded data amount is evaluated. It can be observed that user's offloaded data amount increases with the increase of user $i$.

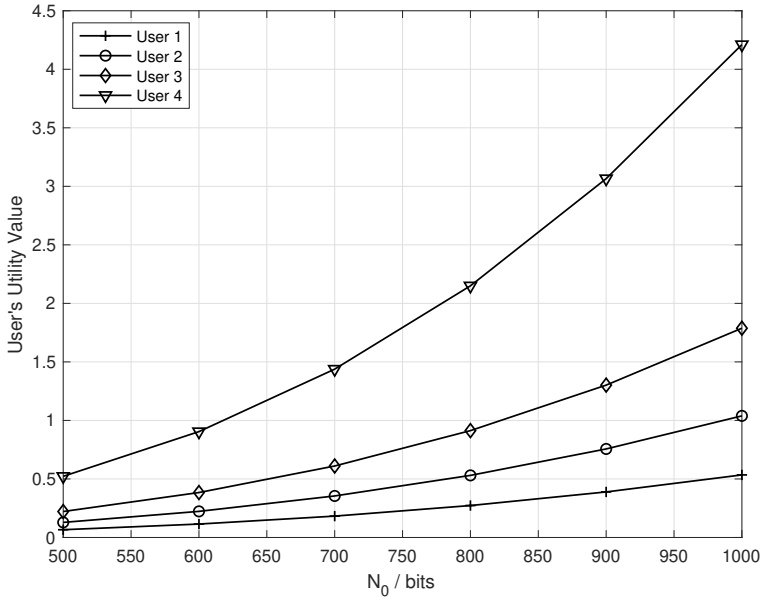


Figure 5.3: The user's utility value in our algorithm.

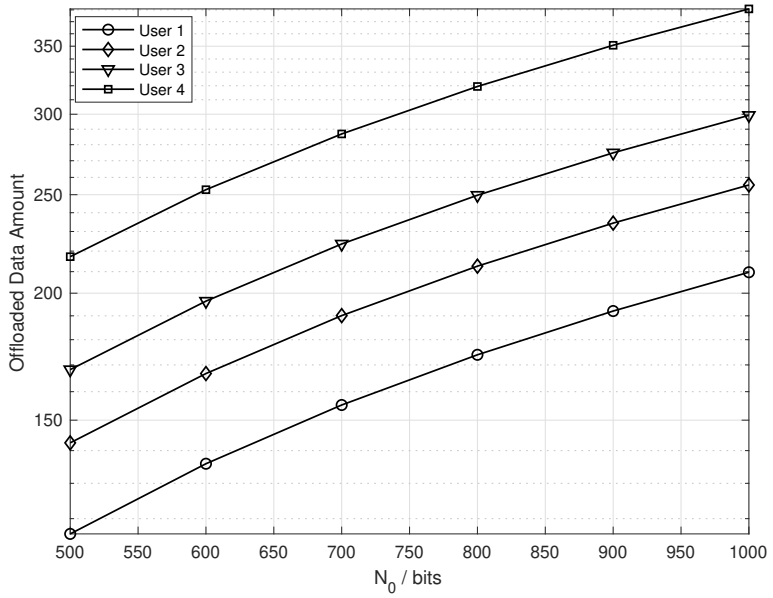


Figure 5.4: Different user's offloaded data amount in our algorithm.

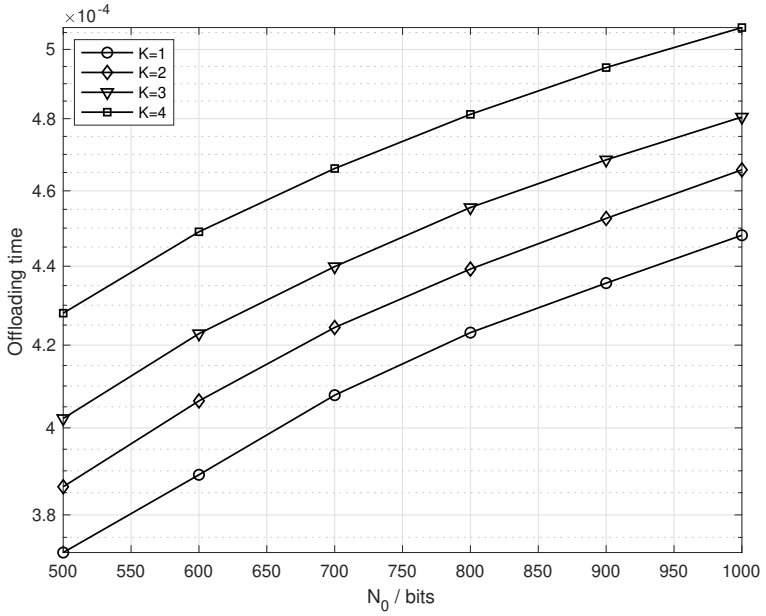


Figure 5.5: The offloading time in our algorithm.

For example, user 4's offloaded data amount is around twice larger than user 1's offloaded data amount. Moreover, the offloading time is illustrated in Fig. 5.5 under different user numbers. The time spent on data offloading goes up with the increase of the number of data bits $N_0$. which is intuitive. Recall that one time slot has a duration of 1ms. We can see that the percentage of time used for data offloading is around 50%.

## 5.5 Conclusion

In this chapter, we provide one design of energy-aware resource allocation in NOMA MEC networks, with the aid of a two-level Stackelberg game. By using the backward induction, after solving the buyer-level game, the seller-level game is a non-convex optimization problem. Then we provide an efficient approach to reach its global optimal point. Specifically, when the allocated time in our system is fixed, we demonstrate that the optimization problem can be efficiently

solved. Subsequently, the monotonic optimization method is utilized to allocate the optimal time resource.

# Chapter 6

# Conclusions and Future Research

## 6.1 Conclusions

Under different networking scenarios, to achieve the goal of efficient transmissions, we study the resource allocation problems in NOMA enabled networks.

Chapter 3 investigates an overlay cognitive NOMA system integrated with energy harvesting. Based on the time switching protocol, the ST harvests energy from the primary signal. When the throughput for the primary system is smaller than a target, the ST helps the PT to relay information. Meanwhile, NOMA transmission is leveraged to send the ST's information. In our system, with the aim of maximizing the secondary throughput, we optimize the time ratio to harvest energy and the power allocation in superposition coding. Two optimization problems are formulated under the SIC case and non-SIC case. We convert the original non-convex problems into some equivalent problems. For the equivalent problems, theoretical proofs are offered to show the quasiconcavity of the objective functions. Then the optimal solutions are obtained by using a designed two-level bisection method. Moreover, we have an interesting insight. We show that the case performing SIC cannot always guarantee a larger performance.

Chapter 4 investigates the Stackelberg game based power allocation problem

in downlink NOMA system. With the aim of maximizing the profit per unit power, the BS optimizes its price and total allocated transmit power. To maximize its profit, each user decides the amount of power. The backward induction is employed to solve the formulated game. Based on the solution at the user side, we have a non-convex optimization problem at the BS. Thus, we propose a method to solve it, which has two stages. In stage 1, an approach is designed to convert the original problem into an equivalent form. Then the optimal solution to the equivalent problem is also found by using one designed iterative algorithm. Afterwards, with the aid of the stage 1 solution, the optimal solution in stage 2 can also be efficiently obtained.

Chapter 5 investigates the resource allocation problem in an energy-aware NOMA MEC system. To promote energy saving from economic views, one approach of resource allocation is proposed by using a two-level Stackelberg game. For the formulated game, a method is developed to solve it. Specifically, we plug the obtained solution of the buyer-level game into the seller-level game, yielding a non-convex optimization problem. To solve the seller-level problem, we first efficiently obtain the optimal solution with given time allocation. Subsequently, how to optimally allocate time resource is also given.

## 6.2 Further Extensions and Future Research

In our future research, we have three possible research topics in wireless networks with NOMA. Firstly, based on our research work in Chapter 3, we can further study the physical layer security concern. In our cognitive NOMA system, we can consider that there exists one eavesdropper who can intercept the information from the ST. Moreover, the ST can be considered to be equipped with multiple antennas. An external jammer can also be used to jam the eavesdropper. With

the aim of enhancing the secrecy performance, besides the harvesting ratio and the power allocation, the design of the beamforming vector at the ST and the jamming vector at the jammer can be investigated.

Secondly, based on our research work in Chapter 4, we can further investigate how to deal with the *free riding* issues in NOMA systems. For example, we can consider one network with multiple NOMA transmitters, in which the energy for multiple NOMA transmitters can be harvested from multiple power beacons. The NOMA transmitters purchase the transmit power from the power beacons. Due to the broadcasting nature of wireless signals, some transmitters may choose to harvest energy without making payments. This is the so-called free riding issue, which can be addressed by using the evolutionary game. Thus, based on our original network, one further research topic is to formulate a Stackelberg game, which is combined with the evolutionary game.

Thirdly, based on our research work in Chapter 5, we can further study the resource allocation in NOMA MEC network over multiple fading blocks. In our considered NOMA MEC network, a single fading block is considered to perform data offloading. However, the offloading time may be larger than one fading block [114]. Therefore, a future research topic is to consider the data offloading for users via uplink NOMA over multiple fading blocks, which has the target of minimizing the average energy consumption. How to determine the data offloading amount and the offloading time can be studied, which can be addressed by using the dynamic programming method.

# References


[1] K. Samdanis and T. Taleb, "The road beyond 5G: A vision and insight of the key technologies," *IEEE Netw.*, vol. 34, no. 2, pp. 135–141, Mar. 2020.

[2] A. Goldsmith, *Wireless Communications*. Cambridge University Press, 2005.

[3] D. Tse and P. Viswanath, *Fundamentals of Wireless Communication*. Cambridge University Press, 2005.

[4] R. Q. Hu and Y. Qian, "An energy efficient and spectrum efficient wireless heterogeneous network framework for 5G systems," *IEEE Commun. Mag.*, vol. 52, no. 5, pp. 94–101, 2014.

[5] C. C. Poon, Y. Zheng, N. Luo, X. Ding, and Y. T. Zhang, "Wearing sensors inside and outside of the human body for the early detection of diseases," in *Wearable Sensors*, E. Sazonov and M. R. Neuman, Eds. Oxford: Academic Press, 2014, pp. 543 – 562.

[6] International Telecommunication Union (ITU), "Minimal requirements related to technical performance for IMT-2020 radio interfaces," Geneva, Switzerland, Feb. 2017, pp. 1–11.

[7] ——, "Requirements related to technical performance for IMT-advanced radio interface(s)," Geneva, Switzerland, Dec. 2008, pp. 1–8.

[8] T. M. Cover and J. A. Thomas, *Elements of Information Theory.* New York: Wiley, 2006.

[9] Y. Saito, Y. Kishiyama, A. Benjebbour, T. Nakamura, A. Li, and K. Higuchi, "Non-orthogonal multiple access (NOMA) for cellular future radio access," in *Proc. IEEE Veh. Technol. Conf.*, Dresden, Germany, June 2013, pp. 1–5.

[10] Y. Saito, A. Benjebbour, Y. Kishiyama, and T. Nakamura, "System-level performance evaluation of downlink non-orthogonal multiple access (NOMA)," in *Proc. IEEE Int. Symp. Pers., Indoor Mobile Radio Commun.*, London, U.K., Sept. 2013, pp. 611–615.

[11] Z. Ding, Y. Liu, J. Choi, Q. Sun, M. Elkashlan, C. L. I, and H. V. Poor, "Application of non-orthogonal multiple access in LTE and 5G networks," *IEEE Commun. Mag.*, vol. 55, no. 2, pp. 185–191, Feb. 2017.

[12] Z. Ding, X. Lei, G. K. Karagiannidis, R. Schober, J. Yuan, and V. K. Bhargava, "A survey on non-orthogonal multiple access for 5G networks: Research challenges and future trends," *IEEE J. Sel. Areas Commun.*, vol. 35, no. 10, pp. 2181–2195, Oct. 2017.

[13] L. Dai, B. Wang, Z. Ding, Z. Wang, S. Chen, and L. Hanzo, "A survey of non-orthogonal multiple access for 5G," *IEEE Commun. Surveys Tuts.*, vol. 20, no. 3, pp. 2294–2323, thirdquarter 2018.

[14] S. M. R. Islam, N. Avazov, O. A. Dobre, and K. Kwak, "Power-domain non-orthogonal multiple access (NOMA) in 5G systems: Potentials and challenges," *IEEE Commun. Surveys Tuts.*, vol. 19, no. 2, pp. 721–742, Secondquarter 2017.

[15] F. Wei, W. Chen, Y. Wu, J. Li, and Y. Luo, "Toward 5G wireless interface technology: Enabling nonorthogonal multiple access in the sparse code domain," *IEEE Veh. Technol. Mag.*, vol. 13, no. 4, pp. 18–27, Dec. 2018.

[16] Z. Chen, Z. Ding, X. Dai, and R. Zhang, "An optimization perspective of the superiority of NOMA compared to conventional OMA," *IEEE Trans. Signal Process.*, vol. 65, no. 19, pp. 5191–5202, Oct. 2017.

[17] M. Giordani, M. Polese, M. Mezzavilla, S. Rangan, and M. Zorzi, "Toward 6G networks: Use cases and technologies," *IEEE Commun. Mag.*, vol. 58, no. 3, pp. 55–61, Mar. 2020.

[18] Z. Ding, P. Fan, and H. V. Poor, "Impact of user pairing on 5G nonorthogonal multiple-access downlink transmissions," *IEEE Trans. Veh. Technol.*, vol. 65, no. 8, pp. 6010–6023, Aug. 2016.

[19] Y. Liu, Z. Ding, M. Elkashlan, and J. Yuan, "Nonorthogonal multiple access in large-scale underlay cognitive radio networks," *IEEE Trans. Veh. Technol.*, vol. 65, no. 12, pp. 10 152–10 157, Dec. 2016.

[20] L. Lv, Q. Ni, Z. Ding, and J. Chen, "Application of non-orthogonal multiple access in cooperative spectrum-sharing networks over Nakagami-$m$ fading channels," *IEEE Trans. Veh. Technol.*, vol. 66, no. 6, pp. 5506–5511, June 2017.

[21] Y. Xu, C. Shen, Z. Ding, X. Sun, S. Yan, G. Zhu, and Z. Zhong, "Joint beamforming and power-splitting control in downlink cooperative SWIPT NOMA systems," *IEEE Trans. Signal Process.*, vol. 65, no. 18, pp. 4874–4886, Sept. 2017.

[22] D. Wang and S. Men, "Secure energy efficiency for NOMA based cognitive radio networks with nonlinear energy harvesting," *IEEE Access*, vol. 6, pp. 62 707–62 716, Oct. 2018.

[23] C. Li, Q. Zhang, Q. Li, and J. Qin, "Price-based power allocation for non-orthogonal multiple access systems," *IEEE Wireless Commun. Lett.*, vol. 5, no. 6, pp. 664–667, Dec. 2016.

[24] Z. Wang, C. Wen, Z. Fan, and X. Wan, "A novel price-based power allocation algorithm in non-orthogonal multiple access networks," *IEEE Wireless Commun. Lett.*, vol. 7, no. 2, pp. 230–233, Apr. 2018.

[25] S. Kim, S. Park, M. Chen, and C. Youn, "An optimal pricing scheme for the energy-efficient mobile edge computation offloading with OFDMA," *IEEE Commun. Lett.*, vol. 22, no. 9, pp. 1922–1925, Sep. 2018.

[26] X. Cao, C. Liu, and M. Peng, "Energy-efficient mobile edge computing in NOMA-based wireless networks: A game theory approach," in *ICC 2020 - 2020 IEEE International Conference on Communications (ICC)*, 2020, pp. 1–6.

[27] S. Haykin, "Cognitive radio: brain-empowered wireless communications," *IEEE J. Sel. Areas Commun.*, vol. 23, no. 2, pp. 201–220, Feb. 2005.

[28] A. Goldsmith, S. A. Jafar, I. Maric, and S. Srinivasa, "Breaking spectrum gridlock with cognitive radios: An information theoretic perspective," *Proceedings of the IEEE*, vol. 97, no. 5, pp. 894–914, May 2009.

[29] Y. C. Liang, Y. Zeng, E. C. Y. Peh, and A. T. Hoang, "Sensing-throughput tradeoff for cognitive radio networks," *IEEE Trans. Wireless Commun.*, vol. 7, no. 4, pp. 1326–1337, Apr. 2008.

[30] R. Fan and H. Jiang, "Optimal multi-channel cooperative sensing in cognitive radio networks," *IEEE Trans. Wireless Commun.*, vol. 9, no. 3, pp. 1128–1138, Mar. 2010.

[31] R. Fan, H. Jiang, Q. Guo, and Z. Zhang, "Joint optimal cooperative sensing and resource allocation in multichannel cognitive radio networks," *IEEE Trans. Veh. Technol.*, vol. 60, no. 2, pp. 722–729, Feb. 2011.

[32] S. Ulukus, A. Yener, E. Erkip, O. Simeone, M. Zorzi, P. Grover, and K. Huang, "Energy harvesting wireless communications: A review of recent advances," *IEEE J. Sel. Areas Commun.*, vol. 33, no. 3, pp. 360–381, Mar. 2015.

[33] L. R. Varshney, "Transporting information and energy simultaneously," in *Proc. IEEE ISIT*, Jul. 2008, pp. 1612–1616.

[34] P. Grover and A. Sahai, "Shannon meets Tesla: Wireless information and power transfer," in *Proc. IEEE ISIT*, Jun. 2010, pp. 2363–2367.

[35] X. Lu, P. Wang, D. Niyato, D. I. Kim, and Z. Han, "Wireless networks with RF energy harvesting: A contemporary survey," *IEEE Commun. Surveys Tuts.*, vol. 17, no. 2, pp. 757–789, Secondquarter 2015.

[36] Y. Mao, C. You, J. Zhang, K. Huang, and K. B. Letaief, "A survey on mobile edge computing: The communication perspective," *IEEE Commun. Surveys Tuts.*, vol. 19, no. 4, pp. 2322–2358, Fourthquarter 2017.

[37] P. Mach and Z. Becvar, "Mobile edge computing: A survey on architecture and computation offloading," *IEEE Commun. Surveys Tuts.*, vol. 19, no. 3, pp. 1628–1656, thirdquarter 2017.

[38] W. Shi, J. Cao, Q. Zhang, Y. Li, and L. Xu, "Edge computing: Vision and challenges," *IEEE Internet Things J.*, vol. 3, no. 5, pp. 637–646, Oct. 2016.

[39] T. Taleb, K. Samdanis, B. Mada, H. Flinck, S. Dutta, and D. Sabella, "On Multi-Access Edge Computing: A survey of the emerging 5G network edge cloud architecture and orchestration," *IEEE Commun. Surveys Tuts.*, vol. 19, no. 3, pp. 1657–1681, thirdquarter 2017.

[40] ETSI, "MEC deployments in 4G and evolution towards 5G," Sophia Antipolis Cedex, France, Feb. 2018, pp. 1–24.

[41] ETSI GS MEC-IEG, "Mobile-Edge Computing proof-of-concept framework, v1.1.1," Sophia Antipolis Cedex, France, Aug. 2015, pp. 1–14.

[42] ETSI. (2016) MEC proofs of concept. [Online]. Available: https://www.etsi.org/technologies/multi-access-edge-computing/mec-poc

[43] D. Fudenberg and J. Tirole, *Game Theory*. MIT Press, 1991.

[44] M. Osborne, *An Introduction to Game Theory*. Oxford Univ. Press, 2004.

[45] M. Vaezi, G. A. Aruma Baduge, Y. Liu, A. Arafa, F. Fang, and Z. Ding, "Interplay between NOMA and other emerging technologies: A survey," *IEEE Trans. on Cogn. Commun. Netw.*, vol. 5, no. 4, pp. 900–919, Dec. 2019.

[46] Z. Ding, Z. Yang, P. Fan, and H. V. Poor, "On the performance of non-orthogonal multiple access in 5G systems with randomly deployed users," *IEEE Signal Process. Lett.*, vol. 21, no. 12, pp. 1501–1505, Dec. 2014.

[47] Z. Ding, M. Peng, and H. V. Poor, "Cooperative non-orthogonal multiple access in 5G systems," *IEEE Commun. Lett.*, vol. 19, no. 8, pp. 1462–1465, Aug. 2015.

[48] Z. Ding, H. Dai, and H. V. Poor, "Relay selection for cooperative NOMA," *IEEE Wireless Commun. Lett.*, vol. 5, no. 4, pp. 416–419, Aug. 2016.

[49] P. Xu, Z. Yang, Z. Ding, and Z. Zhang, "Optimal relay selection schemes for cooperative NOMA," *IEEE Trans. Veh. Technol.*, vol. 67, no. 8, pp. 7851–7855, Aug. 2018.

[50] Y. Liu, Z. Ding, M. Elkashlan, and H. V. Poor, "Cooperative non-orthogonal multiple access with simultaneous wireless information and power transfer," *IEEE J. Sel. Areas Commun.*, vol. 34, no. 4, pp. 938–953, Apr. 2016.

[51] Z. Yang, Z. Ding, P. Fan, and N. Al-Dhahir, "The impact of power allocation on cooperative non-orthogonal multiple access networks with SWIPT," *IEEE Trans. Wireless Commun.*, vol. 16, no. 7, pp. 4332–4343, July 2017.

[52] S. Wang and T. Wu, "Stochastic geometric performance analyses for the cooperative NOMA with the full-duplex energy harvesting relaying," *IEEE Trans. Veh. Technol.*, vol. 68, no. 5, pp. 4894–4905, May 2019.

[53] Z. Ding, P. Fan, and H. V. Poor, "Impact of non-orthogonal multiple access on the offloading of mobile edge computing," *IEEE Trans. Commun.*, vol. 67, no. 1, pp. 375–390, Jan. 2019.

[54] Y. Ye, R. Q. Hu, G. Lu, and L. Shi, "Enhance latency-constrained computation in MEC networks using uplink NOMA," *IEEE Trans. Commun.*, vol. 68, no. 4, pp. 2409–2425, Apr. 2020.

[55] L. Lin, W. Zhou, and Z. Zhao, "Analytical modeling of NOMA-based mobile edge computing systems with randomly located users," *IEEE Commun. Lett.*, pp. 1–4, Accepted.

[56] T. Lv, Y. Ma, J. Zeng, and P. T. Mathiopoulos, "Millimeter-wave NOMA transmission in cellular M2M communications for Internet of Things," *IEEE Internet Things J.*, vol. 5, no. 3, pp. 1989–2000, June 2018.

[57] D. Zhang, K. Yu, Z. Wen, and T. Sato, "Outage probability analysis of NOMA within Massive MIMO systems," in *2016 IEEE 83rd Vehicular Technology Conference (VTC Spring)*, May 2016, pp. 1–5.

[58] J. Chen, L. Yang, and M. Alouini, "Physical layer security for cooperative NOMA systems," *IEEE Trans. Veh. Technol.*, vol. 67, no. 5, pp. 4645–4649, May 2018.

[59] Z. Ding, P. Fan, G. K. Karagiannidis, R. Schober, and H. V. Poor, "NOMA assisted wireless caching: Strategies and performance analysis," *IEEE Trans. Commun.*, vol. 66, no. 10, pp. 4854–4876, Oct. 2018.

[60] S. Timotheou and I. Krikidis, "Fairness for non-orthogonal multiple access in 5G systems," *IEEE Signal Process. Lett.*, vol. 22, no. 10, pp. 1647–1651, Oct. 2015.

[61] P. Xu and K. Cumanan, "Optimal power allocation scheme for non-orthogonal multiple access with $\alpha$ -fairness," *IEEE J. Sel. Areas Commun.*, vol. 35, no. 10, pp. 2357–2369, Oct. 2017.

[62] J. Cui, Z. Ding, and P. Fan, "A novel power allocation scheme under outage constraints in NOMA systems," *IEEE Signal Process. Lett.*, vol. 23, no. 9, pp. 1226–1230, Sept. 2016.

[63] J. Seo and Y. Sung, "Beam design and user scheduling for nonorthogonal multiple access with multiple antennas based on pareto optimality," *IEEE Trans. Signal Process.*, vol. 66, no. 11, pp. 2876–2891, June 2018.

[64] Y. Zhang, H. Wang, T. Zheng, and Q. Yang, "Energy-efficient transmission design in non-orthogonal multiple access," *IEEE Trans. Veh. Technol.*, vol. 66, no. 3, pp. 2852–2857, Mar. 2017.

[65] Q. Liu, T. Lv, and Z. Lin, "Energy-efficient transmission design in cooperative relaying systems using NOMA," *IEEE Commun. Lett.*, vol. 22, no. 3, pp. 594–597, Mar. 2018.

[66] G. Liu, X. Chen, Z. Ding, Z. Ma, and F. R. Yu, "Hybrid half-duplex/full-duplex cooperative non-orthogonal multiple access with transmit power adaptation," *IEEE Trans. Wireless Commun.*, vol. 17, no. 1, pp. 506–519, Jan. 2018.

[67] P. D. Diamantoulakis, K. N. Pappi, Z. Ding, and G. K. Karagiannidis, "Wireless-powered communications with non-orthogonal multiple access," *IEEE Trans. Wireless Commun.*, vol. 15, no. 12, pp. 8422–8436, Dec. 2016.

[68] Q. Wu, W. Chen, D. W. K. Ng, and R. Schober, "Spectral and energy-efficient wireless powered iot networks: NOMA or TDMA?" *IEEE Trans. Veh. Technol.*, vol. 67, no. 7, pp. 6663–6667, July 2018.

[69] H. Zhang, M. Feng, K. Long, G. K. Karagiannidis, and V. C. M. Leung, "Energy-efficient resource allocation in NOMA heterogeneous networks with energy harvesting," in *2018 IEEE Global Communications Conference (GLOBECOM)*, Dec. 2018, pp. 206–212.

[70] Z. Ding, D. W. K. Ng, R. Schober, and H. V. Poor, "Delay minimization for NOMA-MEC offloading," *IEEE Signal Process. Lett.*, vol. 25, no. 12, pp. 1875–1879, Dec. 2018.

[71] Z. Ding, J. Xu, O. A. Dobre, and V. Poor, "Joint power and time allocation for NOMA-MEC offloading," *IEEE Trans. Veh. Technol.*, vol. 68, no. 6, pp. 6207–6211, June 2019.

[72] F. Wang, J. Xu, and Z. Ding, "Multi-antenna NOMA for computation offloading in multiuser mobile edge computing systems," *IEEE Trans. Commun.*, vol. 67, no. 3, pp. 2450–2463, Mar. 2019.

[73] C. Li, H. Wang, and R. Song, "Intelligent offloading for NOMA-assisted MEC via dual connectivity," *IEEE Internet Things J.*, pp. 1–12, Accepted.

[74] J. Cui, Y. Liu, Z. Ding, P. Fan, and A. Nallanathan, "Optimal user scheduling and power allocation for millimeter wave NOMA systems," *IEEE Trans. Wireless Commun.*, vol. 17, no. 3, pp. 1502–1517, Mar. 2018.

[75] Y. Zhang, H. Wang, Q. Yang, and Z. Ding, "Secrecy sum rate maximization in non-orthogonal multiple access," *IEEE Commun. Lett.*, vol. 20, no. 5, pp. 930–933, May 2016.

[76] Y. Sun, D. W. K. Ng, J. Zhu, and R. Schober, "Robust and secure resource allocation for full-duplex MISO multicarrier NOMA systems," *IEEE Trans. Commun.*, vol. 66, no. 9, pp. 4119–4137, Sep. 2018.

[77] L. Xiang, D. W. K. Ng, X. Ge, Z. Ding, V. W. S. Wong, and R. Schober, "Cache-aided non-orthogonal multiple access: The two-user case," *IEEE J. Sel. Topics Signal Process.*, vol. 13, no. 3, pp. 436–451, June 2019.

[78] F. Li, H. Jiang, R. Fan, and P. Tan, "Cognitive non-orthogonal multiple access with energy harvesting: An optimal resource allocation approach," *IEEE Trans. Veh. Technol.*, vol. 68, no. 7, pp. 7080–7095, July 2019.

[79] F. Li, H. Jiang, R. Fan, and P. Tan, "Optimal cooperative strategy in energy harvesting cognitive radio networks," in *2017 IEEE 86th Vehicular Technology Conference (VTC-Fall)*, Sept. 2017, pp. 1–6.

[80] Y. Zhang, Q. Yang, T. Zheng, H. Wang, Y. Ju, and Y. Meng, "Energy efficiency optimization in cognitive radio inspired non-orthogonal multiple access," in *Proc. 2016 IEEE PIMRC*, Sep. 2016, pp. 1–6.

[81] W. Liang, Z. Ding, Y. Li, and L. Song, "User pairing for downlink non-orthogonal multiple access networks using matching algorithm," *IEEE Trans. Commun.*, vol. 65, no. 12, pp. 5319–5332, Dec. 2017.

[82] M. Mohammadi, B. K. Chalise, A. Hakimi, Z. Mobini, H. A. Suraweera, and Z. Ding, "Beamforming design and power allocation for full-duplex non-orthogonal multiple access cognitive relaying," *IEEE Trans. Commun.*, vol. 66, no. 12, pp. 5952–5965, Dec. 2018.

[83] L. Lv, L. Yang, H. Jiang, T. H. Luan, and J. Chen, "When NOMA meets multiuser cognitive radio: Opportunistic cooperation and user scheduling," *IEEE Trans. Veh. Technol.*, vol. 67, no. 7, pp. 6679–6684, Jul. 2018.

[84] L. Lv, J. Chen, Q. Ni, Z. Ding, and H. Jiang, "Cognitive non-orthogonal multiple access with cooperative relaying: A new wireless frontier for 5G spectrum sharing," *IEEE Commun. Mag.*, vol. 56, no. 4, pp. 188–195, Apr. 2018.

[85] S. Boyd and L. Vandenberghe, *Convex Optimization*. New York, NY, USA: Cambridge University Press, 2004.

[86] J. F. Traub and A. G. Werschulz, *Complexity and Information*. Cambridge University Press, 1998.

[87] D. Bertsekas, *Dynamic Programming and Optimal Control*. Athena Scientific, 2001, vol. I and II.

[88] Q. Gu, Y. Jian, G. Wang, R. Fan, H. Jiang, and Z. Zhong, "Mobile edge computing via wireless power transfer over multiple fading blocks: An optimal stopping approach," *IEEE Trans. Veh. Technol.*, vol. 69, no. 9, pp. 10 348–10 361, Sep. 2020.

[89] R. M. Corless, G. H. Gonnet, D. E. Hare, D. J. Jeffrey, and D. E. Knuth, "On the Lambert W function," *Advances in Computational mathematics*, vol. 5, no. 1, pp. 329–359, 1996.

[90] R. Fan, W. Chen, H. Jiang, J. An, K. Yang, and C. Xing, "Dynamic spectrum leasing with two sellers," *IEEE Trans. Veh. Technol.*, vol. 67, no. 6, pp. 4852–4866, Jun. 2018.

[91] J. Gao, S. A. Vorobyov, and H. Jiang, "Cooperative resource allocation games under spectral mask and total power constraints," *IEEE Trans. Signal Process.*, vol. 58, no. 8, pp. 4379–4395, Aug. 2010.

[92] B. Wang, Z. Han, and K. J. R. Liu, "Distributed relay selection and power control for multiuser cooperative communication networks using stackelberg game," *IEEE Trans. Mobile Comput.*, vol. 8, no. 7, pp. 975–990, July 2009.

[93] X. Kang, R. Zhang, and M. Motani, "Price-based resource allocation for spectrum-sharing femtocell networks: A stackelberg game approach," *IEEE J. Sel. Areas Commun.*, vol. 30, no. 3, pp. 538–549, Apr. 2012.

[94] B. Hu, H. V. Zhao, and H. Jiang, "Wireless multicast using relays: Incentive mechanism and analysis," *IEEE Trans. Veh. Technol.*, vol. 62, no. 5, pp. 2204–2219, Jun. 2013.

[95] B. Di, L. Song, and Y. Li, "Sub-channel assignment, power allocation, and user scheduling for non-orthogonal multiple access networks," *IEEE Trans. Wireless Commun.*, vol. 15, no. 11, pp. 7686–7698, Nov. 2016.

[96] L. P. Qian, Y. Wu, H. Zhou, and X. Shen, "Joint uplink base station association and power control for small-cell networks with non-orthogonal multiple access," *IEEE Trans. Wireless Commun.*, vol. 16, no. 9, pp. 5567–5582, Sept. 2017.

[97] L. Seymour, R. S. Murray, and L. John, *Schaum's Outline of Mathematical Handbook of Formulas and Tables.* McGraw-Hill Education, 2017.

[98] M. Carter, *Foundations of Mathematical Economics.* The MIT Press, 2001.

[99] M. S. Bazaraa, H. D. Sherali, and C. M. Shetty, *Nonlinear programming: theory and algorithms.* John Wiley & Sons, 2013.

[100] Wei Yu and R. Lui, "Dual methods for nonconvex spectrum optimization of multicarrier systems," *IEEE Trans. Commun.*, vol. 54, no. 7, pp. 1310–1322, July 2006.

[101] M. Zeng, N. Nguyen, O. A. Dobre, and H. V. Poor, "Delay minimization for NOMA-assisted MEC under power and energy constraints," *IEEE Wireless Commun. Lett.*, vol. 8, no. 6, pp. 1657–1661, Dec 2019.

[102] B. Liu, C. Liu, and M. Peng, "Resource Allocation for Energy-Efficient MEC in NOMA-Enabled Massive IoT Networks," *IEEE J. Sel. Areas Commun.*, pp. 1–1, Accepted.

[103] Y. Huang, Y. Liu, and F. Chen, "NOMA-aided mobile edge computing via user cooperation," *IEEE Trans. Commun.*, vol. 68, no. 4, pp. 2221–2235, Apr. 2020.

[104] W. Wu, X. Wang, F. Zhou, K. Wong, C. Li, and B. Wang, "Resource allocation for enhancing offloading security in NOMA-enabled MEC networks," *IEEE Syst. J.*, pp. 1–4, Accepted.

[105] L. P. Qian, A. Feng, Y. Huang, Y. Wu, B. Ji, and Z. Shi, "Optimal SIC ordering and computation resource allocation in MEC-aware NOMA NB-IoT networks," *IEEE Internet Things J.*, vol. 6, no. 2, pp. 2806–2816, Apr. 2019.

[106] X. Chen, L. Jiao, W. Li, and X. Fu, "Efficient multi-user computation offloading for mobile-edge cloud computing," *IEEE/ACM Trans. Netw.*, vol. 24, no. 5, pp. 2795–2808, Oct. 2016.

[107] W. Sun, J. Liu, Y. Yue, and H. Zhang, "Double auction-based resource allocation for mobile edge computing in industrial Internet of Things," *IEEE Trans. Ind. Informat.*, vol. 14, no. 10, pp. 4692–4701, Oct. 2018.

[108] Q. Pham, H. T. Nguyen, Z. Han, and W. Hwang, "Coalitional games for computation offloading in NOMA-enabled multi-access edge computing," *IEEE Trans. Veh. Technol.*, vol. 69, no. 2, pp. 1982–1993, Feb. 2020.

[109] C. Xu, G. Zheng, and L. Tang, "Energy-aware user association for NOMA-based mobile edge computing using matching-coalition game," *IEEE Access*, vol. 8, pp. 61 943–61 955, 2020.

[110] W. Zhang, Y. Wen, K. Guan, D. Kilper, H. Luo, and D. O. Wu, "Energy-optimal mobile cloud computing under stochastic wireless channel," *IEEE Trans. Wireless Commun.*, vol. 12, no. 9, pp. 4569–4581, Sep. 2013.

[111] W. Press, S. Teukolsky, W. Vetterling, and B. Flannery, *Numerical Recipes: The Art of Scientific Computing*. New York, NY, USA: Cambridge University Press, 2007.

[112] H. Tuy, "Monotonic optimization: Problems and solution approaches," *SIAM Journal on Optimization*, vol. 11, no. 2, pp. 464–494, 2000.

[113] Y. J. A. Zhang, L. Qian, and J. Huang, "Monotonic optimization in communication and networking systems," *Foundations and Trends in Networking*, vol. 7, no. 1, pp. 1–75, 2013.

[114] R. Fan, F. Li, S. Jin, G. Wang, H. Jiang, and S. Wu, "Energy-efficient mobile-edge computation offloading over multiple fading blocks," in *2019 IEEE Global Communications Conference (GLOBECOM)*, Dec. 2019, pp. 1–6.